FRIEDRICH-SCHILLER-
UNIVERSITÄT
JENA

Dynamics of Quantum Information in Many-Body Systems with Nonlocal Interactions

Dissertation

zur Erlangung des akademischen Grades

doctor rerum naturalium
(Dr. rer. nat)

vorgelegt dem Rat der

Physikalisch-Astronomischen Fakultät

der

Friedrich-Schiller-Universität Jena

von

M. Sc. Darvin Wanisch

geboren am 24.01.1994 in Hagen

GUTACHTER:

1. Prof. Dr. Stephan Fritzsche
2. Dr. Pieter W. Claeys
3. Prof. Dr. Stefan Kehrein

TAG DER DISPUTATION: 26.09.2023

Abstract

The dynamics of quantum information lies at the heart of future technologies that aim to utilize the laws of quantum mechanics for practical purposes. Beyond that, it provides a unifying language that shines new light on longstanding problems home to historically separate fields of theoretical physics. Considering how quantum information propagates and spreads over the degrees of freedom of a quantum many-body system far from equilibrium has proven particularly helpful for various subjects, ranging from the emergence of statistical mechanics in isolated quantum systems to the black hole information paradox. Crucial for these developments are impressive experimental advances that nowadays allow us to explore the nonequilibrium physics of paradigmatic, simple, and (almost) isolated quantum many-body systems in the laboratory. In this thesis, we investigate the dynamics of quantum information in one-dimensional systems of interacting qubits, i.e., spin-chains, where we particularly consider systems that embody nonlocal interactions. The latter are ubiquitous in many experimental platforms for quantum simulation. Our results reveal an interesting connection between two complementary probes of quantum information dynamics, i.e., entanglement growth and operator spreading. This connection allows us to characterize different dynamical classes and underlines that nonlocal interactions induce rich behavior, such as slow thermalization accompanied by superballistic information propagation. In particular, we show that the famous slowdown of entanglement growth in systems with powerlaw interactions implies a slowdown of operator dynamics. The latter clearly distinguishes a system with powerlaw interactions from a system possessing fast scrambling, a characteristic property of black holes and holographic duals to theories of quantum gravity.

Zusammenfassung

Die Dynamik von Quanteninformation ist Herzstück künftiger Technologien, welche Gesetze der Quantenmechanik für praktische Zwecke nutzen wollen. Zudem bietet sie eine einigende Sprache, die neues Licht auf alte Probleme wirft, die in historisch getrennten Bereichen der Physik liegen. Die Überlegung, wie sich Quanteninformation über die Freiheitsgrade eines Quantenvielteilchensystems fernab des Gleichgewichts ausbreitet, hat sich als hilfreich für etliche Themen erwiesen, die von der Emergenz statistischer Mechanik in isolierten Quantensystemen bis zum Informationsparadoxon in Schwarzen Löchern reichen. Entscheidend für diese Entwicklungen sind beeindruckende experimentelle Fortschritte, die es uns heute ermöglichen, die Nichtgleichgewichtsphysik paradigmatischer, einfacher und (nahezu) isolierter Quantenvielteilchensysteme im Labor zu erforschen. In dieser Arbeit untersuchen wir Quanteninformationsdynamik in eindimensionalen Systemen aus wechselwirkenden Qubits, d.h. Spin-Ketten, wobei wir insbesondere nichtlokale Wechselwirkungen betrachten. Letztere sind in vielen experimentellen Plattformen für Quantensimulationen allgegenwärtig. Unsere Ergebnisse offenbaren eine interessante Verbindung zwei komplementärer Maße der Quanteninformationsdynamik, nämlich dem Verschränkungswachstum und der Operatorausbreitung. Diese Verbindung erlaubt es uns, dynamische Klassen zu charakterisieren und zeigt, dass nichtlokale Wechselwirkungen ein diverses Verhalten hervorrufen, wie z.B. langsame Thermalisierung, begleitet von superballistischer Informationsausbreitung. Insbesondere zeigen wir, dass das bekannte langsame Verschränkungswachstums in Systemen mit Potenzgesetz-Wechselwirkungen langsame Operatordynamik impliziert. Letzteres unterscheidet ein System mit Potenzgesetz-Wechselwirkungen eindeutig von jenem, das schnelles Scrambling zeigt, eine charakteristische Eigenschaft von Schwarzen Löchern und holographischen Dualen zu Theorien der Quantengravitation.

Acknowledgements

First and foremost, I want to thank Prof. Dr. Stephan Fritzsche for giving me the opportunity to work on this exciting topic and for providing useful advice, especially on what is important to become a good scientist. Furthermore, I warmly thank Prof. Dr. Holger Gies for his support and his advice on my future career. Special thanks go to Juan Diego for our fruitful discussions and the stimulating collaboration. I hope we will continue working together, and I am curious about what the future holds. Also, I would like to thank everyone from my group in Jena for all the interesting discussions and the familiar atmosphere.

Besonderer Dank geht an Romain, Björn und Baghi, die diesen Weg mit mir zusammen gegangen sind. Über die letzten Jahre sind wir Freunde geworden und ich hoffe, das bleibt auch so. Ich danke auch meinen Freunden aus der Heimat für die große Unterstützung, insbesondere Henry und Jens. Ich bin sehr froh, euch zu haben. Vor allem aber möchte ich Carla danken, für ihre Unterstützung während dieser aufregenden Zeit und ihren Mut, diesen Weg mit mir zu gehen.

Zuletzt möchte in meiner Familie danken, insbesondere Stella, Papa und Mama. Ihr könnt euch nicht vorstellen, wie viel Kraft ihr mir gegeben habt. Ich liebe euch.

Publications

The content of this thesis is based on the following publications:

- *Delocalization of quantum information in long-range interacting systems*
  D. Wanisch and S. Fritzsche, Phys. Rev. A, **104**, 042409 (2021).
- *Information scrambling and the correspondence of entanglement dynamics and operator dynamics in systems with nonlocal interactions*
  D. Wanisch, J. D. Arias Espinoza and S. Fritzsche, Phys. Rev. B, **107**, 205127 (2023)

The following publication is not included in this thesis:

- *Driven spin chains as high-quality quantum routers*
  D. Wanisch and S. Fritzsche, Phys. Rev. A, **102**, 032624 (2020).

“You are too concerned with what was and what will be. There is a saying. Yesterday is history, tomorrow is a mystery, but today is a gift. That is why it is called present”

— Master Oogway

Contents

1. Dynamics of Quantum Information 1

2. Entanglement and Scrambling 7

2.1. Entanglement 8
  2.1.1. Nonseparability and Nonlocality 9
  2.1.2. The Entropy of Entanglement 11
  2.1.3. Quantum Mutual Information 13
2.2. Quantum Information Propagation 15
  2.2.1. Locality and the Emergence of Causality 17
  2.2.2. The Breakdown of Locality 19
2.3. Quantum Information Scrambling 21
  2.3.1. Entanglement Growth 22
  2.3.2. The Generalized Hayden-Preskill Protocol 27
  2.3.3. Operator Spreading 31

3. Dynamics of Quantum Information in the Mixed-Field Ising Model 39

3.1. The Generalized Hayden-Preskill Protocol II 40
3.2. Measures of Quantum Information Dynamics 43
3.3. The Operator State 47

4. Dynamics of Quantum Information and Powerlaw Interactions 53

4.1. Strong Thermalization 54
4.2. The Monogamy of Mutual Information 56
4.3. Regimes of Quantum Information Dynamics 61
  4.3.1. The Local Regime 61
  4.3.2. The Nonlocal Regime 64
4.4. The Slowdown of Operator Dynamics 68
4.5. Connecting Entanglement Growth and Operator Spreading 71

5. Fast Scrambling **77**
5.1. A Minimal Model for Fast Scrambling 78
5.2. Fast Scrambling and Powerlaw Interactions 79

6. Discussions and Future Directions **85**

A. Numerics **91**
A.1. Time-Evolution 91
A.2. Entanglement Entropy and the Partial Trace 92
A.3. Operator Dynamics 92
A.4. Finite Size Scaling of Operator Size 94
A.5. Kac Normalization 95
A.6. Additional TDVP Data 96

B. Derivations and Useful Relations **101**
B.1. Derivation of Eq. (2.34) 101
B.2. Further Operator Relations 102

Bibliography **105**

Chapter 1.

Dynamics of Quantum Information

"Information is physical."
— Rolf Landauer

Despite the immediate success of quantum mechanics after its invention almost a century ago, the physical relevance of one of its characteristic traits, *quantum entanglement*, was more or less unclear at that time, and the sheer existence of entanglement triggered debates about the completeness of quantum mechanics as a theory itself [1]. Decades later, the development of quantum information theory established entanglement as a fundamental resource for quantum information processing tasks, essential for future quantum technologies [2, 3]. Nowadays, physicists are well aware that entanglement plays a crucial role in classifying complex quantum systems, for example, the detection of quantum phase transitions [4], or topological states of matter [5]. The amount of entanglement in a given quantum state is, in some sense, a measure of its complexity, as it relates to the difficulty of simulating the quantum state on a classical computer [6]. Recently, the dynamics of isolated quantum many-body systems enjoyed particular attention [7]. In this regard, concepts and techniques originating from quantum information theory, such as measures of entanglement and other types of correlations, have greatly enhanced our understanding of nonequilibrium quantum matter and shined new light on longstanding questions of theoretical physics.

Key drivers for the growing interest in nonequilibrium quantum many-body physics are impressive technological advances over the last two decades regarding the control and manipulation of single atoms and ions. These advances brought us the first pioneering platforms for analog quantum simulation and potential candidates for universal quantum computing. Already four decades ago, Richard Feynman proposed the idea of a *quantum simulator* [8]. He argued that the most efficient way to simulate a complex quantum system is to use a physical quantum system and manipulate it such that its Hamiltonian is sufficiently close to the Hamiltonian of the system one aims to simulate. Of course, this requires immense control over the system that serves as a simulation platform, which was unthought-of at the time of Feynman's proposal. Today, however, several platforms for quantum simulation exist, for instance, systems of trapped ions [9, 10], cold atoms in optical lattices [11, 12], or systems of Rydberg atoms [13, 14]. These platforms allow us to explore the nonequilibrium physics of paradigmatic quantum lattice models of widespread importance. For example, models of interacting Fermions [15, 16] and Bosons [17] like the Hubbard model, or models of interacting spins (qubits) [18, 19] such as the Ising model. The resulting quantum many-body systems are in good approximation isolated from their environment, at least up to a certain timescale, which enables the simulation of coherent dynamics. Noteworthy, these platforms are currently at a stage where they compete with the scope of classical computers or even overcome it. Thus, considering the current developments on the experimental side, one may expect that it is just a matter of time until quantum simulators are able to explore complex quantum many-body systems beyond the scope of (future) classical computers.

Inspired by the technical possibilities of the above-mentioned experimental platforms, a popular protocol to study the nonequilibrium physics of quantum many-body systems is a *quantum quench*. In such a protocol, the system is prepared in an uncorrelated initial state $|\Psi_0\rangle$. Generally, such a state is not an eigenstate of the respective many-body Hamiltonian $\mathcal{H}$. Hence, the system will evolve in time according to

$$|\Psi(t)\rangle = e^{-i\mathcal{H}t}|\Psi_0\rangle \,, \tag{1.1}$$

where we assume a time-independent Hamiltonian $\mathcal{H}$ here, which is not a necessary condition, though. Under unitary evolution, interactions between the system's constituents result in the build-up of entanglement. In this regard, the *growth of entanglement* following the quantum quench protocol depicted in Eq. (1.1) has become an integral diagnostic tool of nonequilibrium quantum matter. In particular, it is crucial for understanding whether quantum many-body systems initialized far from equilibrium eventually equilibrate. Although not many conditions are necessary for the general equilibration of local observables [20], whether their late-time expectation values are determined by a few macroscopic quantities consistent with statistical mechanics is a question that caught much more attention recently [21]. This phenomenon goes under the name of *quantum* *thermalization*. Accordingly, considering the quench protocol (1.1), local observables *thermalize* under unitary evolution. That is, the late-time expectation value of a local observable $\mathcal{O}$ is determined by an effective thermal ensemble

$$\lim_{T\to\infty} \frac{1}{T} \int_0^T \langle \Psi\,(t)|\mathcal{O}|\Psi\,(t)\rangle \,\mathrm{d}t = \mathrm{Tr}\left\{\rho_\beta\,\mathcal{O}\right\} \,, \tag{1.2}$$

where ρ_β is a suitable thermal ensemble with effective invserse temperature β. The latter is determined by the energy expectation value of the initial state, i.e.,

$$E = \langle \Psi_0|\mathcal{H}|\Psi_0\rangle \overset{!}{=} \mathrm{Tr}\left\{\rho_\beta\,\mathcal{H}\right\} \,. \tag{1.3}$$

Equation (1.2) implies *microscopic thermalization*, therefore, expectation values of local observables solely depend on the energy of the initial state at late times. Typically, the expectation value is reasonably close to the expected thermal value after some *relaxation time* t_R, i.e.,

$$\langle \Psi\,(t)|\mathcal{O}|\Psi\,(t)\rangle \simeq \mathrm{Tr}\left\{\rho_\beta\,\mathcal{O}\right\} \,, \text{ for } t > t_\mathrm{R}\,, \tag{1.4}$$

where t_R may depend on the considered Hamiltonian, the initial state, and the respective observable.

Microscopic thermalization is a consequence of entanglement and, thus, a quantum phenomenon. Hence, due to extensive entanglement between a local region and its environment, the latter acts as an effective thermal bath. The *eigenstate thermalization hypothesis* (ETH) [22, 23] offers an explanation of this phenomenon by arguing that individual many-body eigenstates are locally indistinguishable from thermal ensembles. However, the generality of quantum thermalization is still an open field of research, as there are certain classes of systems that seem to escape thermalization [24, 25]. The latter further provides an interesting perspective on how quantum information evolves under unitary evolution in quantum many-body systems. If we follow Eq. (1.4), it becomes evident that two (orthogonal) initial states $|\Psi_0\rangle$, and $|\Phi_0\rangle$ with the same energy expectation value are effectively indistinguishable by local measurements after the relaxation time. However, due to unitary evolution, the two states remain orthogonal at all times, i.e., $\langle \Phi\,(t)\,|\Psi\,(t)\rangle = \langle \Phi_0|\Psi_0\rangle = 0$. In principle, one could distinguish them by a global measurement, however, they are locally indistinguishable since only the average energy determines local expectation values at late times. Thus, from a local perspective, any detail of the initial state seems to be lost. This apparent loss of initial state information under unitary evolution is nowadays believed to originate from *quantum information scrambling*. That is, under unitary evolution, quantum information spreads over nonlocal degrees of freedom and thereby becomes inaccessible to local measurements.

Due to its inherent connection to thermalization, quantum information scrambling enjoyed increasing attention over the last years as a promising diagnostic of nonequilibrium quantum matter [26, 27]. Furthermore, quantifying how quantum information propagates and spreads over the system's degrees of freedom is fundamentally important for future quantum technologies. Such a perspective on the dynamics of complex quantum many-body systems has additionally proven useful in the domain of high-energy physics and quantum gravity. In particular, quantum entanglement might be a crucial ingredient for the unification of quantum mechanics and general relativity, for example, through the correspondence between anti-de-Sitter space and conformal field theories (AdS/CFT) [28]. Moreover, quantum information scrambling was linked to the black hole information paradox. Correspondingly, information that falls into a black hole is not lost but scrambled such that it is almost impossible to reconstruct. However, assuming one collects all the Hawking radiation that is emitted by the black hole, it may be possible to reconstruct the information that fell in [29]. Black holes were also conjectured to possess a particular form of information scrambling, known as *fast scrambling* [30]. The latter is defined via the process of *operator spreading*, a rather novel view on the dynamics of quantum many-body systems, which considers the growth of initially local operators in size and complexity [26, 31]. This growth is usually diagnosed by *out-of-time-order correlation functions* (OTOCs). The latter allow us to probe the propagation of quantum information in thermalizing systems, contrary to traditional correlation functions. Moreover, they are connected to the emergence of fundamental speed limits in quantum lattice models [32]. Together, these complementary probes, namely, entanglement growth and operator spreading, offer a comprehensive language for the description of quantum many-body dynamics, i.e., *the dynamics of quantum information* [27].

How the constituents of the system interact with each other is one of the defining elements of its dynamics. Within the scope of condensed matter physics, one typically considers systems that embody *local interactions*. It is well established that these systems are generally associated with ballistic operator spreading [26, 32–34] accompanied by a linear growth of entanglement [35–38]. However, several platforms for analog quantum simulations naturally embody *nonlocal interactions*, for example, interactions that decay like a powerlaw with distance, such as Coulomb [9, 10], dipolar [39–41], or van der Waals interactions [13, 14]. The presence of powerlaw interactions can fundamentally change nonequilibrium physics. For example, it can induce superballistic operator spreading [42], which is exploited by improved protocols for quantum information processing tasks [43–46]. Furthermore, it is of current debate whether fast scrambling can be observed in systems with powerlaw interactions [47], which would enable the observation of (believed) features of quantum gravity in current laboratories. At the same time, powerlaw interactions can induce anomalous thermalization behavior [10,48,49], and a counterintuitive slow growth of entanglement [50–52].

In this thesis, we build upon these results and establish a more refined picture of quantum information dynamics, particularly in systems with powerlaw interactions. In Chap. 2, we cover the theoretical foundation, that is, we discuss important diagnostics such as entanglement growth and operator spreading, and present the current status of the field. Following this foundation, in Chap. 3, we exemplify the dynamics of quantum information on a paradigmatic model, i.e., the mixed-field Ising model. In particular, we reproduce known results from the literature and complement them to develop a thorough picture of quantum information dynamics in many-body systems with local interactions. Building up on this, in Chap. 4, we study how powerlaw interactions alter this picture. Crucially, we resolve the apparent discrepancy of slow entanglement growth and superballistic operator spreading by connecting these two processes, which grants us a unifying picture of quantum information dynamics in systems with powerlaw interactions. We further review this established connection in Chap. 5, where we consider a recent, experimental accessible proposal for a fast scrambler. Finally, in Chap. 6, we conclude our results, pose open questions, and talk about future directions.

Chapter 2.

Entanglement and Scrambling

"I would not call entanglement one but rather the characteristic trait of quantum mechanics, the one that enforces its entire departure from classical lines of thought."
— Erwin Schrödinger

This chapter provides an overview of the necessary concepts we use throughout this thesis to explore the dynamics of quantum information in quantum many-body systems. We consider systems that are defined on a spatial lattice Q, which has N lattice sites. Each lattice site i is associated with a local Hilbert space $\mathbb{H}_i$. The (normalized) state of the system is an element of the composite Hilbert space, $|\Psi\rangle \in \mathbb{H}$, where $\mathbb{H} = \bigotimes_{i\in Q} \mathbb{H}_i$. Time-evolution is generated by a Hamiltonian $\mathcal{H}$ that is independent of time, if not mentioned otherwise. Hence, the time-evolution operator is the matrix exponential of the Hamiltonian, $\mathcal{U}(t) = e^{-i\mathcal{H}t}$, and we set $\hbar = 1$. We will focus particularly on one-dimensional (1D), cubic lattices, where each lattice site is associated with a spin-1/2 degree of freedom, a *qubit*, with local Hilbert space $\mathbb{H}_i = \mathbb{C}^2$. The eigenstates of any Pauli operator span a complete orthonormal basis of $\mathbb{C}^2$. For example, the *computational basis* is given by $\{|0\rangle, |1\rangle\}$, where $\mathcal{Z}|0\rangle = -|0\rangle$, $\mathcal{Z}|1\rangle = |1\rangle$, and $\mathcal{Z}$ is the Pauli Z operator. The interactions among the qubits are of two-body nature, hence, the Hamiltonian consists of terms that act nontrivially on one, or two lattice sites, i.e.,

$$\mathcal{H} = \sum_{i<j\in Q} \mathcal{H}_{ij} \, .$$

The *operator space* associated with $\mathbb{H}_i$ is spanned by the Pauli operators, i.e., $\mathbb{O}_i = \text{span}\{\mathbf{1}, \mathcal{X}, \mathcal{Y}, \mathcal{Z}\}$, where $\mathbf{1}$ is the idenity. Hence, an operator $\mathcal{O}$ acting on the composite Hilbert space $\mathbb{H}$ is an element of the composite operator space, $\mathcal{O} \in \mathbb{O}$, where $\mathbb{O} = \bigotimes_{i \in Q} \mathbb{O}_i$. Throughout, we utilize different matrix norms for particular derivations and expressions. Given an operator $\mathcal{O}$ with singular values[1] λ_i, its *operator norm* is determined by the largest singular value, i.e.,

$$||\mathcal{O}|| = \max\{\lambda_i\} \ . \tag{2.1}$$

Furthermore, the *Frobenius norm* is given by

$$||\mathcal{O}||_{\mathrm{F}} = \sqrt{\mathrm{Tr}\{\mathcal{O}^\dagger \mathcal{O}\}} = \sqrt{\sum_i \lambda_i^2} \ . \tag{2.2}$$

The chapter is organized as follows. We cover the concept of entanglement in Sec. 2.1, where we discuss, in particular, its characteristic traits through the lens of quantum information. In Sec. 2.2 we address the propagation of quantum information, i.e., we discuss the emergence of effective limits on information propagation in quantum many-body systems. Finally, in Sec. 2.3, we introduce the concept of quantum information scrambling and discuss its connection to entanglement growth and information propagation.

2.1. Entanglement

Without a doubt, entanglement is one of the most puzzling aspects of quantum mechanics that led to intense debates among its founders. In the famous *EPR paradox* [1], Einstein, Podolsky, and Rosen argued that the existence of entangled particles is inconsistent with locality, a fundamental assumption of theoretical physics. In particular, they pointed out that the measurement of one particle would have an instantaneous effect on the measurement results of the second particle, independent of the distance between them. They inferred that quantum mechanics might be incomplete and proposed a theory of *local hidden variables* to restore locality. At that time, however, the physical relevance of entanglement was rather unclear and there was no known experimental procedure to test their proposal. Almost three decades later, John Stewart Bell proposed a set of inequalities [53] that any theory of local hidden variables must obey. In 1981, Alain

---

[1] The singular values λ_i of an operator $\mathcal{O}$ are given by the square roots of the eigenvalues of the hermitian operator $\mathcal{O}^\dagger \mathcal{O} = \sum_i \lambda_i^2 |i\rangle\langle i|$, where $\{|i\rangle\}$ spans a complete orthonormal basis of $\mathbb{H}$.

Aspect and his collaborators conducted experiments that demonstrated a significant violation of *Bell's inequalities* [54, 55], thereby putting the existence of local hidden variables in doubt. This first experimental evidence in favor of a nonlocal physical reality marked the beginning of a new era that brought forth an unseen level of control and understanding of the quantum realm. Due to these pioneering experiments, Alain Aspect was one of the Nobel laureates in Physics 2022, together with Anton Zeilinger and John Clauser.

In this section, we introduce the formal definition of entanglement in a mathematical sense, and discuss a simple thought experiment that underlines why entanglement is so special, and differs from any other correlation present in a physical system. Moreover, we discuss the information-theoretic interpretation of entanglement, introduce diagnostic probes of entanglement and other correlations that we use throughout this thesis.

2.1.1. Nonseparability and Nonlocality

Formally, entanglement is defined via the separability of a quantum state. Let us consider a bipartition of the Hilbert space $\mathbb{H} = \mathbb{H}_A \otimes \mathbb{H}_B$. A quantum state $|\Psi\rangle \in \mathbb{H}$ is *separable* with respect to this bipartition if and only if one can write it as a product state, $|\Psi\rangle = |\psi_A\rangle \otimes |\psi_B\rangle$, where $|\psi_A\rangle \in \mathbb{H}_A$ and $|\psi_B\rangle \in \mathbb{H}_B$. A quantum state is *entangled* if it is *nonseparable*, i.e., $|\Psi\rangle \neq |\psi_\mathrm{A}\rangle \otimes |\psi_\mathrm{B}\rangle$. In this work, we will predominantly choose spatial degrees of freedom to partition the Hilbert space $\mathbb{H}$. Correspondingly, nonseparabilty of the system's state implies entanglement between a set of neighboring lattice sites, i.e., a *region A* and its *environment B*, which is the rest of the system.

Let us try to understand this formal definition by a simple thought experiment. Consider two parties, Alice and Bob, that share a system of two qubits in the state

$$|\Psi\rangle = \frac{1}{\sqrt{2}}\left(|00\rangle + |11\rangle\right) , \tag{2.3}$$

where each of them has one qubit in their possession. Equation (2.3) is a nonseparable state. As one of the four *Bell pairs*[2], it is considered as a maximally entangled state of two qubits. Now, Alice and Bob measure their qubit and record the result. To obtain a proper statistics of their measurement outcomes, they repeat the measurement process many times with a new copy of the state. From Alice's (or Bob's) perspective, each measurement outcome occurs with equal probability for any given measurement basis.

---

[2] Due to historical reasons, these states are also called EPR pairs.

Thus, if Alice measures in the computational basis, she is going to find her qubit in the state $|0\rangle$ or $|1\rangle$ with a probability of $1/2$ respectively. The same holds for any other basis choice. Given Alice's (or Bob's) measurement outcomes, a single qubit therefore appears to be in any possible state with equal probability. However, if the two compare their records later on, they will notice something very odd. Every time they chose the same measurement basis, they obtained the same outcome, every single time. Apparently, there is a strong correlation between the respective measurement outcomes of Alice and Bob, which roots in the entanglement between the two qubits. What makes it so special is that after performing a measurement, Alice can predict Bob's measurement outcome with certainty if he chooses the same measurement basis. Therefore, Alice's basis choice affects the measurement statistics of Bob and vice versa. Crucially, this effect is instantaneous[3], independent of the distance between Alice and Bob, and thereby *nonlocal*. The nonlocal character of entanglement, famously known as *spooky action at a distance*, is a unique trait of quantum mechanics with no classical analog. The importance of understanding entanglement became at first evident in quantum information processing. In particular, novel protocols such as quantum teleportation [57, 58], or quantum key distribution [59, 60], utilize the entanglement of Bell pairs.

An important remark to the above example is that the state $|\Psi\rangle$ in Eq. (2.3) is a *pure state*. Hence, the system is completely isolated from its environment and in a definite state without any uncertainty. Therefore, Alice and Bob could in principle perform a two-qubit measurement and verify that the system is indeed in the state $|\Psi\rangle$. This is not true for a single qubit though. If Alice tries to reconstruct the state of her qubit with her records only, she would conclude that it is in the *maximally mixed state* concerning her local Hilbert space, i.e., $\rho_A = \frac{1}{2}\left(|0\rangle\langle 0| + |1\rangle\langle 1|\right)$. A mixed state generally describes a lack of information about the system, for instance, due to an imperfect preparation of the quantum state. In the above example, the lack of information about Alice's qubit stems from the entanglement with Bob's qubit. Apparently, there is information about Alice's qubit that she can not access just by local measurements on her qubit. This information is stored nonlocally and only accessible by a joint measurement on both qubits. Quantifying this lack of information corresponds to quantifying the amount of entanglement. In the following subsection, we discuss one of the most important quantifiers of entanglement in pure quantum states.

---

[3] Entanglement does not allow for communication faster than the speed of light since a classical communication channel is required to send information via a Bell pair [56].

2.1.2. The Entropy of Entanglement

In order to quantify entanglement in a pure quantum state, let us first establish that for any state $|\Psi\rangle$ and a bipartition $\{A, B\}$, there exists a decomposition such that

$$|\Psi\rangle = \sum_{i=1}^{d} \sqrt{p_i}\, |\psi_{A,i}\rangle |\psi_{B,i}\rangle \,, \tag{2.4}$$

where the states $\{|\psi_{A,i}\rangle\}$, $\{|\psi_{B,i}\rangle\}$ form an orthonormal basis of $\mathbb{H}_A$, $\mathbb{H}_B$ respectively, and $d = \min\{\dim \mathbb{H}_A, \dim \mathbb{H}_B\}$. Without loss of generality, let us assume $\dim \mathbb{H}_A \leq \dim \mathbb{H}_B$ from now on. Equation (2.4) is known as the *Schmidt decomposition* [3] with *Schmidt coefficients* p_i, where $p_i \geq 0$, and $\sum_{i=1}^{d} p_i = 1$. The state $|\Psi\rangle$ is entangled regarding the bipartition $\{A, B\}$ if and only if there is more than one nonzero Schmidt coefficient, and it is separable otherwise.

As discussed above, entanglement between a region A and its environment B manifests in a lack of information about A. This becomes more evident if we consider the *reduced state*[4] of A, i.e., ρ_A, which is obtained by the partial trace operation with respect to B. Accordingly, one finds

$$\begin{aligned} \rho_A &= \mathrm{Tr}_B \{|\Psi\rangle\langle\Psi|\} \\ &= \sum_{i,j=1}^{d} \sqrt{p_i p_j}\, |\psi_{A,i}\rangle\langle\psi_{A,j}|\, \mathrm{Tr}\{|\psi_{B,i}\rangle\langle\psi_{B,j}|\} \\ &= \sum_{i=1}^{d} p_i\, |\psi_{A,i}\rangle\langle\psi_{A,i}| \,. \end{aligned} \tag{2.5}$$

If, for example, $p_k = 1$, and $p_i = 0$, $\forall\, i \neq k$, it follows that $\rho_A = |\psi_{A,k}\rangle\langle\psi_{A,k}|$. Hence, if there is only one nonzero Schmidt coefficient, the reduced state of A is a projector onto the pure state $|\psi_{A,k}\rangle$. All information about the state of A is thereby contained in A and, in principle, accessible by measurements on A. In contrast, if there is more than one nonzero Schmidt coefficient, the reduced state (2.5) is a mixed state, which diagnoses a lack of information. The more mixed the reduced state ρ_A is, i.e., the closer the Schmidt coefficients p_i are to a uniform distribution, the higher the amount of entanglement.

---

[4] The reduced state of a subsystem $A \subset Q$ is an effective description of that subsystem in the sense that it leads to the correct measurement statistics. Hence, $\mathrm{Tr}\{\mathcal{O}_A\, \rho_A\} = \langle\Psi|\mathcal{O}_A|\Psi\rangle$ holds for all hermitian operators $\mathcal{O}_A$ that act trivially on B.

One can quantify this amount by the *entanglement entropy*, which is defined as the von Neumann entropy of the reduced state ρ_A

$$S_A\left(|\Psi\rangle\right) = -\operatorname{Tr}\left\{\rho_A \log \rho_A\right\} = -\sum_{i=1}^{d} p_i \log p_i \,. \tag{2.6}$$

Out of convenience, we will occasionally neglect the argument of $S_A\left(|\Psi\rangle\right)$ throughout this thesis. Nevertheless, it is usually clear from the context which quantum state $|\Psi\rangle$ we are discussing. The Schmidt decomposition (2.4) implies that ρ_A and ρ_B have the same spectrum and, therefore, $S_A = S_B$ holds for any bipartition of the Hilbert space. The entanglement entropy (2.6) vanishes if and only if ρ_A is a pure state. Moreover, it takes its maximum value if and only if ρ_A is the maximally mixed state regarding $\mathbb{H}_A$, i.e., $\rho_A \sim \mathbf{1}_A$. If not stated otherwise, we take the logarithm to base 2 throughout this thesis. For systems of qubits, $\dim \mathbb{H}_A = 2^{|A|}$, where $|A|$ is the volume of A, i.e., the number of lattice sites that belong to A. Thus, in summary we have

$$0 \leq S_A \leq |A| \,. \tag{2.7}$$

The entanglement entropy satisfies a number of mathematical properties necessary to be an *entanglement measure* in accordance with quantum information theory [2]. Furthermore, it is *subadditive* [61], that is

$$S_A + S_B \geq S_{AB} \tag{2.8}$$

holds for any state ρ_{AB} (pure or mixed) with reduced states ρ_A and ρ_B. An even stronger relation is the *strong subadditivity* [62]

$$S_{ABC} + S_B \leq S_{AB} + S_{BC} \,, \tag{2.9}$$

which holds for any state ρ_{ABC} with respective reduced states. The relations in Eq. (2.8) and Eq. (2.9) have important implications on correlations in a quantum system, as we will see later on.

The entanglement entropy (2.6) is typically difficult to access analytically, numerically and also experimentally. A generalization of the von Neumann entropy, i.e., the *Rényi entropy*, can be more practical in certain scenarios. As it will be of use later, let us introduce the *second Rényi entanglement entropy*, which is given by

$$S_A^{(2)}\left(|\Psi\rangle\right) = -\log\left(\mathrm{Tr}\left\{\rho_A^2\right\}\right) \,. \tag{2.10}$$

The second Rényi entanglement entropy (2.10) has many similarities with the entanglement entropy (2.6). For example, it vanishes if and only if the reduced state ρ_A is pure. Moreover, it attains its maximal value if and only if the reduced state ρ_A is maximally mixed. Thus, it is commonly used as an alternative diagnostic of entanglement in pure quantum states.

We want to emphasize that throughout this thesis, we mainly discuss *bipartite entanglement*, i.e., entanglement between two entities. Quantifying entanglement between several entities, i.e., *multipartite entanglement*, is considerably more complicated and a research topic on its own [2].

2.1.3. Quantum Mutual Information

The entanglement entropy quantifies the amount of entanglement between a region $A \subset Q$, and its environment $B = Q/A$, see Fig. 2.1 (a). For many occasions, however, it is of particular interest how two regions that do not form a bipartition of the whole system are correlated to each other, i.e., $A \cup B \subset Q$, where $A \cap B = \emptyset$. For example, two distant sites of the lattice, see Fig. 2.1 (b). With the aid of the entanglement entropy, one can define the *mutual information*

$$I_{A:B} = S_A + S_B - S_{AB} \,, \tag{2.11}$$

where $AB = A \cup B$. If $AB = Q$, it follows immediately that the mutual information (2.11) reduces to twice the entanglemmant entropy, $I_{A:B} = 2S_A$. In the general case, $AB \subset Q$, the mutual information measures the total correlation between the two regions [63], and thereby contains both, classical, and quantum correlations[5]. The subadditivity of entropy (2.8) implies that the mutual information is strictly nonnegative, $I_{A:B} \geq 0$, where the equality holds if and only if A and B are uncorrelated, i.e., $\rho_{AB} = \rho_A \otimes \rho_B$. Furthermore, it follows from the strong subadditivity (2.9) that mutual information does not increase under reduction, $I_{A:BC} \geq I_{A:B}$. This provides an intuitive interpretation of

---

[5] The mixed state $\rho_{AB} = \frac{1}{2}\left(|0\rangle\langle 0| \otimes |0\rangle\langle 0| + |1\rangle\langle 1| \otimes |1\rangle\langle 1|\right)$, for example, is not entangled, but $I_{A:B} = 1$ since it contains classical correlations.

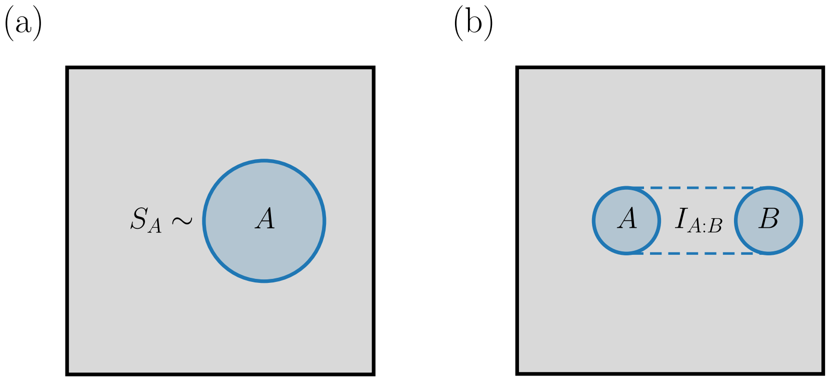

Figure 2.1.: Partitionings of the system Q and respective correlation measures. (a) The system is divided into two parts A and B, i.e., $A \cup B = Q$. The entanglement entropy (2.6) measures the amount of entanglement between the region A and its environment B. (b) The mutual information (2.11) measures the total correlation between two regions A and B, where $A \cup B \subset Q$.

strong subadditivity, that is, the correlation between two subsystem A and B can not decrease if we enlarge one of the subsystems.

Correlations between (local) regions are traditionally measured by connected correlation functions of the form $\langle \mathcal{O}_A \mathcal{O}_B \rangle_c = \langle \mathcal{O}_A \mathcal{O}_B \rangle - \langle \mathcal{O}_A \rangle \langle \mathcal{O}_B \rangle$, where $\langle \ldots \rangle = \langle \Psi | \ldots | \Psi \rangle$ is the expectation value in the state $|\Psi\rangle$. While these functions may depend on the choice of the operators $\mathcal{O}_A$ and $\mathcal{O}_B$, the mutual information (2.11) provides an observable-independent measure of correlation. As such, it serves as an upper bound for connected correlation fucntions [64], i.e.,

$$I_{A:B} \geq \frac{\langle \mathcal{O}_A \mathcal{O}_B \rangle_c^2}{2 \ln 2 \, ||\mathcal{O}_A||^2 \, ||\mathcal{O}_B||^2} \,, \tag{2.12}$$

where $\mathcal{O}_A$, $\mathcal{O}_B$ are operators that act on $\mathbb{H}_A$, $\mathbb{H}_B$ respectively, and $||\ldots||$ is the operator norm (2.1).

To capture correlations between more than two regions, let us consider the *tripartite mutual information* (TMI)

$$I_{A:B:C} = I_{A:B} + I_{A:C} - I_{A:BC} \,, \tag{2.13}$$

where A, B, and C are three disjoint regions of Q. If the the latter is in a pure state $|\Psi\rangle$, the TMI (2.13) is symmetric under permutations of A, B, C, and D, where D refers to the complement of ABC. In addition, $I_{A:B:C} = 0$, if the system's state is separable with respect to any partitioning of these regions, for example, $|\Psi\rangle = |\Psi_{AB}\rangle \otimes |\Psi_{CD}\rangle$.

The TMI probes how quantum information distributes among the three regions A, B, and C. In particular, unlike the mutual information (2.11), the TMI has no definite sign. If $I_{A:B:C} < 0$, quantum information is predominantly shared globally, as the total correlation between A and BC as a whole is larger than the total correlation between A and B, C individually. On the other hand, if $I_{A:B:C} > 0$, quantum information is rather shared among the individual regions.

Noteworthy, nonpositivity of the TMI, $I_{A:B:C} \leq 0$, implies *monogamy of mutual information*, i.e.,

$$I_{A:BC} \geq I_{A:B} + I_{A:C} \,. \tag{2.14}$$

Monogamy is an important concept in quantum information theory and a characteristic trait of entanglement [65, 66]. Accordingly, entanglement is not a shareable resource, implying that strong entanglement between A and B limits the amount of entanglement between A and C. This is typically formalized via inequalities of the form $E_{A:BC} \geq E_{A:B} + E_{A:C}$, where $E_{A:B}$ is some measure of entanglement between A and B. Since the mutual information (2.11) is a measure of total correlation, it is generally not monogamous. In a recent work [67], it was shown that quantum field theories with holographic duals obey the monogamy condition (2.14), which motivated the authors to argue that entanglement is the dominant correlation in these theories. Originally, the TMI (2.13) was introduced to characterize multipartite entanglement in ground states of topologically ordered, two-dimensional systems [68]. Recently, it was further studied in the context of nonequilibrium quantum many-body physics [69–73], and unitary quantum channels [74, 75]. As we shall see later, it will be helpful to characterize different regimes of quantum information dynamics in isolated quantum many-body systems.

2.2. Quantum Information Propagation

If a quantum many-body system is prepared in a nonstationary state in accordance with the quench protocol (1.1), correlations among its constituents will build up in the subsequent evolution. An intuitive thought in this regard is whether one can utilize the dynamics of a quantum system to process and transmit quantum information. Partially, this connects to understanding how quantum information propagates under unitary evolution. How fast can a signal propagate through a quantum many-body system? Are there any fundamental limits on this propagation, and if so, what determines them?

These questions are, of course, of great importance for future quantum technologies. Beyond, studying the propagation of quantum information in many-body systems has proven particularly helpful for understanding and classifying various dynamical regimes of quantum matter, as we will further discuss throughout this chapter.

In this section, we elaborate on why the unitary evolution of initially local operators sets fundamental bounds on the propagation of quantum information. In Sec. 2.2.1, we recall important results from the literature that establish a maximal velocity at which information can propagate in local quantum systems. How the presence of powerlaw interactions may alter this behavior is the subject of Sec. 2.2.2.

For a simple thought experiment[6], let us revisit Alice and Bob, who have partial access to a many-body system in an initial state $|\Psi_0\rangle$. Alice has access to a local region A and perturbs the initial state by applying a local unitary operator $\mathcal{W}_A$[7]. For example, she flips one qubit by applying a Pauli operator. Afterward, the system evolves for a time t. Bob controls a local region B, some distance away from Alice. He tries to figure out how she perturbed the system by applying a local measurement. After many repetitions of this protocol, the expectation value of Bobs observable $\mathcal{V}_B$ is given by

$$\begin{aligned}\langle \mathcal{V}_B \rangle &= \langle \Psi_0 | \mathcal{W}_A \, e^{i\mathcal{H}t} \, \mathcal{V}_B \, e^{-i\mathcal{H}t} \, \mathcal{W}_A | \Psi_0 \rangle \\ &= \langle \Psi(t) | \mathcal{W}_A(-t) \; \mathcal{V}_B \, \mathcal{W}_A(-t) \, | \Psi(t) \rangle \\ &= \langle \Psi(t) | \mathcal{V}_B | \Psi(t) \rangle + \langle \Psi(t) | \left[\mathcal{W}_A(-t) \, , \mathcal{V}_B \right] \mathcal{W}_A(-t) \, | \Psi(t) \rangle \, , \end{aligned} \tag{2.15}$$

where $\mathcal{W}_A(-t) = e^{-i\mathcal{H}t} \mathcal{W}_A e^{i\mathcal{H}t}$ is the Heisenberg picture of $\mathcal{W}_A$, and $|\Psi(t)\rangle = e^{-i\mathcal{H}t}|\Psi_0\rangle$. The last line in Eq. (2.15) provides us with a meaningful result. As long as the commutator $[\mathcal{W}_A(-t) \, , \mathcal{V}_B]$ vanishes, the expectation value of Bob's measurement is given by $\langle \Psi(t) | \mathcal{V}_B | \Psi(t) \rangle$, which is the unperturbed expectation value, and thus independent of $\mathcal{W}_A$. Therefore, the commutator determines whether or not Bob can (in principle) detect a signal of the perturbation that Alice applied.

---

[6] A similar thought experiment was presented in the recent tutorial of Xu and Swingle [76].

[7] For simplicity, we assume that the operator is also hermitian. This assumption is not necessary for the main argument, though.

We can further bound the second term in the last line of Eq. (2.15) by virtue of

$$
\begin{aligned}
&\left|\left\langle\Psi\left(t\right)\right|\left[\mathcal{W}_{A}\left(-t\right),\mathcal{V}_{B}\right]\mathcal{W}_{A}\left(-t\right)\left|\Psi\left(t\right)\right\rangle\right| \\
&\leq\sqrt{\left\langle\Psi\left(t\right)\right|\left[\mathcal{W}_{A}\left(-t\right),\mathcal{V}_{B}\right]\left[\mathcal{W}_{A}\left(-t\right),\mathcal{V}_{B}\right]^{\dagger}\left|\Psi\left(t\right)\right\rangle} \\
&\leq\left|\left|\left[\mathcal{W}_{A}\left(-t\right),\mathcal{V}_{B}\right]\right|\right| ,
\end{aligned}
\tag{2.16}
$$

where the Cauchy-Schwarz inequality yields the second line of Eq. (2.16), and the last line follows from the definition of the operator norm, see also Appendix B.1. Equation (2.16) bounds the *information front* of Alice's perturbation, i.e., no signal of her perturbation can arrive at Bob's region as long as the operator norm of the commutator vanishes. Noteworthy, this statement is independent of the initial state $|\Psi_0\rangle$, and it thereby establishes a general bound on the propagation of a local perturbation under unitary evolution.

The example above underlines that the possibility of Bob detecting a signal of Alice's perturbation at a given time t depends on the structure of $\mathcal{W}_A\left(-t\right)$. Hence, the dynamics of (local) operators under unitary evolution closely relates to the process of information propagation. Initially, the support of $\mathcal{W}_A$ is restricted to Alice's region. Therefore, it does not overlap with the support of $\mathcal{V}_B$, which implies $[\mathcal{W}_A, \mathcal{V}_B] = 0$. As time evolves, the support of $\mathcal{W}_A\left(-t\right)$ grows, i.e., the operator acts nontrivially on an increasing number of sites. This growth of a local operator is known as *operator spreading*, and will be discussed in more detail in Sec. 2.3.3. For now, it is sufficient to acknowledge that once the support of $\mathcal{W}_A\left(-t\right)$ has grown such that it fails to commute with $\mathcal{V}_B$, Bob can, in principle, detect a signal of Alice's perturbation. On the other hand, as we shall later see, it is not guaranteed that he can detect a signal if he applies only local measurements.

2.2.1. Locality and the Emergence of Causality

The discussion above underlines that the dynamics of local operators under unitary evolution sets bounds on information propagation in a quantum many-body system. But how fast can quantum information actually propagate? Of course, we expect that no information can travel faster than the speed of light. However, the postulates of quantum mechanics do not enforce relativistic causality. Therefore, it is natural to ask whether fundamental limits on information propagation exist in systems that do not incorporate relativistic causality by default. In fact, for local quantum lattice models, there exists an analogous to the speed of light. Locality, in this case, means that a single lattice site interacts only with its immediate surrounding, i.e., with its neighboring lattice sites. In one spatial dimension, a generic *local Hamiltonian* with open boundary conditions is given by

$$\mathcal{H} = \sum_{i=1}^{N-1} \mathcal{H}_{i,i+1} \,, \tag{2.17}$$

where $\mathcal{H}_{i,i+1}$ acts nontrivially on site i, and $i+1$. For Hamiltonians such as Eq. (2.17), the *Lieb-Robinson bound* [32] establishes an effective bound on the propagation of quantum information.

To formulate the bound, let us recall the previous example of Alice and Bob. In particular, Alice perturbs the system at site $i \in A$ by applying the unitary $\mathcal{W}_i$, and Bob measures the observable $\mathcal{V}_j$ at site $j \in B$. According to Eq. (2.16), the propagation of Alice's perturbation is bounded by $||[\mathcal{W}_i\,(t)\,, \mathcal{V}_j]||$. The Lieb-Robinson bound further restricts the operator norm of the commutator by

$$\frac{||[\mathcal{W}_i\,(t)\,, \mathcal{V}_j]||}{||\mathcal{W}_i||\;||\mathcal{V}_j||} \leq a\, e^{b\,(t-r/v_{\mathrm{LR}})} \,, \tag{2.18}$$

where $r = |i-j|$ is the distance between Alice and Bob, and a, b, and v_{LR} typically depend on details of the Hamiltonian. Equation (2.18) implies[8] that as long as $t \ll r/v_{\mathrm{LR}}$, the operator norm is bounded by an exponentially small number, and Bob has effectively no chance to detect a signal of Alice's initial perturbation. At $t \sim r/v_{\mathrm{LR}}$, the operator norm can become sizeable, and if so, Bob might be able to detect a signal of the perturbation. The Lieb-Robinson bound, therefore, establishes an effective *lightcone* that bounds the support of $\mathcal{W}_i\,(t)$, and thereby the propagation of quantum information. Accordingly, at time t, the support of $\mathcal{W}_i\,(t)$ can not be much larger than $2tv_{\mathrm{LR}}$, where v_{LR} is the *Lieb-Robinson velocity.* Thus, it follows that as long as the support of $\mathcal{V}_j$ does not overlap with the lightcone of $\mathcal{W}_i\,(t)$, the two operators will (in good approximation) commute, see Fig. 2.2 (a). It is important to emphasize that the Lieb-Robinson bound does not describe how fast information propagates but rather how fast it can propagate in principle. The Lieb-Robinson velocity v_{LR}, therefore, serves as an effective speed limit for information propagation in local quantum lattice models. Crucially, however, the bound ensures that information can not propagate *superballistically.* Thus, in local quantum lattice models,

---

[8] For the sake of brevity, we set $||\mathcal{W}_i|| = ||\mathcal{V}_j|| = 1$ here, which holds for any Pauli operator.

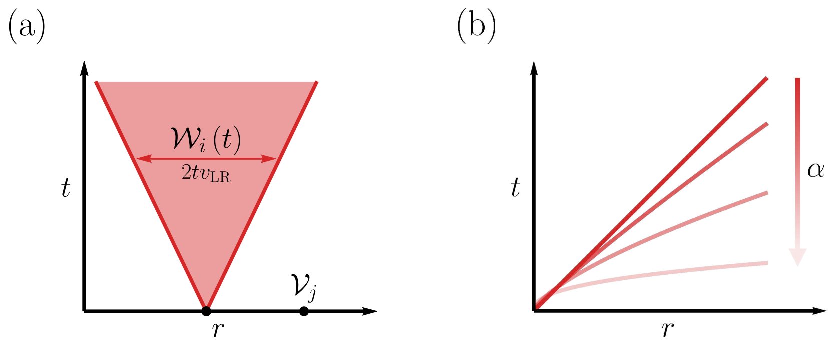

Figure 2.2.: Pictorial illustration of Lieb-Robinson bounds. (a) In local quantum lattice models, the propagation of quantum information is bounded by an effective lightcone. The latter is determined by the Lieb-Robinson velocity v_{LR}. Accordingly, information about a local perturbation $\mathcal{W}_i$ can at best propagate with v_{LR}. (b) Quantum lattice models that incorporate powerlaw interactions, i.e., $||\mathcal{H}_{ij}|| \sim 1/r_{ij}^{\alpha}$, can induce a nonlinear lightcone. With decreasing exponent α, and thereby a slower decay of the interaction strength with distance, the lightcone becomes increasingly nonlinear. A nonlinear lightcone implies the possibility of superballistic propagation of quantum information.

information propagates *ballistically* at best. That is, it takes information at least a time proportional to r to propagate a distance r or, put differently, $t_{\mathrm{I}} \gtrsim r$.

2.2.2. The Breakdown of Locality

The Lieb-Robinson bound (2.18) applies if the system's dynamics is governed by local Hamiltonian. Yet, as mentioned in the introductory part of this thesis, many experimental platforms for analog quantum simulation naturally embody nonlocal interactions. A Hamiltonian simulated on these platforms might, therefore, not comply with the local structure of Eq. (2.17), as a single site effectively interacts with many sites beyond its nearest neighbors. However, the interactions among the system's constituents usually incorporate a spatial structure. That is, the interaction strength between two sites i and j typically decays with the distance r_{ij} between them. For a number of experimental platforms, this decay is in good approximation algebraically, which results in an interaction strength that follows a powerlaw. Hence, considering the part of the Hamiltonian that describes the interaction between site i and j, i.e., $\mathcal{H}_{ij}$, this implies $||\mathcal{H}_{ij}|| \sim 1/r_{ij}^{\alpha}$, where the decay exponent $\alpha \geq 0$ determines the spatial decay of the interaction strength. In systems of trapped ions, for example, one typically encounters $\alpha \leq 3$ [9,10], while dipolar molecules are characterized by $\alpha = 3$ [39–41], and Rydberg atoms by $\alpha = 6$ [13,14].

Due to their immediate experimental relevance, it is particularly important to understand if and how powerlaw interactions alter the propagation of quantum information. As the Lieb-Robinson bound does, in general, not apply, one may ask whether similar bounds on information propagation still exist in this case. For potential applications in quantum information processing, it is of special interest if systems with powerlaw interactions allow for superballistic propagation of quantum information. The latter implies an effective *nonlinear lightcone* that bounds the information front. That is, the time it takes information to propagate a distance r is bounded by a nonlinear function of r, i.e., $t_{\mathrm{I}} \gtrsim f(r)$, where $f(r) \lesssim r$. Over the last two decades, many works aimed at generalizing the Lieb-Robinson bound for systems with powerlaw interactions [44, 77–82]. Moreover, seminal theoretical works on correlation dynamics [50, 83, 84] and related experiments with trapped ions [85, 86] indicated that systems with powerlaw interactions allow for superballistic propagation of quantum information, given the decay exponent α is sufficiently small.

Indeed, generalized Lieb-Robinson bounds for various regimes of the exponent α have been derived. Although a Hamiltonian with powerlaw interactions is not local in a strict sense, sufficiently large values of α can lead to entirely local dynamics. Accordingly, in D-dimensional quantum lattice models, a linear lightcone bounds the information front as long as $\alpha > 2D + 1$ [44]. In addition, for $\alpha > 2D$, it was shown recently that $t_{\mathrm{I}} \gtrsim r^{\gamma}$, where $\gamma = \min\{1, \alpha - 2D\}$ [82], yielding a polynomial lightcone for $2D < \alpha \leq 2D + 1$ and, therefore, the possibility for superballistic propagation of quantum information. For $D < \alpha \leq 2D$, the best known result is that the lightcone is at least logarithmic [77], i.e., $t_{\mathrm{I}} \gtrsim \log(r)$. In summary, we have the following generalized Lieb-Robinson bounds for systems with powerlaw interactions

$$t_{\mathrm{I}} \gtrsim \begin{cases} r \,, \; 2D + 1 < \alpha \leq \infty \\ r^{\gamma} \,, \; 2D < \alpha \leq 2D + 1 \\ \log(r) \;, \; D < \alpha \leq 2D \,. \end{cases} \tag{2.19}$$

Thus, with decreasing exponent α, the lightcone becomes increasingly nonlinear, which is pictorially illustrated in Fig. 2.2 (b). Let us stress once again that even in systems with powerlaw interactions, information may propagate significantly slower than allowed by the generalized Lieb-Robinson bounds (2.19), as the latter only establish limits on information propagation. Nevertheless, in a fine-tuned scenario, it is possible to saturate these bounds, as achieved by several protocols for quantum state transfer [43–46]. Hence, compared to their local counterparts, systems with powerlaw interactions can be advantageous in quantum information processing tasks.

2.3. Quantum Information Scrambling

From now on, lets us consider chaotic, nonintegrable systems, i.e., systems which we generally expect to thermalize [21]. In these systems, information does not seem to propagate very far at all, at least from a local perspective. To make this more explicit, we return to the previous thought experiment with Alice and Bob. Let us further specify that Alice's perturbation does not significantly increase the system's energy, which implies $\langle\Psi_0|\mathcal{H}|\Psi_0\rangle \approx \langle\Psi_0'|\mathcal{H}|\Psi_0'\rangle$, where $|\Psi_0'\rangle = \mathcal{W}_A|\Psi_0\rangle$. As discussed in the previous section, the information front of Alice's perturbation is bounded by an effective lightcone, $t_{\mathrm{I}} \gtrsim f(r)$, where $f(r)$ is a monotonically increasing function of r. The time at which Bob may detect a signal of Alice's perturbation will, therefore, scale with $f(r)$ at best and thereby grow with increasing distance r between them.

As discussed in the introductory part of this thesis, thermalization implies that expectation values of local observables depend solely on the energy of the initial state after the relaxation time t_{R}. Hence, following Eq. (1.4), for any local observable $\mathcal{V}_B$ that Bob measures, we have

$$\langle\Psi'(t)|\mathcal{V}_B|\Psi'(t)\rangle \simeq \frac{\mathrm{Tr}\left\{e^{-\beta\mathcal{H}}\mathcal{V}_B\right\}}{\mathrm{Tr}\left\{e^{-\beta\mathcal{H}}\right\}}, \text{ for } t > t_{\mathrm{R}}.$$

Since, by assumption, $|\Psi_0'\rangle$ has the same energy as $|\Psi_0\rangle$, Bob can not distinguish these two states with local measurements once his region is thermal. Thus, after the relaxation time, he can not reconstruct Alice's perturbation or even detect a signal of it. If the distance r is large enough, Bob's region is already thermal before the arrival of the information front, i.e., $t_{\mathrm{R}} < t_{\mathrm{I}}$. Thus, from a local perspective, the information about Alice's perturbation does not propagate very far, as it appears to get lost on the way.

However, since the evolution is unitary, the information about Alice's perturbation can not get lost, and it seems odd that it stops propagating through the system, so what happens? The mechanism behind this phenomenon is nowadays called quantum information scrambling. Typically, quantum information does not propagate in a localized form in nonintegrable systems but rather spreads over increasingly many nonlocal degrees of freedom and thereby becomes inaccessible to local measurements. This mechanism is responsible for the apparent loss of initial state information in systems that thermalize, and it prevents Bob from detecting a signal of Alice's perturbation.

This section aims to provide a solid understanding of quantum information scrambling. In that respect, we introduce the main diagnostic tools that allow us to probe this phenomenon in quantum many-body systems. Moreover, we recall important results from the literature and underline the relevance of these probes for classifying (nonequilibrium) quantum matter. In Sec. 2.3.1, we argue that information scrambling is fundamentally connected to the growth of entanglement. Furthermore, we discuss the typical behavior of entanglement growth in nonintegrable quantum many-body systems and its connection to thermalization. Section 2.3.2 is devoted to the generalized Hayden-Preskill protocol, which offers a simplified view on information scrambling. We return to the dynamics of local operators in Sec. 2.3.3, where we discuss the process of operator spreading in quantum many-body systems and its connection to information scrambling.

2.3.1. Entanglement Growth

In a quantum quench protocol (1.1), an initial product state $|\Psi_0\rangle$ will usually not remain a product state under unitary evolution but rather evolve into a complex superposition of product states. The reduced state $\rho_A(t) = \mathrm{Tr}_B\left\{|\Psi(t)\rangle\langle\Psi(t)|\right\}$, which is initially pure, becomes thus increasingly mixed as the system evolves in time. Accordingly, the region A becomes entangled with increasingly many degrees of freedom of its environment B, which manifests in the growth of entanglement over time. Following our arguments from Sec. 2.1, the growth of entanglement diagnoses how information, initially confined to A, 'leaks out'. That is, it flows into nonlocal degrees of freedom and thereby becomes inaccessible to measurements on A. Quantum information scrambling is, therefore, deeply connected to the growth of entanglement. The latter is quantified by the entanglement entropy (2.6), which generally exhibits a monotonic growth at early to intermediate times, following a saturation at late times. The particular saturation value of entanglement entropy and its temporal dependence before saturation are powerful diagnostics of nonequilibrium physics. Most importantly, the growth of entanglement lies at the heart of thermalization, which is essentially a strong form of quantum information scrambling.

Although thermalization is a dynamic phenomenon, it is constructive to discuss the structure of individual eigenstates in view of entanglement entropy. It is nowadays well established that ground states of quantum many-body systems are typically only weakly entangled. In particular, the ground state of a local Hamiltonian with a finite energy gap is expected to obey an *area law* [87–89], that is, the entanglement entropy (2.6) of a region A scales with the area of that region

$$S_A\left(|E_0\rangle\right) \sim |\partial A| \ . \tag{2.20}$$

In one spatial dimension, the area law (2.20) becomes particularly simple since the entanglement entropy remains constant as the volume of A is increased. Novel numerical techniques for 1D systems, such as matrix product states (MPS) [90], or the density-matrix renormalization group (DMRG) [91] owe their success to the area law, as their computational cost relates to the scaling of entanglement entropy. More precisely, these techniques approximate a quantum state by a set of matrices whose size is determined by the *bond dimension* χ. Such an approximation provides an accurate representation of the quantum state if the maximal entanglement entropy of the latter is not larger than $\log\left(\chi\right)$.

Highly excited eigenstates, on the other hand, obey a *volume law.* In particular, within the framework of ETH, the entanglement entropy is expected to coincide with the thermodynamic entropy at the same energy [92–94], that is,

$$S_A\left(|E_i\rangle\right) \simeq |A|\, s_\beta \,, \tag{2.21}$$

where $s_\beta = S\left(\rho_\beta\right)/N$ is the thermal entropy density, determined by the thermal ensemble ρ_β with effective inverse temperature β, i.e.,

$$\rho_\beta = \frac{e^{-\beta\mathcal{H}}}{\mathrm{Tr}\left\{e^{-\beta\mathcal{H}}\right\}} \ .$$

Similar to Eq. (1.3), the effective inverse temperature β is determined by the energy of the eigenstate $|E_i\rangle$. Equation (2.21) should be understood to hold at leading order in the system size. Eigenstates whose energy lies in the middle of the spectrum are associated with infinite effective temperature. In this case, the entanglement entropy is expected to attain a value associated with a random pure state drawn from the Haar measure, known as the *Page value* [95]. For systems of qubits, this value is given by

$$S_{\mathrm{Page}} = |A| - \frac{1}{2\ln 2} 2^{2|A|-N} \,, \tag{2.22}$$

where we assume $|A| \leq N/2$. Thus, in this extreme case, every region A that contains slightly less than half of the system's degrees of freedom is effectively maximally entangled with its environment, since the second term in Eq. (2.22) decays exponentially as $|A|$ becomes smaller.

The thermal nature of highly excited eigenstates then transfers to the nonequilibrium setting. Accordingly, in a quantum quench protocol (1.1) with a highly excited initial state $|\Psi_0\rangle$, the entanglement entropy is expected to saturate at the respective thermodynamic entropy at late times, i.e.,

$$S_A\left(|\Psi\left(t\rightarrow\infty\right)\rangle\right)\simeq|A|\,s_\beta\,, \tag{2.23}$$

where in this case, the effective thermal ensemble is determined by the energy of the initial state $|\Psi_0\rangle$, as described by Eq. (1.3). Equation (2.23) implies that the reduced state ρ_A approaches the respective thermal state. Once the former is sufficiently close to the latter, the entanglement entropy reaches its saturation value, and any detail about the initial state is (locally) lost. Furthermore, entanglement entropy follows a volume law at late times, which underlines the challenge of the numerical treatment of late-time dynamics. In particular, extensions of the above-mentioned numerical techniques to the nonequilibrium domain, for example, the time-dependent variational principle (TDVP) [96], or time-dependent DMRG [97], require a bond dimension that scales exponentially with the system size to capture the volume law. Nevertheless, these techniques are still among the most successful in simulating nonequilibrium quantum many-body physics at early to intermediate times.

The growth of entanglement entropy under unitary evolution is best understood for local quantum many-body systems, described by a Hamiltonian such as Eq. (2.17). These systems are generally associated with linear growth in time accompanied by a growth rate that follows an area law [35–38, 98]. A universal form is, hence, given by

$$S_A\left(|\Psi\left(t\right)\rangle\right)=|\partial A|\;v_{\mathrm{E}}\,t\,, \tag{2.24}$$

where $|\partial A|$ is the number of sites at the boundary of the respective region A, and v_{E} is the *entanglement velocity*, which may depend on the energy of the initial state and further details of the Hamiltonian. The linear temporal dependence in Eq. (2.24) implies that the time it takes for the entanglement entropy to saturate scales linearly with the volume $|A|$ of the considered region. Moreover, the area law growth rate originates from the local structure of the Hamiltonian. To be more explicit, let us divide the Hamiltonian into three parts,

$$\mathcal{H} = \mathcal{H}_A + \mathcal{H}_B + \mathcal{H}_{A:B} \,. \tag{2.25}$$

In Eq. (2.25), we denote $\mathcal{H}_A$ as the part of the Hamiltonian containing all operators that act only nontrivially on A. Similarly, $\mathcal{H}_B$ contains all operators that act only nontrivially on the environment B. Consequently, $\mathcal{H}_{A:B}$ contains all operators that connect A with its environment B, that is, all operators that act nontrivially on A and B. If this latter part vanishes, $\mathcal{H}_{A:B} = \mathbf{0}$, an initial product state will remain a product state under unitary evolution with respect to the bipartition $\{A, B\}$. Accordingly, $\mathcal{H}_{AB}$ is responsible for the growth of entanglement between A and B. For a local Hamiltonian, the support of $\mathcal{H}_{A:B}$ is confined close to the boundary of A, resulting in a growth rate proportional to $|\partial A|$. We can, thus, understand the universal behavior (2.24) as follows. Under unitary evolution, information about the region A flows through its boundary ∂A into nonlocal degrees of freedom at a constant velocity v_E, see Fig. 2.3 (a) for a pictorial illustration.

At this point, let us say a few words about the experimental accessibility of entanglement entropy, which is not an observable as it is a nonlinear function of the reduced state ρ_A and, therefore, not directly measurable. One approach to access entanglement entropy is full quantum state tomography [99, 100]. The latter involves a complete reconstruction of the quantum state, which scales poorly with the system size and is thus limited to systems of a few lattice sites. More efficient experimental techniques, directly tailored to probe entanglement entropy, have also been developed recently [17, 101–104]. On a trapped-ion quantum simulator, for example, entanglement growth was 'measured' for a system of $N = 20$ qubits [104]. Moreover, the linear entanglement growth expected for local systems (2.24) has been observed in a quantum simulation of the Bose-Hubbard Hamiltonian [17]. As hinted earlier, these advantageous experimental schemes usually consider the second Rényi entropy (2.10).

Although Eq. (2.24) provides an accurate description of entanglement growth for a broad range of nonequilibrium settings, dissent from this behavior generally diagnoses fundamentally different physics. For example, the presence of local disorder can induce a significant slowdown of entanglement growth and may even inhibit thermalization, given the disorder strength is sufficiently strong. This failure of thermalization due to local disorder is known as many-body localization (MBL), a novel phase of matter that currently enjoys broad attention [24]. At intermediate disorder strength, the system is still expected to thermalize, however, the presence of disorder will slow down the dynamics. In particular, the linear entanglement growth described by Eq. (2.24) will become sublinear at intermediate disorder strength, $S_A\left(|\Psi\left(t\right)\rangle\right) \sim t^{\gamma}$, where $\gamma < 1$ [105]. For sufficiently strong disorder strength, the system enters the MBL phase, which is characterized by a logarithmically slow entanglement growth, $S_A\left(|\Psi\left(t\right)\rangle\right) \sim \log\left(t\right)$ [106]. The transition to the MBL phase is thereby characterized by a fundamental change of entanglement growth. In this phase, entanglement entropy saturates at a value expected in the diagonal ensemble, i.e., $\rho_{\mathrm{D}} = \sum_i \left|c_i\right|^2 |E_i\rangle\langle E_i|$, where the coefficients c_i are the overlaps of the eigenstates $|E_i\rangle$ with the initial state, i.e., $|\Psi_0\rangle = \sum_i c_i|E_i\rangle$. Even though the diagonal ensemble implies that entanglement entropy follows a volume law, this ensemble retains a memory of the initial state. We want to emphasize that despite the extensive interest and effort put towards MBL, see Ref. [24] for a recent review, its general existence for arbitrarily large systems is still a matter of current debate.

After discussing important results for local quantum many-body systems, let us now elaborate on how powerlaw interactions alter the growth of entanglement. In this case, the support of $\mathcal{H}_{A:B}$ in Eq. (2.25) is generally not confined to the boundary of A, but reaches deep into the bulk of A and the environment B. We, therefore, expect a volume law contribution to the growth rate of entanglement entropy, i.e.[9], $\partial_t\, S_A\left(|\Psi\left(t\right)\rangle\right) \sim |A|$, see also Fig. 2.3 (b) for an illustration. Although the support of $\mathcal{H}_{A:B}$ may reach far beyond the boundary of A, and technically extends over the whole system, the weight of $\mathcal{H}_{A:B}$ is increasingly suppressed as we move away from the boundary since the interaction strength decays as $1/r^{\alpha}$. For sufficiently large α, we thus expect the area law contribution to dominate. Indeed, it was proven that the universal growth (2.24) survives in D-dimensional systems with powerlaw interactions as long as $\alpha > D + 1$ [107]. For smaller decay exponents, though, entanglement growth can change drastically.

Intuitively, one might expect that the presence of powerlaw interactions results in faster entanglement growth. Although this may be true at early times due to the volume-law contribution to the growth rate, several works discovered that powerlaw interactions generally induce a slowdown of entanglement growth [50–52, 108]. That is, in particular, a sublinear temporal dependence of entanglement entropy, $S_A\left(|\Psi\left(t\right)\rangle\right) \sim t^{\gamma}$, where $\gamma < 1$. The slowdown of entanglement growth becomes even more severe if the decay exponent α is smaller than the spatial dimension, $\alpha < D$. In this case, logarithmically slow growth of entanglement was found, $S_A\left(|\Psi\left(t\right)\rangle\right) \sim \log\left(t\right)$. Contrary to MBL, though, the system is still expected to thermalize [109]. The approach toward local thermal equilibrium,

---

[9] This notation should emphasize that there is a volume law contribution to the growth rate. However, the area law contribution may still be relevant, and the growth rate could further depend on time.

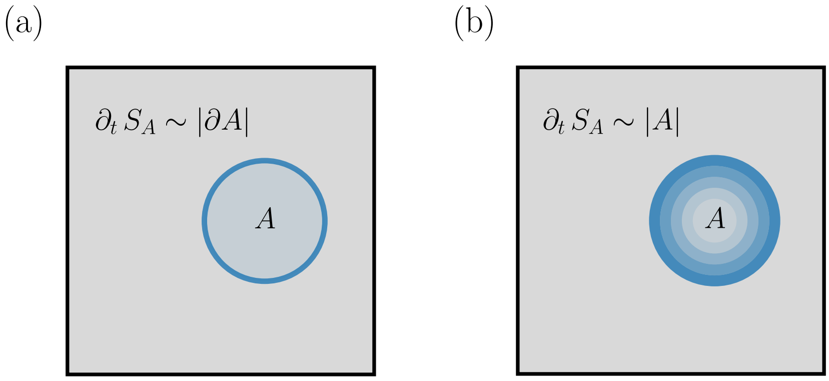

Figure 2.3.: Pictorial illustration of entanglement growth. (a) In local systems, the growth rate of the entanglement entropy is proportional to the area $|\partial A|$ of the considered region A. This can be understood by the fact that all terms of the Hamiltonian that act nontrivially on A and its environment B are located at the boundary of A. (b) In systems with powerlaw interactions $\sim 1/r^{\alpha}$, also terms that act nontrivially on the bulk of A contribute to the growth of entanglement, resulting in a volume law contribution to the growth rate.

however, may be considerably more complicated. For instance, powerlaw interactions can lead to *prethermalization* [21, 48, 49], i.e., the system first relaxes to an intermediate prethermal state before ultimately thermalizing. Such a prethermalization plateau was recently observed in an experiment with trapped ions [10]. Considering systems with local disorder, powerlaw interactions can prevent a transition to the MBL phase given the decay exponent α is sufficiently small [110–112].

In summary, power law interactions can significantly alter the dynamics of entanglement and, thus, the nonequilibrium physics of a quantum many-body system. Putting systems with disorder aside from now, what is particularly important for us, is the counterintuitive slowdown of entanglement growth for sufficiently small decay exponents α. Consequently, this will result in a slower approach toward local equilibrium, i.e., slower thermalization. Interestingly, this is accompanied by the possibility of superballistic propagation of quantum information, as discussed in Sec. 2.2. Later, in Sec. 2.3.3, we will revisit this issue. In the next section, we consider a simple protocol that underlines the connection between entanglement growth and information scrambling more explicitly.

2.3.2. The Generalized Hayden-Preskill Protocol

To make the rather abstract concept of information scrambling more tangible, let us discuss a simple but sufficient protocol, i.e., the generalized Hayden-Preskill protocol [76, 98].

Consider a system Q, which consists of N qubits, and its dynamics is governed by the Hamiltonian $\mathcal{H}$. Moreover, let us introduce an auxiliary qubit R, *the reference*, that is completely isolated and undergoes no dynamics. Initially, the reference is entangled with the first qubit of the system in form of a simple Bell pair (2.3). Hence, the composite initial state is given by

$$|\Psi_0\rangle = \frac{1}{\sqrt{2}} \left(|0_R\rangle |\psi_0\rangle + |1_R\rangle |\psi_1\rangle \right) , \tag{2.26}$$

where $|\psi_0\rangle$, and $|\psi_1\rangle$ denote the states of the system with the first qubit in the state $|0\rangle$, and $|1\rangle$ respectively, i.e.,

$$|\psi_0\rangle = |0\rangle|\psi\rangle \, , \quad |\psi_1\rangle = |1\rangle|\psi\rangle \, ,$$

and $|\psi\rangle$ is the initial state of the remaining $N-1$ qubits. The time-evolution of the initial state (2.26) is then given by

$$|\Psi\left(t\right)\rangle = \frac{1}{\sqrt{2}} \left(|0_R\rangle |\psi_0\left(t\right)\rangle + |1_R\rangle |\psi_1\left(t\right)\rangle \right) , \tag{2.27}$$

where $|\psi_0\left(t\right)\rangle = e^{-it\mathcal{H}}|\psi_0\rangle$, and $|\psi_1\left(t\right)\rangle$ is defined likewise. A pictorial illustration of this protocol is displayed in Fig. 2.4. From Eq. (2.27), it follows immediately that the reference stays maximally entangled with the system at all times, i.e., $S_R = 1 \, \forall \, t$. The initial entanglement is, therefore, never lost, which is not surprising since the evolution is unitary. However, due to information scrambling, we expect the initially localized entanglement between the reference and the system to become increasingly complex over time and to involve a growing number of qubits in the system. To quantify the process of information scrambling, one may ask the following question. How many degrees of freedom are sufficient to recover the initial entanglement with the reference at a given time t?

We can quantify the entanglement between the reference and a given region of the system via the mutual information (2.11). Note that $I_{R:Q} = 2$ holds at all times, emphasizing that the reference is always maximally entangled with the system. Furthermore, it is straightforward to show that $I_{R:A} + I_{R:\bar{A}} = 2$ always holds, where $A \cup \bar{A} = Q$. Thus, any region $A \subset Q$ that attains almost maximal mutual information is sufficient to recover the initial entanglement with the reference. Since the reference is initially only entangled with the first qubit, one finds $I_{R:A} = 2$ for $A = \{1\}$, diagnosing maximal entanglement with the reference and the first qubit of the system at $t = 0$. Therefore,

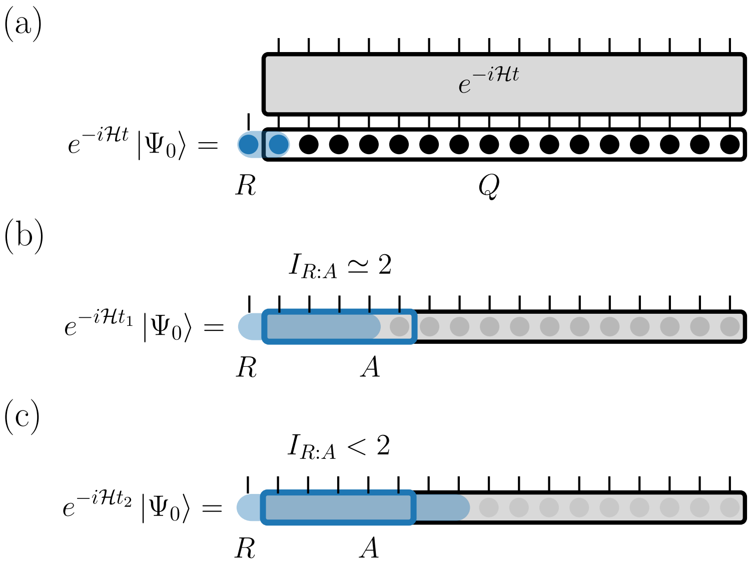
(a)
$e^{-i\mathcal{H}t}$
$e^{-i\mathcal{H}t}\,|\Psi_0\rangle =$
R
Q
(b)
$I_{R:A} \simeq 2$
$e^{-i\mathcal{H}t_1}\,|\Psi_0\rangle =$
R
A
(c)
$I_{R:A} < 2$
$e^{-i\mathcal{H}t_2}\,|\Psi_0\rangle =$
R
A

Figure 2.4.: A simple protocol for information scrambling. (a) An isolated reference qubit R is initially entangled with the first site of the system Q. Afterward, the system evolves in time, while the reference stays isolated. Under unitary evolution, the initially localized entanglement with the reference is spread over the nonlocal degrees of freedom of the system. Hence, an increasing number of sites is necessary to recover the entanglement with the reference. (b) Time-evolved state at time $t_1 > 0$. As long as the entanglement with the reference only involves sites in the region A, the entanglement is in principle recoverable if one has control over A, which reflects in an almost maximal value of the mutual information between R and A, i.e., $I_{R:A} \simeq 2$. (c) Time-evolved state at time $t_2 > t_1$. Once the entanglement with the reference involves sites that are not in A, the entanglement is not recoverable in A anymore, i.e., $I_{R:A} < 2$.

the mutual information between the reference and any other set of qubits that does not contain the first qubit will vanish at $t = 0$. Under unitary evolution, we can then track how fast the entanglement with the reference spreads over the system's degrees of freedom by calculating the mutual information between the reference and the first ℓ qubits, $A = \{1, 2, \ldots, \ell\}$. As long as the mutual information is close to its maximal value, i.e., $I_{R:A} \simeq 2$, it is possible to recover the entanglement with the reference as it is confined to the region A, see also Fig. 2.4 (b) and (c).

How large does the region A need to be at a given time such that it contains the entanglement with the reference? Or, in other words, how long does it take until the entanglement with the reference begins to leak out of A? Since the overall state (2.27) is pure, one finds

$$I_{R:A} = S_R + S_A - S_{RA} = 1 + S_A - S_{\bar{A}}\,,$$

where $\bar{A} = RA$ is the complement of A. If we consider a local Hamiltonian such as Eq. (2.17), entanglement will grow linear in time, with an area law growth rate, see Eq. (2.24). Hence, until S_A saturates, S_A and $S_{\bar{A}}$ will grow at the same rate, yielding $I_{R:A} = 2$. Once S_A begins to saturate, it follows that $S_A < S_{\bar{A}} - 1$ and, therefore, $I_{R:A} < 2$. Thus, for a local Hamiltonian, one can recover the entanglement with the reference in a region A as long as its entanglement entropy has not yet saturated. For a more sophisticated derivation of this statement, see Ref. [98].

This is an interesting result for several reasons. First, it underlines that entanglement growth fundamentally connects to the process of information scrambling. Second, the linear growth of entanglement entropy results in a linear growth of the region A, necessary to recover the entanglement with the reference. Hence, the *scrambling time* t_s is given by the saturation time of the entanglement entropy

$$t_s = \frac{|A|\, s_\beta - 1}{|\partial A|\; v_{\mathrm{E}}} \,. \tag{2.28}$$

Note that the additional term in Eq. (2.28) is due to the fact that $S_A = 1$ at $t = 0$, as A includes the first site of the system. Thus, the linear scaling of the scrambling time (2.28) with the size of A implies the ballistic propagation of the information front regarding the entanglement with the reference. If the Hamiltonian is not local, a straightforward generalization of these statements is not possible, as entanglement growth may not follow the universal behavior described by Eq. (2.24). However, entanglement growth still determines whether one can recover the entanglement with the reference. Generally, one can recover the entanglement in a given region A as long as $\partial_t \left(S_A - S_{\bar{A}}\right) \simeq 0$, which implies $I_{R:A} \simeq 2$. Thus, as long as S_A grows at the same rate as $S_{\bar{A}}$, the entanglement with the reference is recoverable in A. In the case of a local Hamiltonian, this agrees with the saturation time of S_A.

What we have not discussed so far is the possibility of a localized propagation of quantum information. In this case, Bob may not need access to the full region A, but only to a small region close to the boundary of A, to recover the initial entanglement with the reference. Quantum information scrambling implies that this is actually not possible. More explicitly, let us consider that at time t_1, we can recover the entanglement with the reference in the region A, i.e., $I_{R:A} = 2$. Let us further assume that the information front of the entanglement with the reference is close to the boundary of A, but still confined to a slightly smaller region $A_1 \subset A$. Hence, we have $I_{R:A} = I_{R:A_1} = 2$, and consequently $I_{R:A_2} = 0$, where A_2 is a small region at the boundary of A. Note that by construction,

$A_1 \cup A_2 = A$, where $|A_2| \ll |A_1|$. A bit later, at time $t_2 > t_1$, the information front arrives at A_2. If the initial entanglement with the reference propagates in a localized form, we expect the mutual information $I_{R:A_2}$ to grow significantly, once the information front arrives, which indicates a strong correlation between the small region A_2 and the reference R. However, before arrival of the information front at A_2, the entanglement with the reference is confined to A_1, implying $I_{R:A_2} = 0$ and, therefore, $S_{RA_2} = S_R + S_{A_2}$. Since A_2 is much smaller than A_1, and the arrival of the information front is determined by the saturation time of A_1, the entanglement entropy of A_2 is long saturated upon arrival of the information front. Monotonic growth of entanglement entropy, therefore, implies that $I_{R:A_2} = 0$ at all times, given A_2 is much smaller than A_1. Hence, only the region A can recover the entanglement with the reference and not a smaller region close to the information front, which underlines the phenomenon of information scrambling.

2.3.3. Operator Spreading

The generalized Hayden-Preskill protocol provides a simplified view of how initially local quantum information spreads over a growing number of degrees of freedom under unitary evolution. Crucially, it connects the growth of entanglement entropy to the number of degrees of freedom necessary to recover the initial entanglement with the reference at a given time. However, in the ordinary quantum quench protocol (1.1), the relationship between entanglement growth and the spread of quantum information over spatial degrees of freedom is less clear. As discussed in Sec. 2.3.1, the growth of entanglement entropy probes how quantum information about a given region A becomes inaccessible due to entanglement with its environment. However, it does not probe how many degrees of freedom from the environment are entangled with A, i.e., how many degrees of freedom are sufficient to recover the information about A.

The dynamics of local operators offers a complementary perspective on the process of information scrambling. As discussed in Sec. 2.2, the former determines how fast a local perturbation can propagate through a quantum many-body system. Quantum information scrambling then implies that this propagation is not localized, as already discussed above. Accordingly, as the perturbation propagates through the system, control over a growing number of degrees of freedom is necessary to reconstruct it. This process goes under the name of *operator spreading* and has received increased attention from several communities over the last few years [26].

Let us first motivate the notion of operator spreading more appropriately. Consider a local operator $\mathcal{W}$, supported on a single site, that evolves in time according to the Heisenberg picture

$$\mathcal{W}\left(t\right) = e^{i\mathcal{H}t}\,\mathcal{W}\,e^{-i\mathcal{H}t}\,. \tag{2.29}$$

We can rewrite Eq. (2.29) by virtue of the Baker–Campbell–Hausdorff formula [113],

$$\mathcal{W}\left(t\right) = \sum_{k=0}^{\infty} \frac{\left(it\right)^{k}}{k!} \left[\mathcal{H}, \mathcal{W}\right]_{k}\ , \tag{2.30}$$

where $\left[\mathcal{H}, \mathcal{W}\right]_{k}$ is the nested commutator, i.e., $\left[\mathcal{H}, \mathcal{W}\right]_{k} = \left[\mathcal{H}, \left[\mathcal{H}, \mathcal{W}\right]_{k-1}\right]$, and $\left[\mathcal{H}, \mathcal{W}\right]_{0} = \mathcal{W}$. For now, let us consider a local, 1D Hamiltonian[10] such as Eq. (2.17). The first nontrivial term in Eq. (2.30) is just the commutator between the Hamiltonian and the local operator, that is, $\left[\mathcal{H}, \mathcal{W}\right]$. The terms in the Hamiltonian that may not commute with $\mathcal{W}$ are the ones that act on the same site as $\mathcal{W}$. Accordingly, these are either single-site terms or terms that act on the neighboring sites of $\mathcal{W}$ as well. Commuting once with the Hamiltonian, therefore, can result in operators that act on three sites. Generally, the k-th term in Eq. (2.30) can result in operators that act on $2k+1$ sites [26]. An initially local operator, therefore, grows in size and complexity under unitary evolution, and may eventually extend over the entire system. As a result, information about this operator is spread over increasingly many degrees of freedom.

We can diagnose the spread of $\mathcal{W}\left(t\right)$ via the *squared commutator* with an auxiliary local operator $\mathcal{V}$ located at a distant site r

$$C_{r}\left(t\right) = \frac{1}{2}\left\langle \left[\mathcal{W}\left(t\right), \mathcal{V}_{r}\right]^{\dagger} \left[\mathcal{W}\left(t\right), \mathcal{V}_{r}\right] \right\rangle\ . \tag{2.31}$$

As long as the support of $\mathcal{W}\left(t\right)$ does not overlap with the support of $\mathcal{V}$, the squared commutator (2.31) vanishes as the two operators still commute, see Fig. 2.5 (a). Once $\mathcal{W}\left(t\right)$ has spread such that its support overlaps with that of $\mathcal{V}$, the squared commutator becomes sizeable, see Fig. 2.5 (b). By varying r, one can then track how the operator spreads over the system's degrees of freedom. If $\mathcal{W}$, and $\mathcal{V}$ are unitary, for instance, two

---

[10] We make this restriction for simplicity. The notion of operator spreading applies likewise to systems with nonlocal (few-body) interactions. In these systems, it also takes a finite time until the support of an initially local operator can attain a certain size. For systems with powerlaw interactions, this follows immediately from the generalized Lieb-Robinson bounds presented in Sec. 2.2.2. A generalization of operator spreading to higher dimensions is also straightforward.

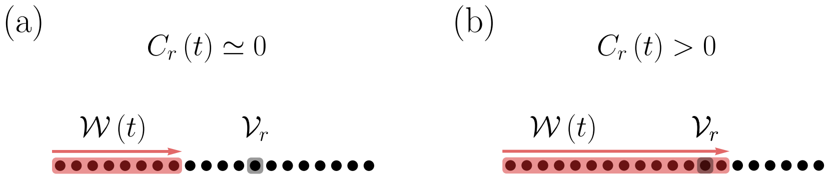

Figure 2.5.: Pictorial illustration of operator spreading. An initially local operator $\mathcal{W}$ grows in support under unitary evolution, determined by the Heisenberg picture, i.e., $\mathcal{W}(t) = e^{i\mathcal{H}t}\,\mathcal{W}\,e^{-i\mathcal{H}t}$. To probe the spread of $\mathcal{W}(t)$, we take an auxiliary local operator $\mathcal{V}$ located at a distant site r. (a) As long as the support of $\mathcal{W}(t)$ does not overlap with that of $\mathcal{V}$, the two operators commute and the squared commutator (2.31) vanishes. (b) Once the support of $\mathcal{W}(t)$ overlaps with that of $\mathcal{V}_r$, the two operators fail to commute, which is reflected by a sizeable value of the squared commutator.

Pauli operators, Eq. (2.31) reduces to

$$C_r(t) = 1 - \mathfrak{Re}\,\{F_r(t)\}\ , \tag{2.32}$$

where the nontrivial part in Eq. (2.32) is given by the *out-of-time-order correlator* (OTOC)

$$F_r(t) = \langle \mathcal{W}(t)\,\mathcal{V}_r\mathcal{W}(t)\,\mathcal{V}_r\rangle\ . \tag{2.33}$$

From here on, we place the operator $\mathcal{W}$ on the first site of the system, i.e., the leftmost site, if not mentioned otherwise. The expectation value in Eq. (2.31) is either taken with respect to a pure state $|\Psi\rangle$, or a thermal state $\rho_\beta \sim e^{-\beta\mathcal{H}}$. Throughout this thesis, we evaluate Eq. (2.31) in the same initial state $|\Psi_0\rangle$ that we consider for the quench protocol (1.1), probing how information about a local operator spreads in this particular scenario. In addition, we may consider a thermal state at infinite temperature, i.e., $\rho_\beta \sim \mathbf{1}_{\mathbb{H}}$. Hereinafter, if we refer to Eq. (2.31), the expectation value is evaluated in either of those two states. Evaluating the squared commutator at infinite temperature equals an average value for all possible product states in a given basis[11].

The squared commutator appeared already earlier in Eq. (2.16). Accordingly, it bounds the time at which Bob can, in principle, detect a signal of the perturbation that Alice applied to the initial state $|\Psi_0\rangle$. Furthermore, it follows from Eq. (2.16) that the squared commutator is bounded by the operator norm of the commutator, i.e.,

$$2\,C_r(t) \leq \left|\left|[\mathcal{W}(t)\,,\mathcal{V}_r]\right|\right|^2\ . \tag{2.34}$$

---

[11] Note that at infinite temperature $\rho_\beta = 2^{-N}\mathbf{1}_{\mathbb{H}}$ and, therefore, $\langle\mathcal{O}\rangle = 2^{-N}\,\mathrm{Tr}\,\{\mathcal{O}\}$. Moreover, $\mathrm{Tr}\,\{\mathcal{O}\} = \sum_i \langle\Psi_i|\mathcal{O}|\Psi_i\rangle$, where $\{|\Psi_i\rangle\}$ is a complete orthonormal basis of $\mathbb{H}$.

For a derivation of Eq. (2.34), see Appendix B.1. The factor 2 in Eq. (2.34) arises due to our definition of $C_r(t)$ in Eq. (2.31). The operator norm of the commutator, $||[\mathcal{W}(t), \mathcal{V}_r]||$, is the central object of the Lieb-Robinson bound (2.18) and its generalizations (2.19). While these bounds determine how fast information can maximally propagate, the squared commutator provides a more practical measure of information propagation. Most importantly, it allows us to probe information propagation in nonintegrable quantum many-body systems. In contrast, ordinary correlation functions, such as $\langle \mathcal{W}(t) \mathcal{V}_r \rangle$, are not suited for that, as they usually decay rapidly due to information scrambling [26].

The unconventional temporal structure in Eq. (2.31) renders the explicit determination of the squared commutator challenging both theoretically and experimentally. Nevertheless, on the experimental side, first measurement schemes have been carried out already. While one exploits randomized measurements [114, 115], others actually implement forward and backward time-evolution, necessary for the Heisenberg picture [116, 117]. Challenges that arise in a numerical treatment of operator spreading are discussed in Appendix A.3.

At large, probing operator spreading allows us to understand the propagation of quantum information in nonintegrable quantum many-body systems. Beyond, it has found applications in different areas of physics, for example, in the detection of (dynamical) quantum phase transitions [118], or quantum many-body scars [119]. The latter are specific highly excited eigenstates that do not obey the expected thermal structure discussed in Sec. 2.3.1. Consequently, an initial state that has a high overlap with these 'scarred' eigenstates may eventually fail to thermalize [25]. Our understanding of operator spreading in nonintegrable systems has further motivated new numerical techniques [120] that exploit effective constraints like the Lieb-Robinson bound (2.18). Moreover, operator spreading is considered crucial for the dynamics of black holes and theories of quantum gravity. In particular, the property of fast scrambling [30] has attracted much attention recently, also within the realm of quantum many-body physics [47, 121–123]. We discuss this subject extensively in Chap. 5.

Before we review the typical behavior of the squared commutator (2.31), let us further discuss operator dynamics in general, which received increased attention in the last years as an alternative, state-independent perspective on quantum many-body physics [31, 33, 34, 124–128]. Generally, we can expand any operator by means of a complete orthonormal operator basis, i.e.,

$$\mathcal{W}\left(t\right)=\sum_{\mathcal{S}}c_{\mathcal{S}}\left(t\right)\mathcal{S}\,, \tag{2.35}$$

where the *Pauli strings* $\mathcal{S}$ are constructed from tensor products of the local operator basis, i.e., $\mathcal{S}\in\mathbb{O}=\bigotimes_{i\in Q}\mathbb{O}_i$, where $\mathbb{O}_i=\operatorname{span}\left\{\mathbf{1},\mathcal{X},\mathcal{Y},\mathcal{Z}\right\}$, and we have $\operatorname{Tr}\left(\mathcal{S}\mathcal{S}'\right)/2^N=\delta_{\mathcal{S}\mathcal{S}'}$. Hence, the Pauli strings $\mathcal{S}$ are hermitian, and if $\mathcal{W}$ is hermitian too, the coefficients in Eq. (2.35) are real.

A useful diagnostic of operator dynamics based on the expansion (2.35) is given by the *operator density* [33, 124, 129]

$$p_\ell\left(t\right)=\sum_{|\mathcal{S}|=\ell}\left|c_{\mathcal{S}}\left(t\right)\right|^2\,, \tag{2.36}$$

where the sum runs over all Pauli strings $\mathcal{S}$ whose rightmost non-identity site is ℓ. If $\mathcal{W}$ is unitary, which is true for any local Pauli operator[12], we have $\sum_\ell p_\ell\left(t\right)=1\;\forall\;t$. Thus, Eq. (2.36) measures how much weight of the operator $\mathcal{W}\left(t\right)$ attributes to strings whose support ranges from the first to the ℓ-th site, i.e., strings of size ℓ. Let us, for example, consider a system of $N=3$ sites. In this case, the string $\mathcal{X}\otimes\mathbf{1}\otimes\mathcal{Z}$ has size $\ell=3$, $\mathbf{1}\otimes\mathcal{Y}\otimes\mathbf{1}$ has size $\ell=2$, and $\mathcal{Z}\otimes\mathbf{1}\otimes\mathbf{1}$ has size $\ell=1$, for example. Initially, the operator density is localized at the first site, i.e., $p_1\left(0\right)=1$ and $p_\ell\left(0\right)=0\;\forall\;\ell>1$. As time evolves, $\mathcal{W}\left(t\right)$ grows in size and complexity, which implies that the operator density flows toward increasingly larger ℓ. Thus, as a consequence of the spread of $\mathcal{W}\left(t\right)$, its *operator front*, i.e., $\max_\ell p_\ell\left(t\right)$, propagates through space. The squared commutator (2.31), therefore, probes the propagation of the operator front. For the sake of clearer expressions and derivations, we will occasionally neglect the time dependence of the operator density throughout this thesis.

Since it will be useful later on, let us further define the operator density on a region A that incorporates the initial position of $\mathcal{W}$, i.e.,

$$P_{\ell\leq|A|}\left(t\right)=\sum_{\ell\leq|A|}p_\ell\left(t\right)\,. \tag{2.37}$$

---

[12] The Pauli strings $\mathcal{S}$ also include the local Pauli operators. Generally, we have $\mathcal{S}=\mathcal{S}^\dagger$, and $\mathcal{S}^2=\mathbf{1}$.

In addition, we define the *operator size* as [126, 129, 130]

$$L\left[\mathcal{W}\left(t\right)\right]=\sum_{\ell}\ell\, p_{\ell}\left(t\right)\,. \tag{2.38}$$

Considering our discussion above, we generally expect the operator size (2.38) to grow monotonically and saturate at late times at some value close to N.

In certain instances, random unitary dynamics provides an effective description of quantum many-body dynamics at late times. Regarding the expansion in Eq. (2.35), this implies a uniform distribution of the coefficients $c_{\mathcal{S}}$ (excluding the identity) [131]. Therefore, the operator density p_ℓ is (on average) determined by the number of strings with size ℓ, i.e., $p_\ell = 3\cdot 4^{\ell-1}/\left(4^N-1\right)$, which grows exponentially with ℓ. Hence, under random unitary dynamics, most of the operator density attributes to the largest strings, i.e., strings of size N. For the operator size (2.38), random unitary dynamics results in the (average) operator size of a random unitary drawn from the Haar measure, i.e.,

$$L_{\mathrm{Haar}}=N\left(1+\frac{1}{4^N-1}\right)-\frac{1}{3}\approx N-\frac{1}{3}\,. \tag{2.39}$$

In the later chapters, we will show for a specific Hamiltonian that the operator dynamics at late times is, in certain cases, well described by random unitary dynamics.

More generally, the expectation for nonintegrable quantum many-body systems is that an initially local operator becomes as complex as possible, considering potential symmetries of the Hamiltonian. Thus, at late times, we also expect that most of the operator density attributes to the largest Pauli strings [31], although the detailed structure might differ from that expected by random unitary dynamics. The typical behavior of the squared commutator is then as follows. Before arrival of the operator front at site r, the squared commutator vanishes as $\mathcal{W}\left(t\right)$ has effectively no weight on site r, see Fig. 2.6 (a). The arrival of the operator front at site r manifests in a rapid growth of the squared commutator, following a saturation at some finite value, see Fig. 2.6 (b). The propagation of the operator front is then usually diagnosed by the time t_θ at which the squared commutator becomes sizeable, i.e., $C_r\left(t_\theta\right)=\theta$, where θ is some fraction of the expected saturation value. While the onset of the growth of $C_r\left(t\right)$ probes how fast the operator front propagates, a finite saturation value of the squared commutator indicates that information propagation is indeed not localized. That is, $\mathcal{V}_r$ fails to commute with $\mathcal{W}\left(t\right)$ although a long time passed since the operator front reached site r. If information propagation is localized, the squared commutator should decay after the arrival of the

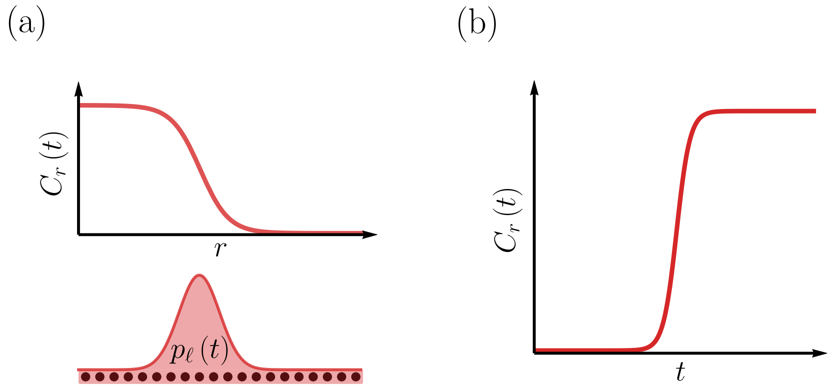

Figure 2.6.: Typical behavior of the squared commutator (2.31) and the operator density (2.36). The spread of the Heisenberg operator $\mathcal{W}(t)$ can be understood through the propagation of the operator front, i.e., $\max_\ell p_\ell(t)$. (a) At a fixed time t, the squared commutator vanishes for all sites r that have not been reached by the operator front. (b) Temporal evolution of the squared commutator for a fixed r, characterized by rapid growth upon arrival of the operator front and a subsequent saturation at a finite value.

operator front at site r, and vanish at late times, diagnosing that information about $\mathcal{W}(t)$ is localized at the operator front. We present further details on the relation between the operator density and the squared commutator in Appendix B.2.

A central goal of the recent effort toward operator dynamics is the characterization of universal behavior. For local systems, studies of random unitary circuits [33, 124, 125] established an effective hydrodynamic description of operator dynamics, characterized by a ballistic propagation of the operator front accompanied by a defusive broadening of the front. This hydrodynamic description is expected to hold for systems described by nonintegrable, local Hamiltonians [34]. Thus, in accordance with the Lieb-Robinson bound (2.18), a local operator typically spreads ballistically in time with a characteristic velocity v_B. The latter is known as the *butterfly velocity*, which owns its name to the relation between operator spreading and quantum chaos [132, 133]. The butterfly velocity v_B, therefore, establishes an effective lightcone that bounds the squared commutator (2.31). In particular, $C_r(t)$ vanishes for $t \ll r/v_\mathrm{B}$, increases rapidly at $t \sim r/v_\mathrm{B}$, and saturates afterwards. Note that Eq. (2.34) implies $v_\mathrm{B} \leq v_\mathrm{LR}$. While the Lieb-Robinson velocity serves as a maximum speed at which information can propagate, the butterfly velocity may as well depend on the state Eq. (2.31) is evaluated in, and the particular choice of the operators $\mathcal{W}$, and $\mathcal{V}$.

Beyond local systems, that is, for systems with powerlaw interactions, much less is known. Using an effective stochastic model, a recent work [127] aimed to generalize the hydrodynamic description of operator dynamics to systems with powerlaw interactions. Furthermore, several numerical studies investigated operator spreading in these systems [42, 134, 135]. Overall, these works observed that the squared commutator (2.31) is generally bounded by a nonlinear lightcone for sufficiently small decay exponents α, in agreement with the generalized Lieb-Robinson bounds (2.19). Thus, the superballistic spreading of quantum information seems to be a generic feature of nonintegrable quantum many-body systems that does not require a particularly fine-tuned setup. The quantitative shape of the lightcone as a function of the decay exponent α, however, is yet not fully resolved and is of particular interest for certain communities, as we discuss later in more detail.

In summary, although information propagates superballistically through space, the loss of initially local information due to the growth of entanglement slows down, as discussed in Sec. 2.3.1. This emphasizes that the process of information scrambling becomes considerably more diverse in systems with powerlaw interactions. At first sight, it appears to be that operator spreading and entanglement growth have opposite behavior in these systems. One of the main objectives of this thesis is to resolve this apparent discrepancy.

Chapter 3.

Dynamics of Quantum Information in the Mixed-Field Ising Model

"Imagination is more important than knowledge. For knowledge is limited, whereas imagination embraces the entire world, stimulating progress, giving birth to evolution."
— Albert Einstein

In this chapter, we want to deepen the previously introduced concepts and techniques by applying them to a specific quantum many-body system. In particular, we want to establish a solid understanding of quantum information dynamics in systems with local interactions, described by Hamiltonians such as Eq. (2.17). We reproduce known results from the literature for diagnostic probes of quantum information dynamics, such as the entanglement entropy, and the squared commutator. Moreover, we provide further insights into the relationship between these quantities. These results will serve as a baseline for the following chapters, where we explore how the presence of nonlocal interactions may alter the dynamics of quantum information.

The paradigmatic model we consider in this thesis is the mixed-field Ising (MFI) model in one spatial dimension, which has been the focus of many recent works on quantum information dynamics [38, 73, 74, 98, 136]. Its particular Hamiltonian reads

$$\mathcal{H} = -\sum_{\langle i,j\rangle \in Q} J \mathcal{Z}_i \mathcal{Z}_j - \sum_{i \in Q} h_x \mathcal{X}_i - \sum_{i \in Q} h_z \mathcal{Z}_i \,, \tag{3.1}$$

where the first sum indicates a summation over nearest-neighbors, N is the number of qubits (spins), and $\mathcal{X}_i, \mathcal{Z}_i$ are Pauli X, Z operators acting on the lattice site i. Throughout this thesis, we choose open boundary conditions in agreement with experimental conditions of quantum simulation platforms, which are capable of simulating one-dimensional systems of interacting qubits. The interaction strength among nearest neighbors is given by J, which we choose as our unit of energy. If both h_x, and h_z are finite, the Hamiltonian from Eq. (3.1) is generally nonintegrable. If either h_x, or h_z is zero, the Hamiltonian becomes integrable. In particular, one obtains the longitudinal-, or transverse-field Ising model, which are both exactly solvable by a Jordan-Wigner transformation [137]. We fix $h_x/J = -1.05$, and $h_z/J = 0.5$ throughout this thesis, if not explicitly mentioned otherwise. For these parameters, the Hamiltonian is considered to be far away from any integrable point [138].

An analytical treatment of nonintegrable quantum many-body systems far from equilibrium is highly nontrivial and, in many instances, just impossible. Therefore, we rely heavily on numerical simulations in this thesis. Even a numerical treatment of such a system, for example, the MFI Hamiltonian from Eq. (3.1), requires immense computational resources due to the exponential growth of the Hilbert space with the system size and is typically limited to the order of ten lattice sites. We deploy several complementary numerical techniques with the following abbreviations that we use throughout. Exact diagonalization (ED), a numerically exact method to obtain the action of the time-evolution operator on an initial state (EXPM) [139], and a matrix product state technique based on the time-dependent variational principle (TDVP) [96]. In Appendix A, we present further details on our numerical approaches.

3.1. The Generalized Hayden-Preskill Protocol II

At first, we want to revisit the generalized Hayden-Preskill protocol from Sec. 2.3.2 and demonstrate the ballistic spreading of quantum information, given the MFI Hamiltonian from Eq. (3.1). Furthermore, we show that for this particular Hamiltonian, random unitary dynamics is well suited to describe the late-time dynamics of the systems, if the latter is initialized in a highly excited state with zero energy expectation value. Consequently, at late times, it is practically impossible to recover the initial entanglement with the reference in any region that includes slightly less than half of the system's degrees of freedom.

As an initial state of the system, we choose a fully polarized state along the y-direction. More precisely, $|\psi_0\rangle = |Y+\rangle$, where $|Y+\rangle = \bigotimes_{i\in Q} |y+\rangle$, and $|y+\rangle$ is the eigenstate of the Pauli Y operator with positive eigenvalue, $\mathcal{Y}\,|y+\rangle = |y+\rangle$. The state $|\psi_0\rangle$ has zero energy expectation value regarding the MFI Hamiltonian (3.1), i.e., $\langle\psi_0|\mathcal{H}|\psi_0\rangle = 0$. Thus, we expect that, under unitary evolution, the entanglement entropy of any region saturates at the Page value (2.22) at late times. The latter implies that the entanglement with the reference is maximally scrambled over the system's degrees of freedom, as we shall see in the following. Since the reference forms a Bell-pair with the first qubit of the system, see Eq. (2.26), the state $|\psi_1\rangle$ follows by applying a spin-flip to the first site of the system with respect to the y-basis, i.e., $|\psi_1\rangle = -\mathcal{Z}_1|\psi_0\rangle$.

We simulate the generalized Hayden-Preskill protocol numerically using EXPM for a system of $N = 24$ lattice sites. In Fig. 3.1(a), we display the temporal evolution of the mutual information $I_{R:A}\,(t)$ between the reference R and the first ℓ qubits of the system, i.e., $A = \{1, \ldots, \ell\}$. The parallel lines with equidistant separation for different ℓ confirm the ballistic spreading of quantum information. Thus, the size of the region that is sufficient to recover the initial entanglement with the reference grows linearly in time, which results in a scrambling time t_s proportional to the size of A, as described by Eq. (2.28). Apparently, not all curves in Fig. 3.1(a) approach zero at late times, which we want to elaborate on further in the following. If we assume that random unitary dynamics offers a suitable approximation of the late-time dynamics, we may replace the time-evolution operator in Eq. (2.27) with a random unitary operator drawn from the Haar measure. In this case, the mutual information between the reference R and the region A at late times is (on average) given by

$$I_{R:A}\,(t \to \infty) = 1 + \ell_{\text{eff}} - \overline{\ell}_{\text{eff}} + \frac{1}{2^{N+2}\ln 2}\left(2^{2\overline{\ell}_{\text{eff}}} - 2^{2\ell_{\text{eff}}}\right)\,, \tag{3.2}$$

where $\ell_{\text{eff}} = \min\{\ell, N+1-\ell\}$, and $\overline{\ell}_{\text{eff}} = \min\{\ell+1, N-\ell\}$. Due to simplicity, let us in the following assume that N is even. If A contains half of the system's degrees of freedom, i.e., $\ell = N/2$, it follows that $\ell_{\text{eff}} = \overline{\ell}_{\text{eff}}$, and the mutual information attains half of its maximal value, $I_{R:A} = 1$. If A contains less than half of the system's degrees of freedom, $\ell < N/2$, we have $\ell_{\text{eff}} - \overline{\ell}_{\text{eff}} = -1$, and the mutual information is, therefore, determined by the last term in Eq. (3.2). The latter decays exponentially with decreasing ℓ. Hence, if A contains just slightly less than half of the system's degrees of freedom, the mutual information is close to zero, $I_{R:A} \approx 0$. On the other hand, if $\ell > N/2$, we have $\ell_{\text{eff}} - \overline{\ell}_{\text{eff}} = 1$, and the last term, which is now negative, decays exponentially with increasing ℓ. Thus, if A contains slightly more than half of the system's degrees of freedom, the mutual information is close to its maximal value, $I_{R:A} \approx 2$.

In summary, under random unitary dynamics, access to half of the system plus a few additional lattice sites is sufficient to reconstruct the initial entanglement with the reference. On the other hand, any region that contains slightly less than half of the system's degrees of freedom has almost zero correlation with the reference and is thereby insufficient to reconstruct the initial entanglement with the reference. The sharp transition around $\ell \sim N/2$ is due to the purity of the system's initial state. One may also carry out the present protocol with an initial state of the system that is mixed. In this case, the number of degrees of freedom necessary to recover the initial entanglement with the reference becomes larger. For a maximally mixed initial state of the system, it follows that any region containing slightly less than the total number of degrees of freedom of the system is insufficient to recover the initial entanglement with the reference [29, 76].

Thus, random unitary dynamics maximally scrambles the entanglement with the reference over the system's degrees of freedom. In Fig. 3.1(b), we compare the analytical result (3.2) with the late-time dynamics of the MFI Hamiltonian (3.1). In particular, we display the late-time value of the mutual information as a function of ℓ/N. The numerical data nicely agrees with the analytical result for random unitary dynamics, underlining that the latter offers an effective description of the late-time dynamics if the system is initialized in a highly excited state.

The generalized Hayden-Preskill protocol offers a simple framework to understand how initially local quantum information spreads over the system's degrees of freedom and thereby becomes inaccessible to local probes. Regarding the MFI Hamiltonian (3.1), we utilized this protocol to demonstrate the ballistic spreading of quantum information under unitary evolution, as it is expected for a Hamiltonian that incorporates only local interactions. However, in the more realistic quantum quench protocol, introduced in Eq. (1.1), there is no such thing as a reference, and understanding how initially local quantum information spreads and scrambles over the system's degrees of freedom becomes more complicated. In the following section, we build up on the current results for the MFI Hamiltonian and investigate diagnostic probes of quantum information dynamics, such as entanglement growth and operator spreading.

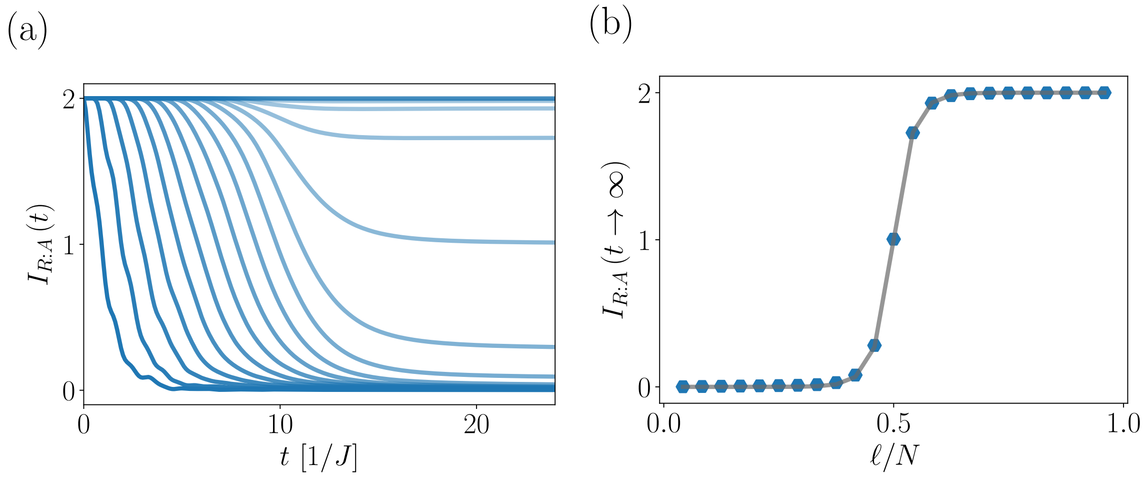

Figure 3.1.: Quantum information scrambling in the generalized Hayden-Preskill protocol. (a) Temporal evolution of the mutual information $I_{R:A}(t)$ between the reference R and the first ℓ qubits of the system, $A = \{1, 2, \dots, \ell\}$, for various ℓ. Data is extracted from a numerical simulation (EXPM) of the MFI Hamiltonian (3.1) for $N = 24$ lattice sites. The initial state (2.26) is constructed from $|\psi_0\rangle = |Y+\rangle$, and $|\psi_1\rangle = -\mathcal{Z}_1|\psi_0\rangle$. (b) Late-time value of $I_{R:A}(t)$ as a function of ℓ/N. Markers represent numerical data, the solid gray line is the analytical result from Eq. (3.2), which assumes random unitary dynamics.

3.2. Measures of Quantum Information Dynamics

Let us first discuss entanglement growth regarding the MFI Hamiltonian described by Eq. (3.1). Accordingly, we consider the quantum quench protocol introduced in Eq. (1.1) for various highly excited initial states $|\Psi_0\rangle$, whose energy expectation value lies in the middle of the energy spectrum. In addition to the state $|Y+\rangle$, which we considered already in the previous section as the initial state of the system, we consider a Néel state in y-direction. The latter is characterized by an alternating local magnetization of the lattice sites, that is, $|Y_{\text{Néel}}\rangle = |y+, y-, y+, \dots\rangle$. Similar to $|Y+\rangle$, also $|Y_{\text{Néel}}\rangle$ as zero energy expectation value. Thus, although these two initial states are orthogonal and remain so under unitary evolution, they will become locally indistinguishable due to thermalization, as discussed in the introductory part of this thesis. Furthermore, we consider initial states where every qubit has the same orientation on the Bloch sphere, i.e.,

$$|\Psi_{\theta,\phi}\rangle = \bigotimes_{i\in Q}\left(\cos\left(\frac{\theta}{2}\right)|1\rangle + e^{i\phi}\sin\left(\frac{\theta}{2}\right)|0\rangle\right) . \tag{3.3}$$

Note that for $\theta = \phi = \frac{\pi}{2}$, we recover the fully polaraized state along the y-direction, i.e., $|\Psi_{\frac{\pi}{2},\frac{\pi}{2}}\rangle = |Y+\rangle$. By slightly rotating away from $|Y+\rangle$, we obtain an initial state with finite energy expectation value that remains in the middle of the spectrum.

In Fig. 3.2 (a), we display the temporal evolution of the half-chain entanglement entropy (2.6) following from a quantum quench with different initial states. One can nicely observe that all considered initial states induce a linear growth of entanglement entropy, in agreement with the universal behavior described by Eq. (2.24). While for initial states with zero energy expectation value, the entanglement entropy saturates at the Page value (2.22) (dashed line), states with a finite energy expectation value exhibit a slightly smaller saturation value, see also the inset in Fig. 3.2 (a). This smaller saturation value is due to a lower effective temperature associated with the initial state. Figure 3.2 (b) shows the temporal evolution of the entanglement entropy following from a quench with initial state $|Y+\rangle$ for various regions A, where the latter is given by the first ℓ qubits of the system, i.e., $A = \{1, \ldots, \ell\}$. The growth rate of the entanglement entropy evidently follows an area law, in agreement with Eq. (2.24). Accordingly, since the system is 1D, all considered regions exhibit the same growth rate until saturation. Moreover, the data confirms that the saturation value of the entanglement entropy follows a volume law, congruent with Eq. (2.23). It is worth noting that the other initial states show the same features.

Hence, for the considered highly excited initial states, entanglement growth exhibits the universal behavior described by Eq. (2.24). The latter implies that the entanglement entropy of a local region saturates at a time proportional to the volume of that region, which suggests that the process of information scrambling is linear. However, at first sight, the growth of entanglement entropy does not tell us how quantum information spreads over spatial degrees of freedom. The same holds for the mutual information (2.11), and due to the bound (2.12), also for ordinary connected correlation functions. As discussed in Sec. 2.3, we may probe how quantum information spreads over spatial degrees of freedom by considering the process of operator spreading, which we do in the following for the MFI Hamiltonian (3.1).

In Fig. 3.3 (a), we display numerical data for the squared commutator (2.31), where we vary the respective operators $\mathcal{W}, \mathcal{V}$, and also the initial state we evaluate the expectation value in. In all cases, we place the operator $\mathcal{W}$ at the left edge of the system, i.e., at the first site, and the operator $\mathcal{V}$ in the middle of the system at site $r = 12$. All curves show qualitatively similar behavior, which agrees with the general picture of operator spreading in local systems, as discussed in Sec. 2.3.3. While the rapid growth upon

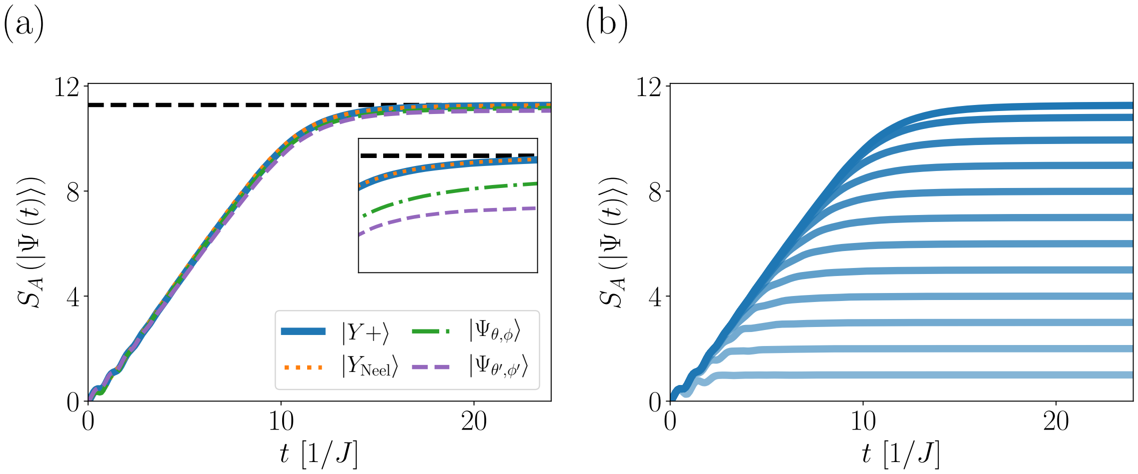

Figure 3.2.: Temporal evolution of entanglement entropy (2.6) following from a quench with a highly excited initial state $|\Psi_0\rangle$. Data is extracted from a numerical simulation (EXPM) of the MFI Hamiltonian (3.1) for $N = 24$ lattice sites. (a) Half-chain entanglement entropy for various initial states. The states $|Y+\rangle$, $|Y_{\text{Néel}}\rangle$, and $|\Psi_{\theta,\phi}\rangle$ are defined in the main text, and we choose $\{\theta, \phi\} = \left\{\frac{7\pi}{16}, \frac{\pi}{2}\right\}$, and $\{\theta', \phi'\} = \left\{\frac{\pi}{2}, \frac{7\pi}{16}\right\}$. The dashed black line indicates the Page value from Eq. (2.22). (b) Entanglement entropy of the first $\ell \leq N/2$ sites following from a quench with initial state $|Y+\rangle$.

arrival of the operator front seems to be universal, one can spot quantitative differences between the curves once the squared commutator approaches its saturation value. Note that these differences originate predominantly from the different choices for $\mathcal{W}$, and $\mathcal{V}$. Differences due to the choice of the initial state are less pronounced, which further supports that states with an energy expectation value that lies in the middle of the spectrum are characterized by generic dynamics. Figure 3.3 (b) shows the spatiotemporal profile of the squared commutator for the initial state $|Y+\rangle$, and $\mathcal{W}, \mathcal{V} = \mathcal{Y}$. The clearly visible linear lightcone of $C_r(t)$ confirms that $\mathcal{W}(t)$ spreads ballistically under unitary evolution. Note that other choices of the operators $\mathcal{W}, \mathcal{V}$, and the initial state will lead to a similar spatiotemporal profile of $C_r(t)$, which follows from the similar behavior shown in Fig. 3.3 (a). Thus, the characteristic velocity of operator spreading, i.e., the butterfly velocity v_{B} is (approximately) universal for the shown cases.

With the following chapters in mind, let us also discuss operator dynamics more generally by analyzing the operator density (2.36) and the operator size (2.38), which are both quantities of the respective operator and therefore independent of any initial state. In Fig. 3.4 (a), we display the operator density regarding the Pauli operator $\mathcal{W} = \mathcal{Y}$, which is initially located at the first site of the system. As time evolves, one can nicely observe the propagation of the operator front. Hence, $\mathcal{W}(t)$ grows in size and complexity as most of the operator density attributes to Pauli strings of increasingly larger size. Moreover, we observe a broadening of the operator front, in agreement with recent works on random unitary circuits [33, 34, 124]. The ballistic operator spreading is further demonstrated in Fig. 3.4 (b), where we display the operator size (2.38) for the three Pauli operators respectively. In all cases, the operator size exhibits a similar linear growth and saturates at a value close to the system size, indicating that the support of the operator extends over the entire system at late times. For $\mathcal{W} = \mathcal{Y}$, the operator size appears to approach the value expected under random unitary dynamics, i.e., L_{Haar} from Eq. (2.39), which is indicated by the dashed line. However, for $\mathcal{W} = \mathcal{X}, \mathcal{Z}$, the saturation value is slightly smaller than L_{Haar}, which we attribute to the nonvanishing overlap between these operators and the Hamiltonian [31].

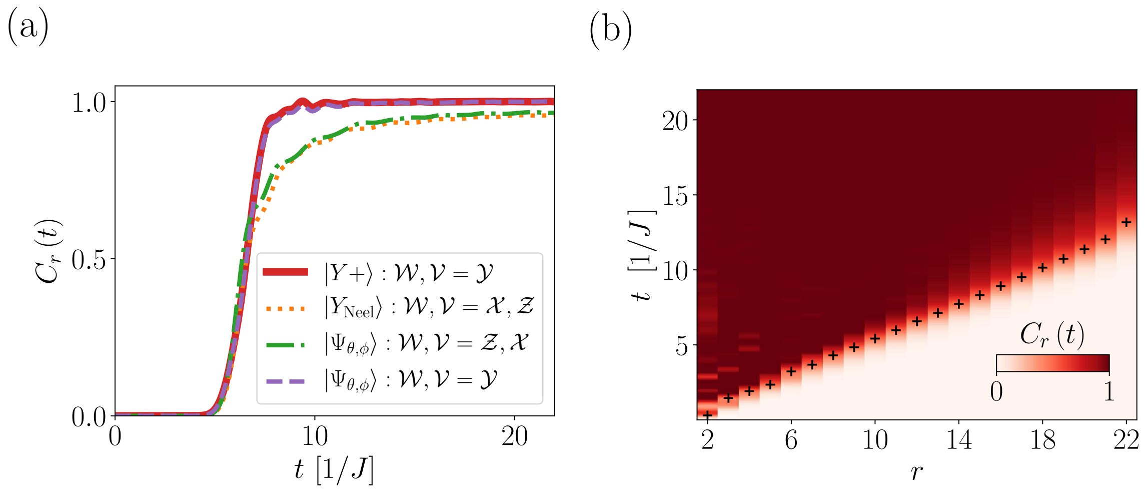

Figure 3.3.: Temporal evolution of the squared commutator (2.31). Data is extracted from a numerical simulation (EXPM) of MFI Hamiltonian (3.1) for $N = 22$ lattice sites. (a) Squared commutator $C_r(t)$ for different choices of $\mathcal{W}$, and $\mathcal{V}$, evaluated in various initial states. The operator $\mathcal{W}$ is located at the first site of the system, and we fix $r = 12$. For the state $|\Psi_{\theta,\phi}\rangle$, we chose the same angles as in Fig. 3.2. The specific choices of the operators $\mathcal{W}$, and $\mathcal{V}$ for each initial state are listed in the legend. (b) Spatio-temporal profile of the squared commutator $C_r(t)$ evaluated in the initial state $|Y+\rangle$, where we choose $\mathcal{W}$, $\mathcal{V} = \mathcal{Y}$. Black markers correspond to the spacetime contour determined by $C_r(t) = 1/2$.

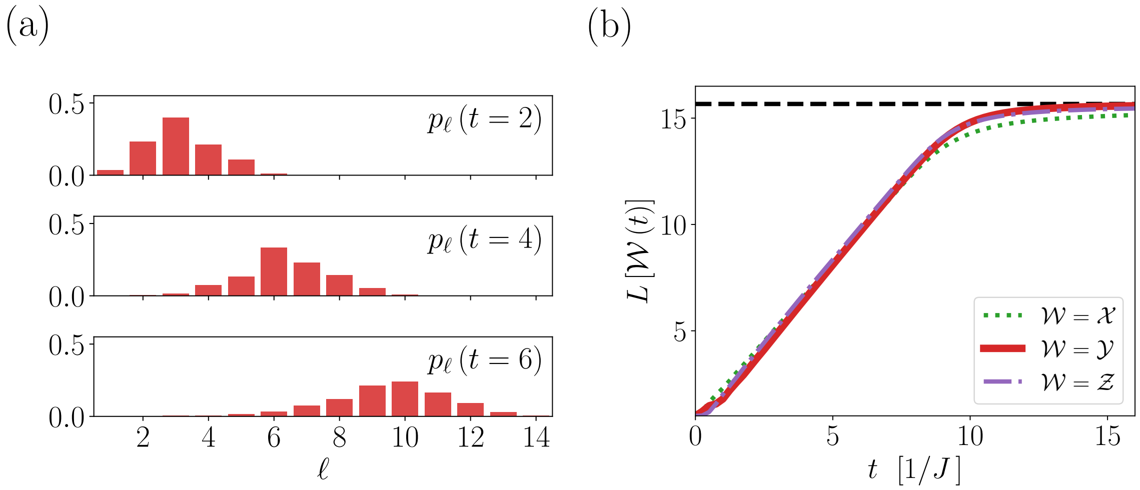

Figure 3.4.: Operator dynamics: (a) Temporal evolution of the operator density (2.36) for $\mathcal{W}=\mathcal{Y}$, initially located at the first site of the system with $N = 14$ lattice sites. (b) Temporal evolution of the operator size (2.38) for $\mathcal{W}=\mathcal{X},\mathcal{Y},\mathcal{Z}$ respectively. The black dashed line indicates the operator size under random unitary dynamics, i.e., L_{Haar} from Eq. (2.39). Data is extracted from a numerical simulation (ED) of the MFI Hamiltonian (3.1).

3.3. The Operator State

The analysis of entanglement growth and operator spreading yields us a consistent picture of quantum information dynamics in local quantum many-body systems like the MFI model (3.1). However, at first glance, it is not evident how these two processes are related. As one of the objectives of this thesis is to understand the interplay between these two processes, we establish a connection between them in the following.

To proceed, let us, for the last time, return to the laboratory of Alice and Bob. They just got a powerful quantum simulator that Bob wants to benchmark. Although he does not know how the simulator works in detail, it enables him to act with the unitary $\mathcal{U}(t) = e^{-i\mathcal{H}t}$ on an arbitrary product state $|\Psi_0\rangle = \bigotimes_{i\in Q} |\psi_i\rangle$ for any time t and Hamiltonian $\mathcal{H}$ he desires. To verify the functionality of the simulator, Bob evolves the system up to a time t, flips the sign of the Hamiltonian, and evolves the system back in time. If the simulator works properly, Bob will recover the initial state $|\Psi_0\rangle$ after this procedure, which he tries to verify with local measurements at site r, located in his part of the laboratory. What Bob does not know is that Alice wants to sabotage his benchmark due to some argument they had earlier. In particular, she applies a local (hermitian) unitary $\mathcal{W}$ between forward and backward time evolution at the leftmost site on her part of the laboratory. Thus, the final state of the system is given by

$$|\Phi(t)\rangle = e^{i\mathcal{H}t}\mathcal{W}e^{-i\mathcal{H}t}|\Psi_0\rangle = \mathcal{W}(t)|\Psi_0\rangle\,. \tag{3.4}$$

This scenario is reminiscent of the one from Sec. 2.2. In a similar vein, Bob can not notice Alice's sabotage as long as the support of $\mathcal{W}(t)$ does not overlap with the site r Bob applies measurements to. Moreover, if we assume that Bob's local measurement $\mathcal{V}_r$ is chosen such that $\mathcal{V}_r|\Psi_0\rangle = |\Psi_0\rangle$, it follows that

$$\langle\mathcal{V}_r\rangle = \langle\Phi(t)|\mathcal{V}_r|\Phi(t)\rangle = \langle\Psi_0|\mathcal{W}(t)\,\mathcal{V}_r\mathcal{W}(t)\,\mathcal{V}_r|\Psi_0\rangle = F_r(t)\ , \tag{3.5}$$

which is the OTOC from Eq. (2.33), evaluated in the initial state $|\Psi_0\rangle$. Note that Eq. (3.5) follows only if $\mathcal{V}_r|\Psi_0\rangle = |\Psi_0\rangle$ holds [1].

The setup from above allows us to establish a connection between entanglement growth and operator spreading. In particular, it is constructive to analyze the entanglement growth that follows from the dynamics of $\mathcal{W}(t)$, as described by the state $|\Phi(t)\rangle$ defined in Eq. (3.4). For a region A that incorporates the initial position of Alice's perturbation, we expect the entanglement entropy of that region to vanish as long as the support of $\mathcal{W}(t)$ is confined A. To make this more explicit, let us recall the operator expansion from Eq. (2.35), and the definition of the operator density (2.36). Accordingly, we can decompose $\mathcal{W}(t)$ such that

$$\mathcal{W}(t) = \mathcal{W}_{\ell\leq|A|} + \mathcal{W}_{\ell>|A|}\,, \tag{3.6}$$

where

$$\mathcal{W}_{\ell\leq|A|} = \sum_{|\mathcal{S}|\leq|A|} c_{\mathcal{S}}\mathcal{S}\,,\ \text{and}\ \mathcal{W}_{\ell>|A|} = \sum_{|\mathcal{S}|>|A|} c_{\mathcal{S}}\mathcal{S}\,.$$

Note that the two parts $\mathcal{W}_{\ell\leq|A|}$, and $\mathcal{W}_{\ell>|A|}$ depend on time, as the coefficients $c_{\mathcal{S}}$ are time-dependent, however, out of convenience, we neglect this dependence in the following. The decomposition in Eq. (3.6) helps us to identify which part of the operator may create entanglement between Bob's side of the laboratory B and its complement A, i.e., Alice's side of the laboratory. While $\mathcal{W}_{\ell\leq|A|}$ acts only nontrivially on A, and trivially on B,

---

[1] Such an observable is, for example, given by $\mathcal{V}_r = |\psi_r\rangle\langle\psi_r| - |\psi'_r\rangle\langle\psi'_r|$, where the set $\{|\psi_r\rangle, |\psi'_r\rangle\}$ spans a complete orthonormal basis of $\mathbb{H}_r$.

$\mathcal{W}_{\ell>|A|}$ acts nontrivially on A as well as on B. Moreover, the unitarity of $\mathcal{W}\left(t\right)$ implies

$$\begin{aligned}1 &= 2^{-N}\,\mathrm{Tr}\left\{\mathcal{W}\left(t\right)\mathcal{W}\left(t\right)\right\}\\ &= 2^{-N}\,\mathrm{Tr}\left\{\mathcal{W}_{\ell\leq|A|}\mathcal{W}_{\ell\leq|A|}\right\} + 2^{-N}\,\mathrm{Tr}\left\{\mathcal{W}_{\ell>|A|}\mathcal{W}_{\ell>|A|}\right\}\\ &= P_{\ell\leq|A|} + P_{\ell>|A|}\,,\end{aligned}$$

where $P_{\ell\leq|A|}$ is the operator density on A, i.e., the weight on all Pauli strings that act only nontrivially on A, which are all strings of size $\ell \leq |A|$, as defined in Eq. (2.37). Consequently, $P_{\ell>|A|} = \sum_{\ell>|A|} p_\ell$ it the total weight of $\mathcal{W}\left(t\right)$ on Pauli strings that act nontrivially on the region B, i.e., all strings of size $\ell > |A|$.

If the support of $\mathcal{W}\left(t\right)$ does not extend beyond A at a given time t, we have $P_{\ell\leq|A|} = 1$, and $\mathcal{W}\left(t\right) = \mathcal{W}_{\ell\leq|A|}$. The reduced state of A is then given by

$$\begin{aligned}\rho_A &= \mathrm{Tr}_B\left\{\mathcal{W}_{\ell\leq|A|}\Psi_0\mathcal{W}_{\ell\leq|A|}\right\}\\ &= \mathcal{W}_{\ell\leq|A|}\Psi_{0,A}\mathcal{W}_{\ell\leq|A|} \otimes \mathrm{Tr}_B\left\{\Psi_{0,B}\right\}\\ &= \mathcal{W}_{\ell\leq|A|}\Psi_{0,A}\mathcal{W}_{\ell\leq|A|}\,,\end{aligned}$$

where we introduced $\Psi_0 = |\Psi_0\rangle\langle\Psi_0|$, and $|\Psi_0\rangle = |\Psi_{0,A}\rangle \otimes |\Psi_{0,B}\rangle$. Since $P_{\ell\leq|A|} = 1$ by assumption, the reduced state ρ_A is a pure state. Thus, as long as the support of $\mathcal{W}\left(t\right)$ is confined to the region A, the perturbation $\mathcal{W}$ could not create entanglement between A and B, implying $S_A\left(|\Phi\left(t\right)\rangle\right) = 0$. Put differently, the entanglement entropy has to vanish as long as all information of the operator $\mathcal{W}\left(t\right)$ is confined to the region A, see Fig. 3.5 (a) for a pictorial illustration. This is somewhat a trivial result, nevertheless, it underlines that a finite entanglement entropy $S_A\left(|\Phi\left(t\right)\rangle\right)$ diagnoses that the support of $\mathcal{W}\left(t\right)$ extends beyond A. Therefore, it allows us to probe the growing support of $\mathcal{W}\left(t\right)$, similar to the squared commutator. Furthermore, the entanglement entropy $S_A\left(|\Phi\left(t\right)\rangle\right)$ provides additional details on the structure of $\mathcal{W}\left(t\right)$ that will also help us in the following chapters, where we analyze the influence of nonlocal interactions on the dynamics of quantum information.

Once the support of $\mathcal{W}\left(t\right)$ extends beyond the region A, entanglement between A and B may build up. In analogy to the previous argument, we expect a finite entanglement entropy as not all information about $\mathcal{W}\left(t\right)$ is confined to A. In this case, we have

$P_{\ell\leq|A|} < 1$, and $P_{\ell>|A|} > 0$. In particular, the reduced state of A is now given by

$$\rho_A = P_{\ell\leq|A|}\,\Omega_{\ell\leq|A|} + P_{\ell>|A|}\,\Omega_{\ell>|A|}, \tag{3.7}$$

where $\Omega_{\ell\leq|A|} = |\Omega_{\ell\leq|A|}\rangle\langle\Omega_{\ell\leq|A|}|$, with the (normalized) pure state

$$|\Omega_{\ell\leq|A|}\rangle = \left(P_{\ell\leq|A|}\right)^{-\frac{1}{2}} \mathcal{W}_{\ell\leq|A|}|\Psi_{0,A}\rangle\,.$$

Since ρ_A, and $\Omega_{\ell\leq|A|}$ are both density operators, it follows that $\Omega_{\ell>|A|}$ is a density operator as well. Generally, it is given by

$$\Omega_{\ell>|A|} = \frac{1}{P_{\ell>|A|}}\,\mathrm{Tr}_B\left\{\mathcal{W}_{\ell>|A|}\Psi_0\mathcal{W}_{\ell>|A|} + \mathcal{W}_{\ell>|A|}\Psi_0\mathcal{W}_{\ell\leq|A|} + \mathcal{W}_{\ell\leq|A|}\Psi_0\mathcal{W}_{\ell>|A|}\right\}\,.$$

Using Eq. (3.7), and the concavity of the von Neumann entropy, we obtain

$$P_{\ell>|A|}\,S\left(\Omega_{\ell>|A|}\right) \leq S_A\left(|\Phi\left(t\right)\rangle\right) \leq P_{\ell>|A|}\,S\left(\Omega_{\ell>|A|}\right) + H\left(P_{\ell>|A|}\right)\,, \tag{3.8}$$

where $S\left(\Omega_{\ell>|A|}\right)$ is the von Neumann entropy of $\Omega_{\ell>|A|}$, and $H(x) = -x\log(x) - (1-x)\log(1-x)$ is the binary entropy. If $\Omega_{\ell>|A|}$ is a mixed state, it follows from Eq. (3.8) that a finite operator density outside of A, $P_{\ell>|A|} > 0$, implies a finite entanglement entropy, $S_A\left(|\Phi\left(t\right)\rangle\right) > 0$. Although it is not *a priori* clear whether $\Omega_{\ell>|A|}$ is pure or mixed, it will most likely be a mixed state. Hence, the entanglement entropy of A is in direct correspondance to the operator density of $\mathcal{W}\left(t\right)$ outside of A, see Fig. 3.5 (b) for an illustration.

Let us complement these analytical arguments with numerical results. In Fig. 3.5 (c), we compare the entanglement entropy $S_A\left(|\Phi\left(t\right)\rangle\right)$ of the left half A with the squared commutator $C_r\left(t\right)$, where r is chosen as either the leftmost or the rightmost site of the right half B, see Fig. 3.5 (b) for an illustration of this setup. The system is initialized in the previously considered state $|Y+\rangle$, and we choose $\mathcal{W}, \mathcal{V} = \mathcal{Y}$. We observe that the growth of entanglement entropy agrees with the spatiotemporal profile of the squared commutator. That is, the entropy of the left block A begins to grow, once the squared commutator diagnoses that the support of $\mathcal{W}\left(t\right)$ overlaps with the right block B. Shortly after the support has reached the rightmost site of B, entanglement entropy saturates in line with the squared commutator. This result shows that most of the operator density is close to the operator front, which should not be confused with localized information propagation. Noteworthy, the growth of entanglement entropy that follows from the

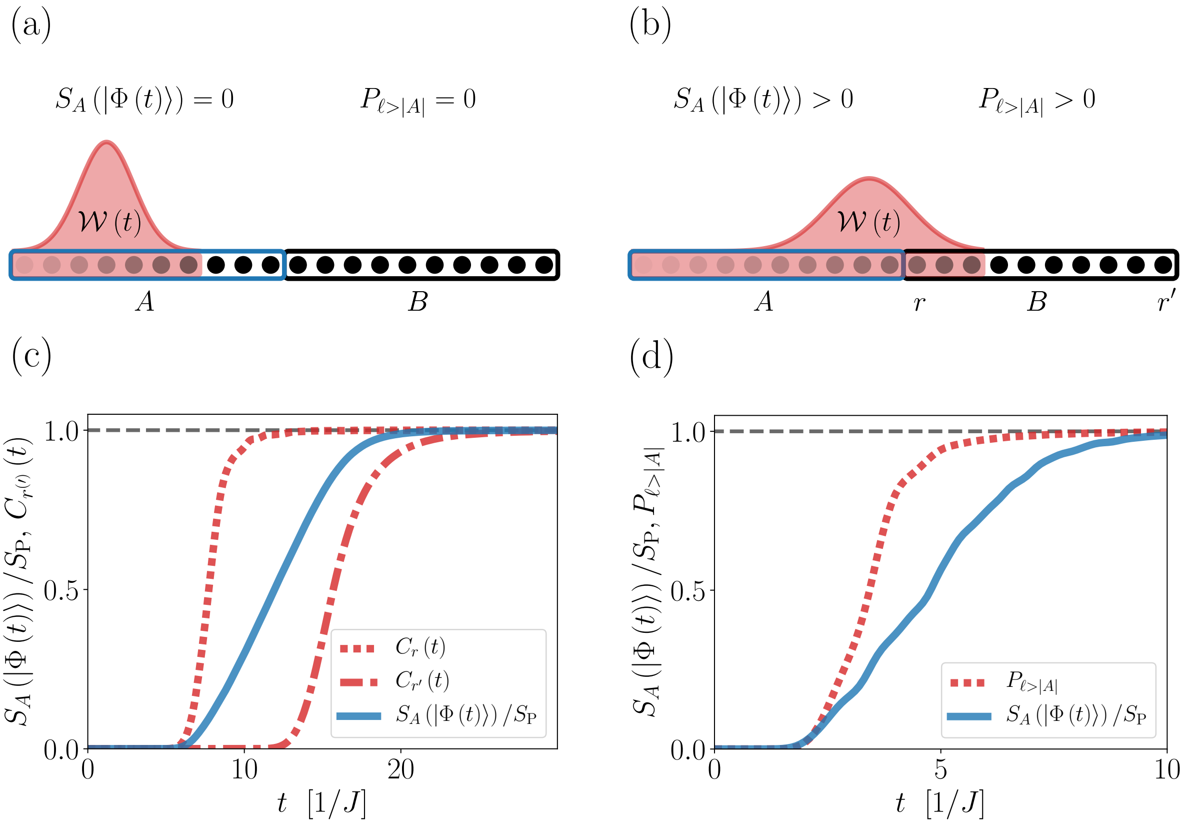

Figure 3.5.: Entanglement growth following the spread of a local operator as described by the operator state (3.4). (a) As long as the support of $\mathcal{W}(t)$ is confined to the region A, its entropy will vanish since the operator density outside of A vanishes. (b) As soon as the support of $\mathcal{W}(t)$ exceeds A, we expect a finite entanglement entropy as the operator density outside of A becomes sizeable. (c) Entanglement entropy $S_A(|\Phi(t)\rangle\rangle)$ (normalized by the Page value S_{P}), where A is the left half of the system, compared to the squared commutator (2.31), where $\mathcal{W}$ is initially located at the leftmost site of the system, and $\mathcal{V}_r$ at the leftmost (dotted) or rightmost (dashdot) site of the right half B. System size is $N = 26$. (d) Total operator density (2.37) on the first five sites of the system $P_{\ell\leq 5}$, compared to the entanglement entropy of that region. System size is $N = 24$. Initial state is chosen as $|Y+\rangle$, and $\mathcal{W}, \mathcal{V} = \mathcal{Y}$. Data is extracted from a numerical simulation (EXPM) of the MFI Hamiltonian (3.1).

dynamics of $\mathcal{W}(t)$ seems to be linear, similar to the growth in the ordinary quantum quench protocol (1.1).

In Fig. 3.5 (d), we display the entanglement entropy $S_A(|\Phi(t)\rangle\rangle)$, where A is now chosen as the first five sites of the system. For this region, moreover, we calculate the total operator density (2.37). We determine the latter by computing the overlap of $\mathcal{W}(t)$ with every possible Pauli string that acts nontrivially on A and trivially on B. To compute the overlap, we approximate the trace by an expectation value in a random pure state drawn from the Haar measure [134, 140], see also Appendix A for further details. The operator density outside of A then follows simply by $P_{\ell \leq |A|} = 1 - P_{\ell > |A|}$, which we display in Fig. 3.5 (d). One can nicely observe the validity of Eq. (3.8), that is, the entanglement entropy begins to grow once $\mathcal{W}(t)$ has spread such that its operator density outside of A begins to grow. Or put differently, entanglement begins to grow once information about $\mathcal{W}(t)$ begins to leak out of the region A.

As discussed earlier in Sec. 2.3.1, considering a quantum quench protocol, we can understand the growth of entanglement for some region A as the leakage of information out of A, resulting in the inaccessibility of that information to measurements on A. With respect to the operator state (3.4), the growth of entanglement can be understood in a similar way. Accordingly, it follows from the decay of the operator density in A, which diagnoses that not all information about the operator $\mathcal{W}(t)$ is accessible by measurements on A. The observed similarities in entanglement dynamics for the operator state (3.4) and the ordinary quench protocol (1.1), then motivate the idea that there is a deeper connection between entanglement growth and operator spreading. In the following chapter, we investigate the influence of powerlaw interactions on the dynamics of quantum information, where we find further evidence for such a connection.

Chapter 4.

Dynamics of Quantum Information and Powerlaw Interactions

“Be less curious about people and more curious about ideas.”
— Marie Curie

The previous chapter illustrates that analyzing entanglement growth and operator spreading provides a complementary and intuitive picture of quantum information dynamics in local quantum lattice models. The presence of nonlocal interactions, however, may drastically change the nonequilibrium physics of a many-body system, as discussed in Chap. 2.

In this chapter, we discuss how powerlaw interactions influence the dynamics of quantum information. To do so, we consider the local MFI Hamiltonian from Eq. (3.1) and incorporate interactions beyond nearest neighbors. In particular, we study the long-range mixed-field Ising (LRMFI) Hamiltonian

$$\mathcal{H}_\alpha = -\sum_{i<j\in Q} J_{ij}^{\alpha} \mathcal{Z}_i \mathcal{Z}_j - \sum_{i\in Q} h_x \mathcal{X}_i - \sum_{i\in Q} h_z \mathcal{Z}_i \,, \tag{4.1}$$

with an interaction strength between the qubits that decays like a powerlaw, $J_{ij}^{\alpha} = J/\left|i-j\right|^{\alpha}$, and J is again the interaction strength between nearest neighbors. Note that one recovers the local Hamiltonian from Eq. (3.1) in the limit $\alpha \to \infty$. In Sec. 4.1, we discuss the counterintuitive phenomenon that sufficiently small decay exponents α drastically slow down the approach toward local equilibrium. The latter suggests a slowdown of quantum information scrambling, which we further investigate in Sec. 4.2, by studying the temporal evolution of the TMI (2.13). Building upon these results, in Sec. 4.3, we discuss explicit regimes of quantum information dynamics regarding the LRMFI Hamiltonian (4.1). These regimes are characterized by a fundamentally different behavior of entanglement growth and operator spreading. Crucially, our analysis suggests that the famous slowdown of entanglement growth for sufficiently strong powerlaw interactions also implies a slowdown of operator dynamics, which we support with numerical data in Sec. 4.4. Finally, in Sec. 4.5, we present analytical arguments for a connection between the growth of entanglement following a quantum quench and the dynamics of Pauli strings under unitary evolution. Using this result, we develop a qualitative picture of the dynamics of quantum information in systems with powerlaw interactions.

4.1. Strong Thermalization

To properly analyze the dynamics of quantum information in the presence of powerlaw interactions, our first objective is to explore whether they have any effect on the late-time dynamics of the system. In particular, we want to examine whether also the LRMFI Hamiltonian from Eq. (4.1) exhibits strong thermalization regarding a quantum quench with initial state $|\Psi_0\rangle = |Y+\rangle$ [138]. Strong thermalization implies that expectation values of local observables approach the respective thermal expectation values under unitary evolution, without considering the time average. Let us, for example, consider the total magnetization in x-direction

$$\mathcal{M}_x = \sum_{i\in Q} \mathcal{X}_i \,, \tag{4.2}$$

which is a sum of local observables and, therefore, we expect it to thermalize. For an initial state with zero energy expectation value, such as $|Y+\rangle$, we expect local observables to approach the thermal expectation value associated with the infinite temperature ensemble. Therefore, we expect the expectation value of the total magnetization to vanish at late times[1]

$$\langle \mathcal{M}_x\,(t)\rangle = \langle \Psi\,(t)|\mathcal{M}_x|\Psi\,(t)\rangle \simeq 2^{-N}\,\mathrm{Tr}\,\{\mathcal{M}_x\} = 0\,.$$

---

[1] Pauli strings are generally traceless, excluding the identity. Hence, the expectation value of any Pauli string in the infinite temperature ensemble vanishes.

In Fig. 4.1 (a), we display the temporal evolution of Eq. (4.2) following a quench from $|Y+\rangle$ for various values of the decay exponent α. For all of these values, the expectation value approaches the infinite temperature result at late times. Noteworthy, with decreasing exponent α, and thereby a slower decay of the interaction strength with distance, the approach toward local equilibrium continues to slow down. For $\alpha \leq 1$, the total magnetization seems to approach its thermal expectation value exponentially slowly, note the logarithmic time scale in Fig. 4.1. This counterintuitive slowdown of thermalization in the presence of powerlaw interactions roots in a slowdown of entanglement growth, which we will cover in more detail in Sec. 4.3. We note that choosing different directions of the magnetization leads to similar conclusions.

For a more general treatment, we probe the approach toward local equilibrium by analyzing the dynamics of local density matrices. We can quantify how close a local density matrix is to the infinite temperature ensemble by calculating, for example, the Frobenius norm of their difference, i.e.,

$$D\left(t\right) = \left|\left|\rho_A\left(t\right) - 2^{-|A|}\,\mathbf{1}_A\right|\right|_{\mathrm{F}} \,. \tag{4.3}$$

Figure 4.1 (b) shows the distance measure from Eq. (4.3), where A is chosen as a set of two neighboring qubits located in the middle of the system. In agreement with the results for the total magnetization, one observes an increasingly slower approach to the thermal density matrix with decreasing decay exponent α. We observe similar behavior for different local regions A. Moreover, the observed slowdown is robust against a change in the system size N, see the inset of Fig. 4.1 (b), suggesting that it is a general phenomenon in the respective system. Thus, also the LRMFI Hamiltonian (4.1) exhibits strong thermalization in the considered quench scenario. Accordingly, local density matrices approach the infinite temperature ensemble at late times, which implies strong thermalization of local observables. However, with decreasing decay exponent α, the relaxation time continues to increase and the system takes longer to thermalize. This slower approach towards local equilibrium becomes very severe for $\alpha \leq 1$. It is common for systems with powerlaw interactions to normalize the interaction strength such that the Hamiltonian is extensive for all values of α. The observed behavior is qualitatively similar if one applies such a normalization, which we discuss further in Appendix A.5.

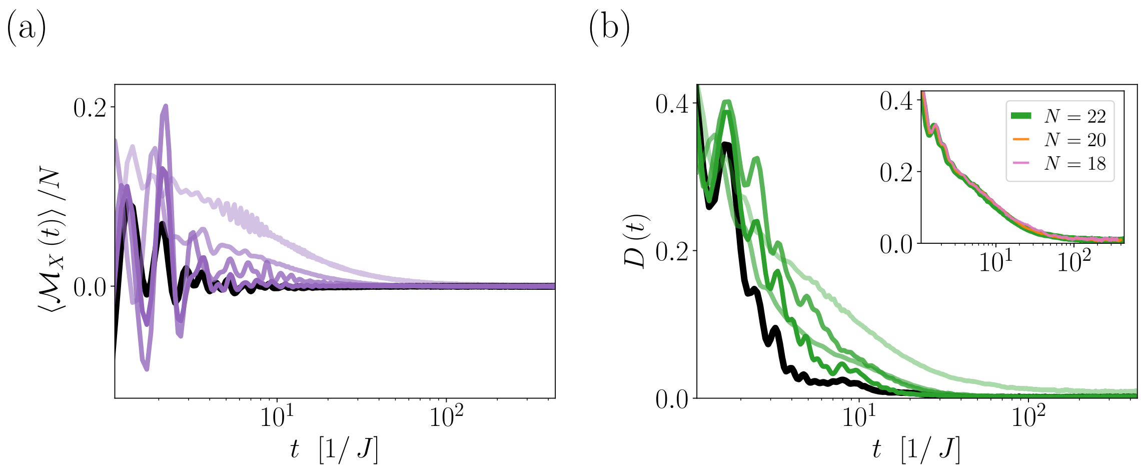

Figure 4.1.: Strong thermalization in the LRMFI model (4.1) following a quantum quench with initial state $|\Psi_0\rangle = |Y+\rangle$ for various values of $\alpha = \{\infty, 3, 2, 1, 0.4\}$. Darker colors indicate larger values of α. Data is extracted from a simulation of $N = 22$ lattice sites (EXPM). (a) Total magnetization in x-direction as defined in Eq. (4.2). (b) Distance between two-qubit reduced density matrix and the maximally mixed state as defined in Eq. (4.3). The inset displays the distance for $\alpha = 0.25$ and different system sizes N.

4.2. The Monogamy of Mutual Information

The continuously slower approach towards local equilibrium with decreasing decay exponent α underlines that powerlaw interactions have a significant and somehow counterintuitive effect on the nonequilibrium physics of a quantum many-body system. Here, we complement this observation by investigating the dynamics of the TMI from Eq. (2.13) in the respective quench protocol. As discussed in Sec. 2.1.3, the sign of the TMI provides information about the correlation structure among three regions A, B, and C. Accordingly, if $I_{A:B:C} \leq 0$, quantum information is scrambled among the three regions and mutual information is monogamous, suggesting that entanglement is the dominant correlation among them. In quantum field theories with holographic duals, mutual information is indeed monogamous, as proven in Ref. [67]. To the best of our knowledge, a similar proof does not exist for general quantum lattice models. However, a recent numerical work [71] considered the temporal evolution of the TMI in the generalized Hayden-Preskill protocol from Sec. 2.3.2 for several integrable, and nonintegrable models of interacting qubits. For local Hamiltonians, mutual information was found to be predominantly monogamous, as only a few initial states where associated with a positive TMI. The latter is merely a consequence of symmetry, as the considered Hamiltonians in Ref. [71] conserve the total magnetization in a particular direction. In the following, we show that for initial states belonging to smallest nontrivial subspace of the magnetization operator, the TMI (2.13) is strictly nonnegative, i.e., $I_{A:B:C} \geq 0$ holds for all disjoint regions A, B, and C.

To proceed, let us consider a Hamiltonian $\mathcal{H}$ that conserves the total magnetization, for example, in z-direction[2]. Accordingly, we have $[\mathcal{H}, \mathcal{M}_z] = 0$, where

$$\mathcal{M}_z = \sum_i \mathcal{Z}_i$$

is the total magnetization operator. Due to the conservation of $\mathcal{M}_z$, one may decompose the Hamiltonian into a direct sum, with each element acting on an invariant subspace associated with a particular eigenvalue of $\mathcal{M}_z$. An initial state $|\Psi_0\rangle$, confined to one of these subspaces, will therefore remain confined to this subspace under unitary evolution. The smallest nontrivial subspace of $\mathcal{M}_z$ is the *one-excitation subspace*[3], which has Hilbert space dimension N. This subspace is spanned by all states with only one qubit in a different state of the computational basis than all the other qubits. The unitary evolution of an initial state from the one-excitation subspace can thus be written as

$$|\Psi(t)\rangle = \sum_i c_i |\boldsymbol{i}\rangle ,$$

where $|\boldsymbol{i}\rangle$ is the state with the qubit at site i in the state $|1\rangle$ and all other qubits in the state $|0\rangle$. Note the coefficients c_i depend on time, however, out of convenience, we drop this dependence here. To evaluate the TMI, let us consider the reduced state of a region A, which is given by

$$\rho_A = \sum_{i,j \in A} c_i c_j^* |\boldsymbol{i}_A\rangle\langle \boldsymbol{j}_A| + \sum_{i \notin A} |c_i|^2 |\boldsymbol{0}_A\rangle\langle \boldsymbol{0}_A| , \tag{4.4}$$

where $|\boldsymbol{i}_A\rangle$ is the reduced state of A regarding the state $|\boldsymbol{i}\rangle$, i.e., $|\boldsymbol{i}_A\rangle\langle \boldsymbol{i}_A| := \mathrm{Tr}_B \{|\boldsymbol{i}\rangle\langle \boldsymbol{i}|\}$, and $|\boldsymbol{0}_A\rangle := \bigotimes_{i\in A} |0\rangle$ is the state with all sites that belong to A in the zero state. If we define $p_A := \sum_{i\in A} |c_i|^2$ and

$$|\boldsymbol{1}_A\rangle := (p_A)^{-1/2} \sum_{i\in A} c_i |\boldsymbol{i}_A\rangle ,$$

---

[2] One may, of course, choose a different direction of the magnetization here.

[3] This name is motivated by the Jordan-Wigner transformation [137], which maps a system of qubits to a system of spinless fermions.

we can diagonalize Eq. (4.4) according to

$$\rho_A = p_A \left|\mathbf{1}_A\right\rangle \left\langle \mathbf{1}_A\right| + (1 - p_A) \left|\mathbf{0}_A\right\rangle \left\langle \mathbf{0}_A\right| . \tag{4.5}$$

Thus, the reduced state of A has at most two nonzero eigenvalues, which correspond to the probability of finding the excitation in the region A, or in its complement B. From Eq. (4.5), it follows that the entanglement entropy of A is given by the binary entropy

$$S_A = H\left(p_A\right) = -p_A \log\left(p_A\right) - \left(1 - p_A\right) \log\left(1 - p_A\right) \leq 1 . \tag{4.6}$$

Equation (4.6) implies that if A contains more then one lattice site, the entanglement entropy is much tighter bounded than in general, see also the bound in Eq. (2.7). The amount of entanglement that can emerge under unitary evolution is, therefore, strongly restricted due to the small Hilbert space the dynamics is confined to. Moreover, given two disjoint regions A and B, it follows straightforwardly that the entanglement entropy of their union S_{AB} is given by $H\left(p_{AB}\right)$, where $p_{AB} = p_A + p_B$. The TMI (2.13) then takes the form

$$I_{A:B:C} = H\left(p_A\right) + H\left(p_B\right) + H\left(p_C\right) + H\left(p_{ABC}\right) - H\left(p_{AB}\right) - H\left(p_{AC}\right) - H\left(p_{BC}\right) . \tag{4.7}$$

According to Eq. (4.7), the TMI is a function of the variables p_A, p_B and p_C. At the boundaries of the parameter space, i.e., $p_A \vee p_B \vee p_C = 0$, and $p_A + p_B + p_C = 1$, Eq. (4.7) vanishes, implying $I_{A:B:C} = 0$. Furthermore, one finds a (positive) maximum of Eq. (4.7) at $p_A = p_B = p_C = 1/4$. Due to the concavity of entropy, we can then conclude that $I_{A:B:C} \geq 0$ holds for all disjoint regions A, B, and C. Thus, in this particular scenario, mutual information is either exactly extensive, i.e., $I_{A:BC} = I_{A:B} + I_{A:C}$, or nonmonogamous. Hence, entanglement can not dominate correlations, because the symmetry of the Hamiltonian strongly constrains the amount of entanglement that can emerge, see Eq. (4.6). Noteworthy, monogamy of mutual information requires more than just nonseparability of the quantum state. For instance, it follows from the above derivation that generalized W-states [141], which are representatives of one class of multipartite entanglement, will never exhibit a negative TMI. This result also clarifies why only a few initial states where associated with a positive value of the TMI in Ref. [71]. However, for most initial states, mutual information appeared to be monogamous. Although the symmetry of the Hamiltonian remains, most initial product states in the computational basis belong to subspaces with large enough dimension such that entanglement can become the dominant correlation.

The LRMFI Hamiltonian from Eq. (4.1) does not obey a simple symmetry such as the conservation of total magnetization. Moreover, regarding the quantum quench considered in the previous section, we do not expect the subsequent dynamics to be confined to any particular subspace of the total Hilbert space. In the following, we investigate how the decay exponent α influences the temporal evolution of the TMI (2.13) in the previously considered quench protocol. In particular, we want to understand whether the TMI diagnoses any fundamental change in the dynamics, depending on the value of α. To proceed, we consider two different partitionings for the regions A, B, and C. First, we take A, B, C as three neighboring qubits in the middle of the system. Second, we divide the system into four connected regions of equal size[4], and choose A, B, and C as one of these quarters respectively. While the first choice probes how quantum information distributes on a local scale, the second captures its distribution on a global scale.

In Fig. 4.2, we display the temporal evolution of the TMI for both of these choices and various values of the decay exponent α. Noteworthy, for the two largest values, i.e., $\alpha = \infty$, and $\alpha = 3$, the TMI appears to be nonpositive for both choices, implying monogamy of mutual information. Moreover, these two values of α are associated with qualitatively similar behavior of the TMI, which we also observe for other values of $\alpha > 2$. Regarding the global partitioning shown in Fig. 4.2 (a), this behavior is characterized by a vanishing value up to a finite time, following an apparent linear decay towards the late-time saturation value. In the following section, we will discuss in more detail why these two values of α are associated with similar dynamics. For the smaller decay exponents α, however, the dynamics of the TMI changes fundamentally. Regarding the global partitioning, the TMI exhibits a positive peak at early times and turns negative afterwards, see also the inset in Fig. 4.2 (a). Furthermore, the subsequent decay of the TMI becomes sublinear, which is most evident for $\alpha = 0.25$. Considering the local partitioning displayed in Fig. 4.2 (b), the TMI remains positive for an increasingly longer time with decreasing exponent α. Thus, while quantum information scrambles rather quickly among global regions, it remains localized among local regions for sufficiently large decay exponents α. The observed behavior is robust upon varying the systems size N, which is exemplified in Fig. 4.3 (a) for $\alpha = 0.25$. Altogether, these results emphasize that the increasingly slower approach towards local equilibrium discussed in the previous section is accompanied by a fundamental change in the correlation structure. In particular,

---

[4] Here, we assume that N is even and divisible by four.

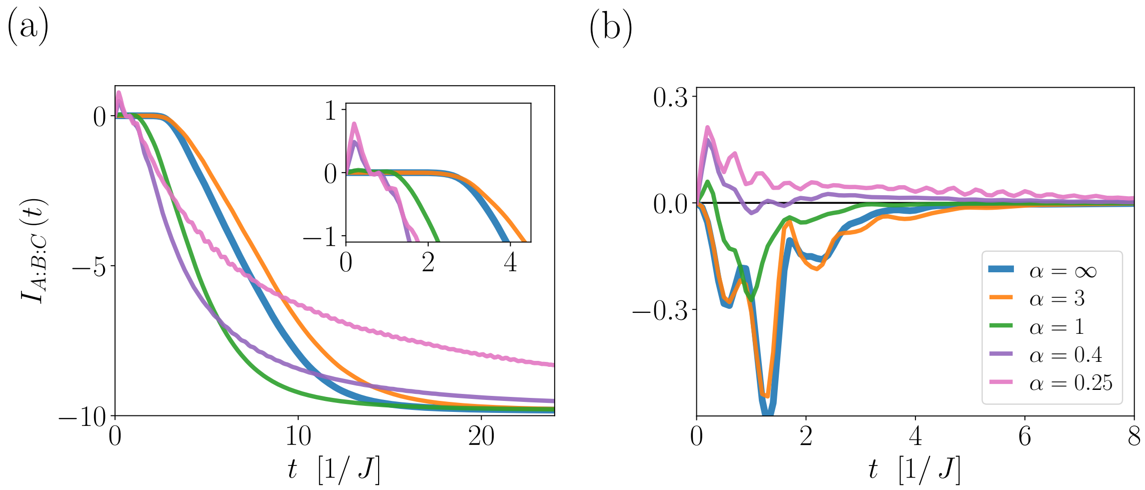

Figure 4.2.: Temporal evolution of the TMI (2.13) following a quantum quench with initial state $|\Psi_0\rangle = |Y+\rangle$ for various values of $\alpha = \{\infty, 3, 1, 0.4, 0.25\}$. Darker colors indicate larger values of α, see also the legend. Data is extracted from a simulation of $N = 24$ lattice sites (EXPM). (a) Global partitioning. The regions A, B, and C are chosen as a connected quarter of the system respectively. (b) Local partitioning. The regions A, B, and C are chosen as neighboring qubits in the middle of the system.

for sufficiently small decay exponents α, the TMI diagnoses that entanglement is not the dominant correlation on a local scale.

To further investigate the sign of the TMI in dependence of the decay exponent α, we display its maximum value during the quench protocol for both partitionings in Fig. 4.3 (b). The data clearly diagnoses a transition at $\alpha = 2$. Accordingly, for both partitionings, $I_{A:B:C} \leq 0$ holds for $\alpha > 2$, while we observe positive values only for $\alpha \leq 2$. We shall note that a similar behavior is observed for other partitionings. Moreover, in Ref. [72], we found the same transition at $\alpha = 2$ for another spin-1/2 Hamiltonian with powerlaw interactions. Our results therefore suggest that mutual information is monogamous in one-dimensional spin-1/2 models with powerlaw interactions for $\alpha > 2$, assuming the dynamics is not confined to a too-small subspace, as discussed above for the one-excitation subspace. Considering this discussion, one may infer that the positive value of the TMI for sufficiently small α diagnoses that the dynamics of the system's state is restricted to an effectively smaller Hilbert space at early to intermediate times, which provides an alternative perspective on the apparent slow thermalization observed in Sec. 4.1. The TMI from Eq. (2.13) is ultimately determined by the dynamics of entanglement entropy. Hence, the observed transition at $\alpha = 2$ diagnoses a fundamental change in entanglement growth, which we explore in more detail in the following section.

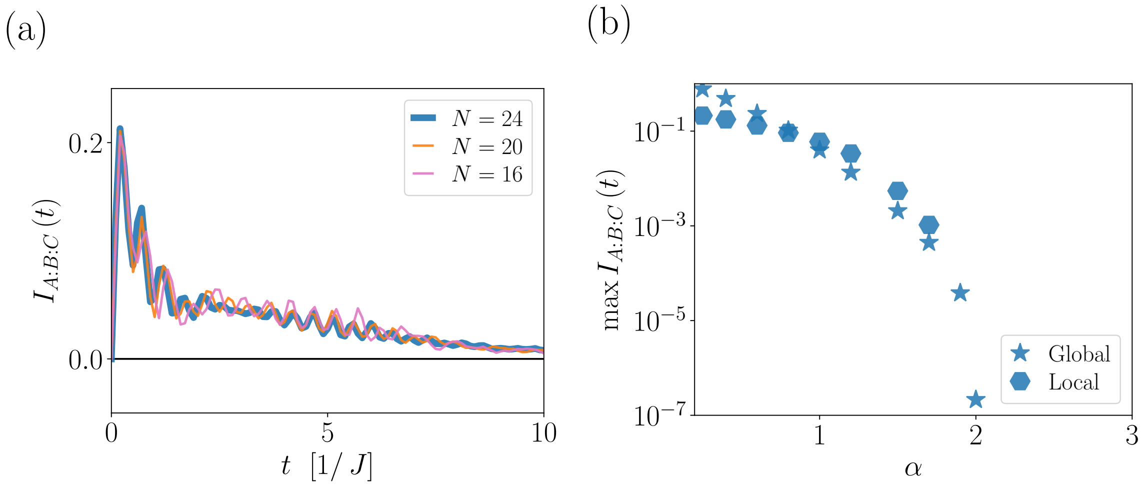

Figure 4.3.: (a) Temporal evolution of the TMI (2.13) for the local partitioning, $\alpha = 0.25$, and different systems sizes N. (b) Maximum of the TMI during the quench protocol in dependence of α for the local, and global partitioning. See the main text for further details.

4.3. Regimes of Quantum Information Dynamics

Building up on the previous two sections, this section aims to establish a more sophisticated understanding of quantum information dynamics in systems with powerlaw interactions. We are particularly concerned with how the decay exponent α influences diagnostics of quantum information dynamics, i.e., entanglement growth and operator spreading, discussed in Sec. 2.3.1 and Sec. 2.3.3. Quantum many-body systems that embody powerlaw interactions will typically undergo several dynamical regimes as the decay exponent α is varied. Transitions between these regimes are characterized by a fundamental change in behavior of the said diagnostics. In the following, we explore these regimes of quantum information dynamics regarding the LRMFI model (4.1).

4.3.1. The Local Regime

For sufficiently large decay exponents α, powerlaw interactions might not alter the dynamics of quantum information fundamentally, as already discussed in Chap. 2. In particular, in a D-dimensional quantum lattice model of spin-1/2 degrees of freedom, the universal growth of entanglement entropy (2.24) is expected to persist for $\alpha > D+1$ [107], while operator spreading remains bounded by a linear lightcone for $\alpha > 2D+1$ [44]. Thus, at least for $\alpha > 2D+1$, the dynamics is entirely local. This bound may not be tight for an individual quantum many-body system though. Here, we consider the LRMFI Hamiltonian from Eq. (4.1) and investigate its *local regime*, i.e., the regime of α associated with effective local behavior of both entanglement growth and operator spreading. Since we rely heavily on numerical results, we can not rigorously prove where the transition to the local regime occurs. However, our results suggest that the local regime persists at least for $\alpha > 2$, which is also the general bound for linear entanglement growth in one spatial dimension. Accordingly, also operator spreading follows effectively local behavior in this regime. Moreover, we find that entanglement growth and operator spreading exhibit an interesting connection in the local regime, a first sign of a deeper relationship between these two complementary perspectives on quantum information dynamics. Determining the local regime for a specific Hamiltonian is also of experimental interest since it may allow simulation of the local dynamics on experimental platforms that naturally embody powerlaw interactions, such as trapped ions, which are typically limited to a decay exponent $0 \leq \alpha \leq 3$.

In the following, we present numerical results for the entanglement velocity v_{E}^{α} and the butterfly velocity v_{B}^{α} in dependence of the decay exponent α. We extract the entanglement velocity from a linear fit to the entanglement entropy (2.6) before saturation, and we choose the region A as the left (right) half of the system. Note that different time intervals for the linear fit do not lead to quantitatively different results. The butterfly velocity follows from a linear fit to the spacetime contour $t_\theta\left(r\right)$, which is determined by a constant value of the squared commutator (2.31), i.e., $C_r\left(t_\theta\left(r\right)\right) = \theta\,, \forall\, r$. Here, we choose $\theta = 1/2$, which is half of the expected late-time value of the squared commutator. Thus, the spacetime contour $t_\theta\left(r\right)$ determines the time at which a significant part of the operator density (2.36) attributes to Pauli strings of size r or larger.

In Fig. 4.4, we present the results of this calculation. Regarding entanglement growth, we consider the quantum quench protocol from the previous sections with initial state $|\Psi_0\rangle = |Y+\rangle$. Moreover, we evaluate the squared commutator in the initial state $|\Psi_0\rangle$, and choose $\mathcal{W}, \mathcal{V} = \mathcal{Y}$. We note that the butterfly velocity barely depends on the choice of $\mathcal{W}$, and $\mathcal{V}$. Figure 4.4 (a) displays the respective velocities v_{E}^{α}, and v_{B}^{α} for various values of the decay exponent α within the local regime. We shall note that the calculated velocities are well converged with the system size N. With decreasing decay exponent α, the entanglement velocity v_{E}^{α}, as well as the butterfly velocity v_{B}^{α} decrease monotonically. This is an interesting result for at least two reasons. First, although the dynamics is effectively local, powerlaw interactions influence the dynamics of quantum information, even in the local regime. Accordingly, they induce an overall slowdown of quantum information scrambling, as the respective velocities of entanglement growth and operator spreading decrease with smaller decay exponent α. This result explains the apparent slowdown of thermalization, at least for decay exponents within the local regime. Second, the similar dependence of v_{E}^{α}, and v_{B}^{α} on the exponent α is a first signature of a deeper connection between entanglement growth and operator spreading. Later on, in Sec. 4.5, we present general analytical arguments for an inherent connection between the growth of entanglement following a quantum quench and the dynamics of Pauli strings under unitary evolution. A recent work on quantum information dynamics in local systems [98] argued that entanglement growth is the bottleneck process of information dynamics, which manifests in $v_{\mathrm{E}} \leq v_{\mathrm{B}}$. Our results suggest that this may also hold in the local regime, as we find $v_{\mathrm{E}}^{\alpha} < v_{\mathrm{B}}^{\alpha}$ for all considered decay exponents α. The influence of powerlaw interactions on operator dynamics is further displayed in Fig. 4.4 (b), which displays the operator size from Eq. (2.38) for $\mathcal{W} = \mathcal{Y}$, and $\alpha = \infty, 2.1$ respectively. In agreement with the previous result, the operator size for $\alpha = 2.1$ exhibits a slowdown, compared to the local system, i.e., $\alpha = \infty$. For both cases, however, a linear growth of the operator size is evident, confirming ballistic operator spreading under unitary evolution.

The effective local dynamics for $\alpha > 2$ is further demonstrated in Fig. 4.5. Figure 4.5 (a) displays the squared commutator (2.31) for a fixed position r and various values of α within the local regime. With decreasing exponent α, the rapid growth of the squared commutator becomes increasingly suppressed, resulting in a smaller butterfly velocity. Thus, the operator front broadens with decreasing exponent α, which becomes more evident upon rescaling time with the respective butterfly velocity v_{B}^{α}, see the inset of Fig. 4.5 (a). Figure 4.5 (b) shows the temporal evolution of the entanglement entropy for various values of α within the local regime. The linear growth of entanglement entropy is clearly visible for all shown values of α. Rescaling time with the respective entanglement velocity leads to a collapse of all curves, see the inset of Fig. 4.5 (b). Hence, the entanglement entropy exhibits a similar growth as for the local Hamiltonian from Eq. (3.1) with a renormalized entanglement velocity v_{E}^{α}, where $v_{\mathrm{E}}^{\alpha} \leq v_{\mathrm{E}}$.

In summary, the analysis of entanglement growth and operator spreading provides a coherent picture. That is, in the local regime, the presence of powerlaw interactions slows down the dynamics of quantum information. In particular, with decreasing decay exponent α, the growth of entanglement entropy continues to slow down, manifesting in a decreasing entanglement velocity. Moreover, we observe an increased broadening of

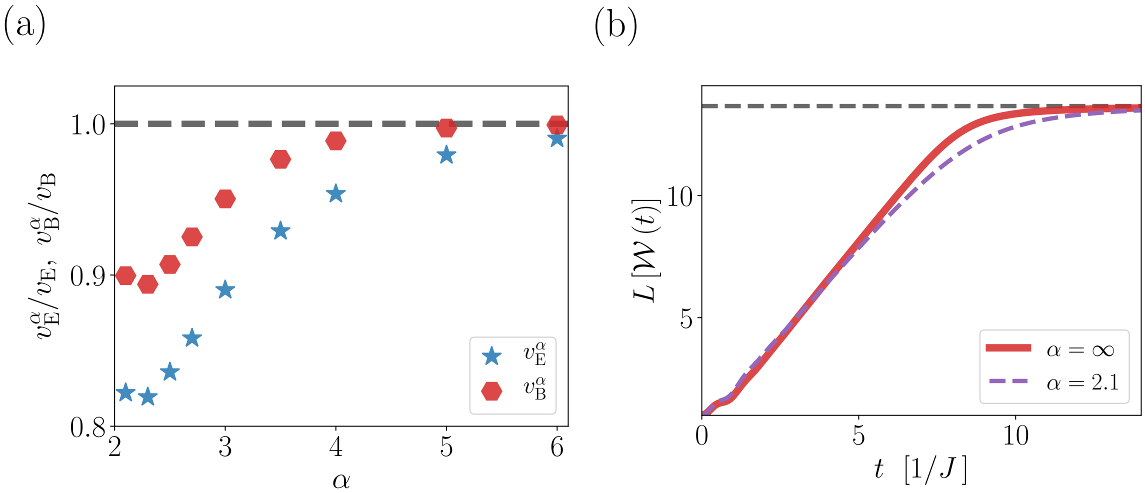

Figure 4.4.: Dynamics of quantum information in the local regime. (a) Entanglement velocity $v_{\rm E}^{\alpha}$ and butterfly velocity $v_{\rm B}^{\alpha}$ in dependence of the decay exponent α, where $|\Psi_0\rangle = |Y+\rangle$, and $\mathcal{W}, \mathcal{V} = \mathcal{Y}$. Gray dashed line indicates the value for the local Hamiltonian $\mathcal{H}_\infty$. Data is extracted from a simulation of $N = 24$ lattice sites (EXPM). (b) Operator size for $\alpha = \infty$, and $\alpha = 2.1$ respectively, where $\mathcal{W} = \mathcal{Y}$. Gray dashed line indicates the operator size following from random unitary evolution, i.e., Eq. (2.39). Data is extracted from a numerical simulation of the LRMFI model (4.1) for $N = 14$ lattice sites (ED).

the operator front, which enforces a less rapid growth of the squared commutator, and a slowdown of the operator size.

4.3.2. The Nonlocal Regime

As discussed in the previous section, determining the exact range of α associated with effectively local dynamics, i.e., the local regime, is not possible in a rigorous sense, given only access to numerical data. It is also not clear whether entanglement growth and operator spreading abandon their local behavior at the same value of α. Beyond the local regime, we generally expect sublinear entanglement growth and superballistic operator spreading, as observed in several recent works on that matter [42, 50, 51, 69, 135]. For the model and the quench protocol we consider here, our data suggest that entanglement growth and operator spreading cease to follow effectively local dynamics for $\alpha \leq 2$. However, the influence on entanglement growth is quite subtle for $1 \leq \alpha \leq 2$. Thus, we primarily focus on the regime $\alpha < 1$ in the following, where the impact of powerlaw interactions on the dynamics of quantum information is most severe.

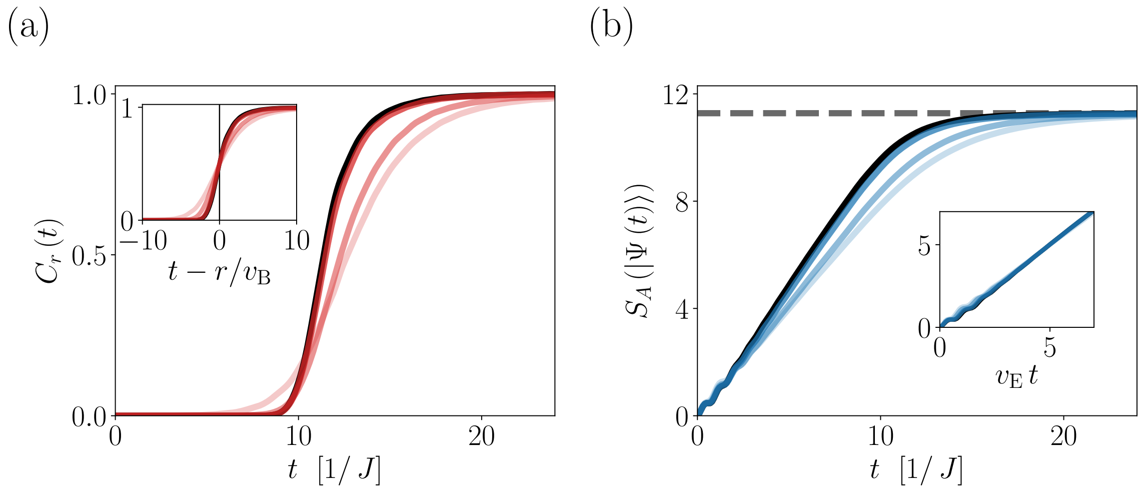

Figure 4.5.: Entanglement growth and operator spreading for various values of the exponent $\alpha = \{\infty, 3.0, 2.5, 2.1\}$ within the local regime. Darker colors indicate larger values of α. (a) Squared commutator $C_r\,(t)$ (2.31) for $r = 20$, and $\mathcal{W}, \mathcal{V} = \mathcal{Y}$, evaluated in the initial state $|\Psi_0\rangle = |Y+\rangle$. The inset shows the collapse at $t \sim 0$ if time is rescaled with the respective butterfly velocity v_B^α. (b) Growth of the half-chain entanglement entropy $S_A\,(|\Psi\,(t)\rangle)$ (2.6) following a quench from $|\Psi_0\rangle = |Y+\rangle$. The inset displays the collapse of all curves if time is rescaled with the respective entanglement velocity v_E^α. Data is extracted from a numerical simulation of the LRMFI model (4.1) for $N = 24$ lattice sites (EXPM).

In this regime, logarithmically slow growth of entanglement entropy was observed in numerical studies [50, 51], and recent works attribute its origin to the dominance of collective spin squeezing [52,108]. In Fig. 4.6 (a), we display the entanglement entropy (2.6) following a quench from the initial state $|\Psi_0\rangle = |Y+\rangle$ for various small values of the decay exponent α regarding the LRMFI Hamiltonian from Eq. (4.1). After initially rapid growth, the entanglement entropy undergoes a drastic slowdown, which becomes more severe as the decay exponent α is decreased. Note also the comparison to the local Hamiltonian from Eq. (3.1). The logarithmic growth is further confirmed in the inset of Fig. 4.6 (a), which displays the entanglement entropy for a fixed value of $\alpha = 0.3$, and different system sizes N. Despite the rapid initial growth, we expect the logarithmic slowdown to dominate at large system sizes, implying that it takes significantly longer until a given region A becomes maximally entangled with its environment. Thus, also for the LRMFI Hamiltonian (4.1), sufficiently strong powerlaw interactions fundamentally change the growth of entanglement. A system with strong powerlaw interactions is, therefore, not scrambling information as fast as a system with local interactions, at least through the lens of entanglement growth, which is in agreement with the slow thermalization discussed in Sec. 4.1, and the analysis of the TMI in Sec. 4.2.

At this point, a few comments regarding the comparability of timescales may be in order. With decreasing decay exponent α, the total interaction strength per lattice site becomes larger. Thus, comparing the temporal evolution of a quantity for different values of α in units of the nearest neighbor interaction strength J is not a fair comparison. Other works on systems with powerlaw interactions compensated this by defining an effective energy per lattice site, for example, by means of the Frobenius norm of the Hamiltonian [50]. However, this rescaling of time does not alter our results in any fundamental way, which is why we do not apply it here.

Contrary to entanglement growth, strong powerlaw interactions seem to have the opposite impact on operator spreading. Based on results from the literature [42, 135], we expect the spatiotemporal profile of the squared commutator to follow a highly nonlinear lightcone for sufficiently small values of the decay exponent α. In particular, a polynomial lightcone, or even a logarithmic lightcone [42]. Note, however, the derived lightcone shapes in Ref. [42] follow from an effective stochastic model and have never been verified in the regime $\alpha < 1$ for an actual quantum many-body system neither numerically, nor analytically. In Fig. 4.6 (b), we display numerical results for the spacetime contour of the squared commutator (2.31) defined by $C_r\left(t_\theta\left(r\right)\right) = \theta$, where $\theta = 1/2$. In agreement with our expectation, the lightcone becomes increasingly nonlinear with decreasing exponent α. Note that $t_\theta\left(r\right)$ will depend on the choice of θ. The functional dependence on r, however, is typically independent of θ, if the latter is chosen as a significant fraction of the late-time value of $C_r\left(t\right)$. For $\alpha = 0.4$, the lightcone appears almost flat, supporting the argument of Ref. [42] for a logarithmic lightcone if $\alpha \leq 1/2$. However, a reliable confirmation of a logarithmic lightcone based on numerical data for such small system sizes is just not possible.

To sum up, while the spatiotemporal profile of the squared commutator suggests that local quantum information spreads rapidly over the system's spatial degrees of freedom, the growth of entanglement entropy between a spatially connected region and its environment is logarithmically slow and thereby follows an entirely different timescale. This apparent discrepancy was acknowledged before, and it was argued in Ref. [69] that entanglement growth and operator spreading are not necessarily related, as the former occurs in state space, and the latter in operator space. Contrary to these arguments, we show in the following sections that there is, in fact, such a relationship. This relationship implies that a slowdown of entanglement growth corresponds to a particular slowdown of operator dynamics.

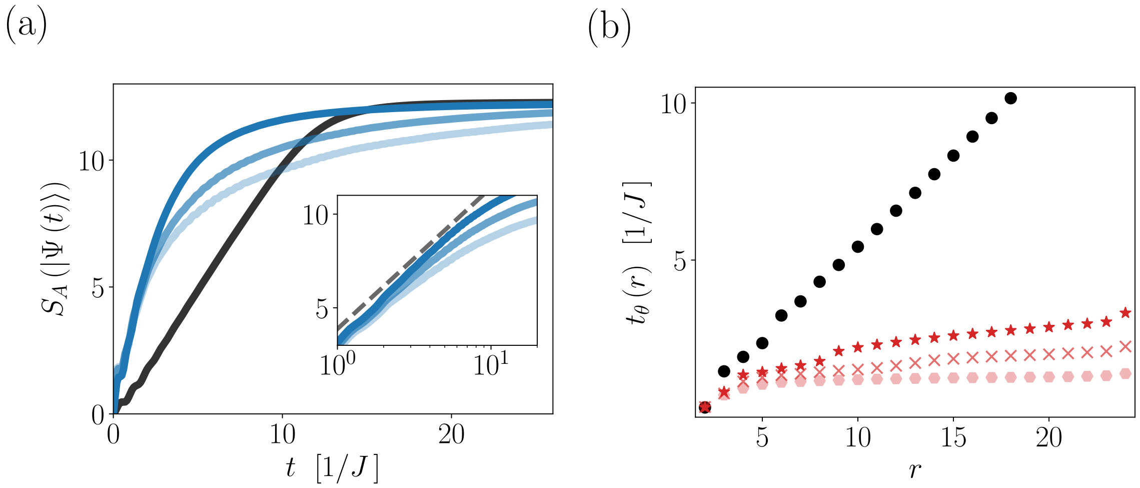

Figure 4.6.: Dynamics of quantum information deep in the nonlocal regime. (a) Temporal evolution of the half-chain entanglement entropy $S_A(|\Psi(t)\rangle)$ following a quench from the initial state $|\Psi_0\rangle = |Y+\rangle$ for a decay exponent $\alpha = \{\infty, 0.5, 0.3, 0.25\}$ respectively, and a system of $N = 26$ lattice sites. The inset depicts the logarithmic growth of entanglement entropy for $\alpha = 0.3$ and a system size of $N = 22, 24, 26$ respectively. The dashed line is proportional to $\log(t)$ (b) Spacetime contour of the squared commutator defined by $C_r(t_\theta(r)) = \theta$, where $\theta = 1/2$ for $\alpha = \{\infty, 0.8, 0.6, 0.4\}$ respectively. Squared commutator is evaluated in the initial state $|\Psi_0\rangle$, and $\mathcal{W}, \mathcal{V} = \mathcal{Y}$. System size is $N = 24$. Darker colors indicate larger values of α in all plots. Data is extracted from a numerical simulation (EXPM) of the LRMFI model (4.1).

4.4. The Slowdown of Operator Dynamics

In Sec. 3.3, we introduced the operator state, which we utilized to establish a connection between the spread of a local operator and the growth of entanglement. Regarding the MFI model (3.1), this approach indicated that most of the entanglement growth regarding some spatial region occurs while the operator front propagates through that region. Based on this result we inferred that most of the operator density is condensed close to the operator front in local systems, which agrees with results for the operator density presented in Sec. 3.2, and recent works on operator spreading in local systems [33,34,124]. Here, we consider the dynamics of the operator state regarding the LRMFI model (4.1) deep in the nonlocal regime.

In Fig. 4.7, we display the entanglement entropy (2.6) of the operator state (3.4) for two small values of α, i.e., we consider $S_A\left(\left|\Phi\left(t\right)\right\rangle\right)$, where A is chosen as the left half of the system, and $\left|\Phi\left(t\right)\right\rangle = \mathcal{W}\left(t\right)\left|\Psi_0\right\rangle$. In addition, we compare this growth to the squared commutator (2.31), similar to the setup in Fig. 3.5. Although the entanglement growth agrees with the squared commutator at early times, we observe a slowdown of entanglement growth at intermediate times, reminiscent of the ordinary quench protocol discussed in the previous section. While the squared commutator diagnoses that the support of $\mathcal{W}\left(t\right)$ extends over the entire system after a short time, the entanglement entropy is still growing. We expect this growth to persist for much longer as our results suggest that also the entanglement entropy of the operator state approaches the Page value (2.22) at late times. We believe the strong oscillations of the squared commutator for smaller α originate from the small system size of our simulation. However, for the system sizes we can access, only a slight decrease of these oscillations is observed, see the inset of Fig. 4.7 (b).

Thus, while information about $\mathcal{W}\left(t\right)$ is still leaking out of A, its support already extents over the entire system. This result is in stark contrast to the result for the MFI Hamiltonian (3.1), which is depicted in Fig. 3.5 (c). Moreover, it points towards a slowdown of operator dynamics in the presence of (strong) powerlaw interactions, similar to the slowdown of entanglement growth following a quantum quench. In particular, it suggests that the operator density behind the superballistically propagating operator front decays significantly slower, compared to a a system with local interactions. However, it is *a priori* not clear how much of the observed slowdown in Fig. 4.7 is due to a slowdown of operator dynamics, and how much originates from the slowdown of entanglement growth we observe in the ordinary quench protocol. In order to support the indication of the operator state, it is therefore desirable to investigate whether there is a general slowdown of operator dynamics, independent of any initial state. For this reason, we consider the squared commutator (2.31) evaluated in the infinite temperature ensemble, which provides a state-independent probe of operator spreading. Moreover, it is connected to the operator density, see also Eq. (B.16) in Appendix B. A slower decay of the operator density behind the operator front then implies a slower approach of the squared commutator towards its saturation value. That is, after a rapid growth upon arrival of the operator front, we expect an increasingly slower approach of the squared commutator towards its late time value with decreasing decay exponent α. To compute the squared commutator at infinite temperature, we approximate the trace by an expectation value in a random pure state drawn from the Haar measure [134, 140]. With this approximation, the computation is similar to that of the squared commutator evaluated in a pure state with an additional averaging over several random states. For further details on this technique, see Appendix A.3.

In Fig. 4.8, we display the approach of the infinite temperature squared commutator towards its late-time value for various values of the decay exponent α. The results complement the previous indication, as one can clearly observe an increasingly slower saturation with decreasing exponent α, see Fig. 4.8 (a). Note that we additionally include data for the MFI Hamiltonian (3.1) for comparison. Our observation does not seem to be an artifact of the small system size of our simulation, since we do not observe any sign of its disappearance as the system size is increased, see Fig. 4.8 (b). This result confirms that the process of operator spreading is fundamentally different in systems with strong powerlaw interactions compared to systems with local interactions. Accordingly, it is characterized by a superballistically propagating operator front and a slow decaying operator density behind this front. This slow decay of the operator density behind the front seems to be diagnosed by the slowdown of entanglement growth following a quantum quench since we observe a similar response to a change of the decay exponent α. However, beyond these numerical observations, an analytic connection between entanglement growth and operator spreading is still lacking. In the next section, we complement these numerical results with further analytical arguments for such a connection.

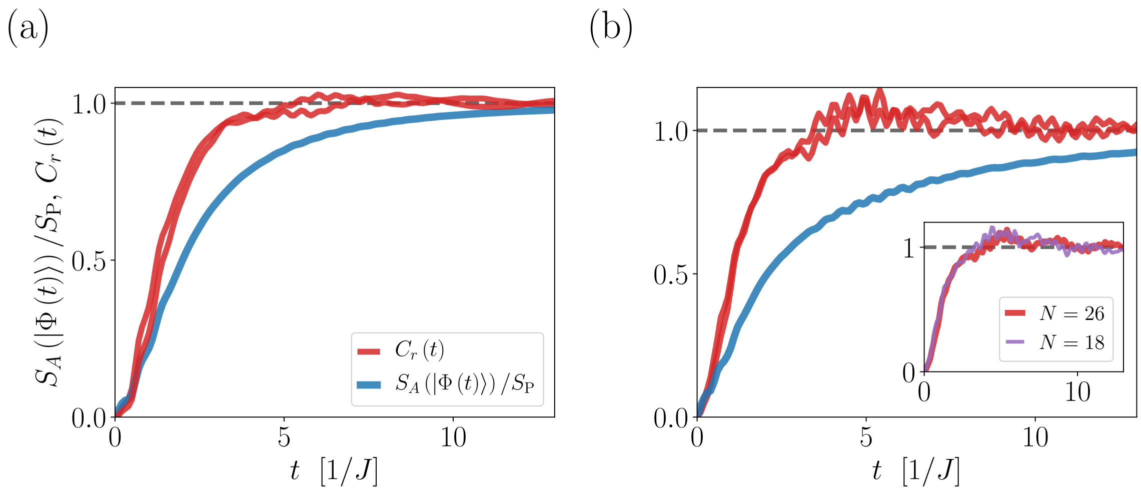

Figure 4.7.: Half-chain entanglement entropy (2.6) regarding the operator state from Eq. (3.4) with initial state $|Y+\rangle$, compared to the squared commutator (2.31) evaluated in the same initial state. The operator $\mathcal{W}=\mathcal{Y}$ is located at the leftmost site of the system, and $\mathcal{V}=\mathcal{Y}$ at the leftmost ($r=14$) and rightmost ($r=26$) site of the right half. (a) $\alpha=0.4$, (b) $\alpha=0.25$. The inset shows the squared commutator for $r=26$ and two values of N. Data is extracted from a numerical simulation (EXPM) of the LRMFI model (4.1) for $N=26$ lattice sites.

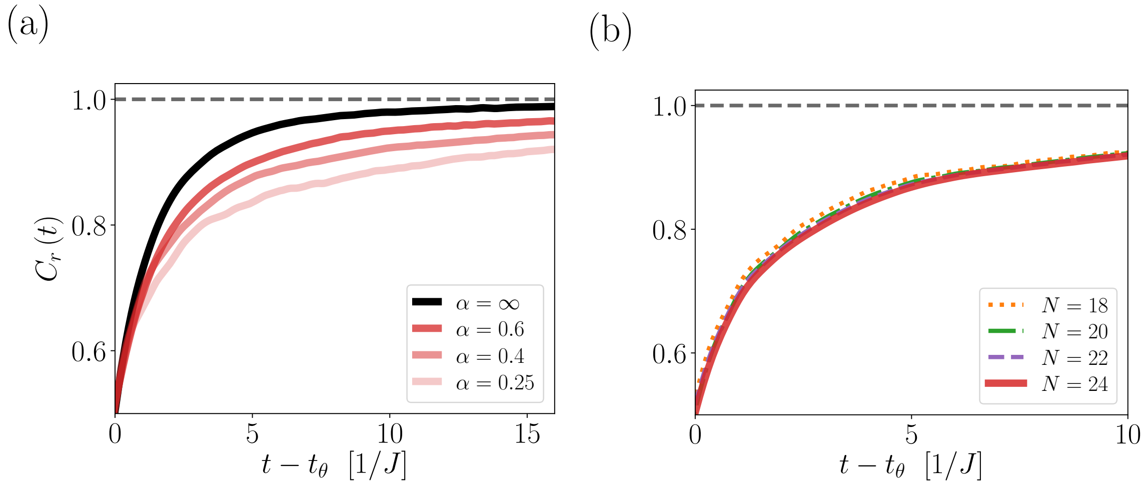

Figure 4.8.: Slow saturation of the squared commutator deep in the nonlocal regime. (a) Squared commutator (2.31) evaluated at infinite temperature, where $\mathcal{W},\mathcal{V}=\mathcal{Y},\mathcal{Z}$ and $r=N$, for $\alpha=\{\infty,0.6,0.4,0.25,0.15\}$ respectively and a system of $N=20$ lattice sites. (b) Squared commutator for $\alpha=0.4$ and different system sizes $N=\{18,20,22,24\}$. Data is extracted from a numerical simulation (EXPM) of the LRMFI model (4.1).

4.5. Connecting Entanglement Growth and Operator Spreading

In the following, we establish a general connection between the dynamics of Pauli strings and the growth of entanglement following a quantum quench. In this regard, let us consider an initial product state $|\Psi_0\rangle = \bigotimes_{i\in Q} |\psi_i\rangle$, where every qubit is prepared in an eigenstate of one of the Pauli operators $\mathcal{X}, \mathcal{Y}$, or $\mathcal{Z}$. We can decompose the projector on this initial state $\rho_0 = |\Psi_0\rangle\langle\Psi_0|$ by virtue of the operator expansion (2.35), i.e.,

$$\rho_0 = 2^{-N} \sum_{\mathcal{S}\in\rho_0} c_{\mathcal{S}}\, \mathcal{S}\,, \tag{4.8}$$

where $c_{\mathcal{S}} = \langle\Psi_0|\mathcal{S}|\Psi_0\rangle = (-1)^s$, and s is either 0 or 1, depending on the Pauli string $\mathcal{S}$. The number of Pauli strings that contribute to the expansion in Eq. (4.8) is given by 2^N. One example of such an initial state is $|Y+\rangle$, which we considered throughout this thesis. In this particular case[5], all Pauli strings that follow from tensor products of the identity and $\mathcal{Y}$ contribute to the expansion (4.8). Thus, the latter includes Pauli strings of all possible sizes. Note that the following derivation is not restricted to initial states like $|Y+\rangle$, where each qubit is prepared in an eigenstate of the same Pauli operator. As long as each qubit is initially in an eigenstate of one of the Pauli operators, the following derivation applies. Under unitary evolution, Eq. (4.8) becomes

$$\rho\left(t\right) = 2^{-N} \sum_{\mathcal{S}\in\rho_0} (-1)^s \mathcal{S}\left(t\right)\,,$$

where $\rho\left(t\right) = e^{i\mathcal{H}t}\rho_0\, e^{-i\mathcal{H}t}$. Thus, the dynamics of the initial state $|\Psi_0\rangle$ is determined by a sum of Pauli strings that evolve under unitary evolution.

Thus, in contrast to previous considerations that addressed operator dynamics of local Pauli strings, we are now confronted with operator dynamics of general Pauli strings. In the latter case, it is useful to generalize the operator density (2.36), which we do in the following. Similar to Eq. (2.35), we can also expand the string $\mathcal{S}\left(t\right)$ by means of a complete operator basis

$$\mathcal{S}\left(t\right) = \sum_{\mathcal{S}'} c_{\mathcal{S}'} \mathcal{S}'\,, \tag{4.9}$$

---

[5] More explicitly, for a system of N lattice sites, it follows that $|Y+\rangle\langle Y+| = 2^{-N} \bigotimes_{i=1}^{N} (\mathbf{1}_i + \mathcal{Y}_i)$.

where we drop the time-dependence of the coefficients $c_{\mathcal{S}'}$ for convenience. In this general case, it is more useful to organize the strings $\mathcal{S}'$ regarding the lattice sites they act nontrivially on. Using Eq. (4.9), we define the operator density on a set of lattice sites A by the total weight on Pauli strings $\mathcal{S}'$ that act only nontrivially on A and trivially on its complement B, i.e.,

$$P_A^{\mathcal{S}} = \sum_{\mathcal{S}'_A \neq \mathbf{0}} |c_{\mathcal{S}'}|^2 \ , \tag{4.10}$$

where $\mathcal{S}'_A := 2^{-|B|} \operatorname{Tr}_B \{\mathcal{S}'\}$ is *the reduced Pauli string* of $\mathcal{S}'$ regarding A, which is only nonzero[6] if $\mathcal{S}'$ acts trivially on the complement B. If we choose $\mathcal{S}$ as a local Pauli string $\mathcal{W}$, located at the left edge of the system, and A as a connected spatial region that incorporates the initial position of $\mathcal{W}$, we can connect the general definition of operator density (4.10) to the operator density in Eq. (2.37), i.e., $P_A^{\mathcal{W}} = P_{\ell \leq |A|}$.

To analyze entanglement growth, we consider the reduced state of a region A, which is given by

$$\rho_A(t) = 2^{-|A|}\mathbf{1}_A + 2^{-|A|} \sum_{\mathcal{S} \in \rho_0 - \mathbf{1}} (-1)^s \, \mathcal{S}_A(t) \ , \tag{4.11}$$

where

$$\mathcal{S}_A(t) = 2^{-|B|} \operatorname{Tr}_B \{\mathcal{S}(t)\} = \sum_{\mathcal{S}'_A \neq \mathbf{0}} c_{\mathcal{S}'} \mathcal{S}'$$

is the reduced Pauli string of $\mathcal{S}(t)$ regarding A. Note the sum in Eq. (4.11) now excludes the identity, which is invariant under unitary evolution. For initial states with zero energy expectation value, such as $|Y+\rangle$, we expect the entanglement entropy to approach the Page value (2.22) under unitary evolution. The latter implies that any region containing slightly less than half of the system's degrees of freedom is maximally entangled with its environment, which results in a maximally mixed reduced state of that region. Equation (4.11), therefore, establishes an interesting connection between the growth of entanglement and the dynamics of Pauli strings under unitary evolution. Accordingly, the reduced state $\rho_A(t)$ is maximally mixed if and only if the sum in Eq. (4.11) vanishes. This does not necessarily imply that every term in the sum vanishes though, since contributions from different $\mathcal{S}_A(t)$ may also cancel out. However, it is possible to connect the generalized operator density (4.10) to the structure of the reduced state $\rho_A(t)$. To probe how close the reduced state is to the maximally mixed state, we calculate the Frobenius norm of their difference, i.e.,

---

[6] This follows from the fact that Pauli strings are traceless, excluding the identity. Thus, if a string $\mathcal{S}'$ acts nontrivially on B, the partial trace over B will result in a vanishing reduced string regarding A.

$$\left\|\rho_A(t) - 2^{-|A|}\mathbf{1}_A\right\|_{\mathrm{F}} = \left\|2^{-|A|} \sum_{\mathcal{S}\in\rho_0-\mathbf{1}} (-1)^s\, \mathcal{S}_A(t)\right\|_{\mathrm{F}} . \tag{4.12}$$

We can upper bound the right hand side of Eq. (4.12) by virtue of the triangle inequality

$$\left\|2^{-|A|} \sum_{\mathcal{S}\in\rho_0-\mathbf{1}} (-1)^s\, \mathcal{S}_A(t)\right\|_{\mathrm{F}} \leq 2^{-|A|} \sum_{\mathcal{S}\in\rho_0-\mathbf{1}} \left\|\mathcal{S}_A(t)\right\|_{\mathrm{F}} = 2^{-|A|/2} \sum_{\mathcal{S}\in\rho_0-\mathbf{1}} \sqrt{P_A^{\mathcal{S}}}\,, \tag{4.13}$$

where we utilized that $P_A^{\mathcal{S}} = 2^{-|A|}\,\mathrm{Tr}\left\{\mathcal{S}_A(t)\,\mathcal{S}_A(t)\right\}$. Combining Eq. (4.12) and Eq. (4.13), we obtain

$$\left\|\rho_A(t) - 2^{-|A|}\mathbf{1}_A\right\|_{\mathrm{F}} \leq 2^{-|A|/2} \sum_{\mathcal{S}\in\rho_0-\mathbf{1}} \sqrt{P_A^{\mathcal{S}}}\,. \tag{4.14}$$

The distance between the reduced state of A and the maximally mixed state thereby lower bounds the total operator densities $P_A^{\mathcal{S}}$. Considering local Pauli strings that have no overlap with the Hamiltonian or any other conserved quantity, we expect universal behavior, as discussed in Sec. 2.3.3. In particular, at late times we expect most of the operator density attributes to strings that act nontrivially on the entire system. If A is small compared to the system size N, this implies a vanishingly small operator density on A at late times. Note, however, we are not restricted to local Pauli strings here, since the expansion in Eq. (4.8) incorporates general Pauli strings. Nevertheless, we do not see any reason why the late-time behavior of $P_A^{\mathcal{S}}$ should change for general strings. In this case, i.e., $P_A^{\mathcal{S}} \approx 0\,\forall\,\mathcal{S}$, Eq. (4.14) implies maximal entanglement between A and its environment. The growth of entanglement following a quantum quench is, therefore, in direct correspondence to the process of operator spreading.

Complementary, we can employ similar arguments to establish a direct connection between the entanglement entropy (2.6) and the operator densities $P_A^{\mathcal{S}}$ from Eq. (4.10). To begin with, let us consider the second Rényi entropy from Eq. (2.10). Using the definition of the Frobenius norm(2.2), it follows that

$$S_A^{(2)}\left(|\Psi(t)\rangle\right) = -\log\left(\|\rho_A(t)\|_{\mathrm{F}}^2\right) . \tag{4.15}$$

Using the reduced state from Eq. (4.11), we can bound the expression in the logarithm of Eq. (4.15) by virtue of the Cauchy-Schwarz inequality

$$\begin{aligned}\left\|\rho_A(t)\right\|_{\mathrm{F}}^2 &= 2^{-|A|} + \left\|2^{-|A|} \sum_{\mathcal{S}\in\rho_0-\mathbf{1}} (-1)^s\, \mathcal{S}_A(t)\right\|_{\mathrm{F}}^2 \\ &\leq 2^{-|A|} + 2^{-2|A|} \left(\sum_{\mathcal{S}\in\rho_0-\mathbf{1}} \left\| \mathcal{S}_A(t) \right\|_{\mathrm{F}} \right)^2 \\ &= 2^{-|A|} + 2^{-|A|} \left(\sum_{\mathcal{S}\in\rho_0-\mathbf{1}} \sqrt{P_A^{\mathcal{S}}} \right)^2 . \end{aligned} \tag{4.16}$$

Since $S_A(|\Psi(t)\rangle) \geq S_A^{(2)}(|\Psi(t)\rangle)$ holds, Eq. (4.16) implies the following bound for the entanglement entropy

$$S_A(|\Psi(t)\rangle) \geq |A| - \log\left(1 + \left(\sum_{\mathcal{S}\in\rho_0-\mathbf{1}} \sqrt{P_A^{\mathcal{S}}}\right)^2\right) . \tag{4.17}$$

Equation (4.17) confirms that the entanglement entropy of the region A bounds the operator densities on that region, i.e., $P_A^{\mathcal{S}}$, which relate to the Pauli strings $\mathcal{S}(t)$ that contribute to the operator expansion (4.8) of the initial state $|\Psi_0\rangle$.

Let us pause for a moment and discuss this connection in more detail. Initially, the system is in the product state $|\Psi_0\rangle$, which implies a vanishing entanglement entropy, $S_A(|\Psi_0\rangle) = 0$. Thus, all information about A is accessible by measurements on A, which implies that $P_A^{\mathcal{S}} = 1$ for all strings $\mathcal{S}$ that act only nontrivially on A and trivially on its complement B, and $P_A^{\mathcal{S}} = 0$ for all strings that act nontrivially on B. As time evolves, the Pauli strings $\mathcal{S}(t)$ grow in size and complexity, which results in the decay of the operator densities $P_A^{\mathcal{S}}$. Thus, information about A becomes inaccessible to measurements on A under unitary evolution. At late times, we expect the operator densities to become vanishingly small, $P_A^{\mathcal{S}} \approx 0\,\forall\,\mathcal{S}$, implying maximal entanglement and the inaccessibility of all information that was initially localized in A. We can, therefore, interpret the decay of $P_A^{\mathcal{S}}$ as the leakage of information out of A, or put differently, the growth of entanglement!

This connection between entanglement growth and operator dynamics provides a qualitative explanation for the numerical observations of the previous section. The slow approach towards maximal entanglement in systems with strong powerlaw interactions thereby implies a slow decay of the operator densities $P_A^{\mathcal{S}}$. For a local string, this implies a slow decay of the operator density behind the superballistically propagating front, in agreement with our numerical results from Sec. 4.4.

It could be interesting to further study the dynamics of general Pauli strings $\mathcal{S}$ and their connection to quench dynamics. In particular, widely different behavior regarding the MFI model (3.1) was observed for quenches with initial states $|X+\rangle$, and $|Z+\rangle$ [138, 142]. Assuming that any string $\mathcal{S}$ that has no overlap with the Hamiltonian becomes effectively Haar random at late times [31], the derivation above implies that the effective thermal ensemble is determined by the dynamics of a few Pauli strings, i.e., strings that describe single-site and two-site terms. Identifying universal behavior of the dynamics of general Pauli strings could therefore help to identify universal behavior in quench dynamics.

Chapter 5.

Fast Scrambling

"We have to give up the idea of realism to a far greater extent than most physicists believe today."
— Anton Zeilinger

Quantum lattice models with nonlocal interactions also appeared recently in connection to the correspondence of anti-de Sitter space and conformal field theories (AdS/CFT), where information scrambling has become a central topic [29, 30, 38, 74, 126, 136, 143, 144]. In this regard, the property of *fast scrambling* is of particular interest. The latter is defined via the squared commutator $C_r\,(t)$ from Eq. (2.31). Accordingly, for a system with N degrees of freedom, fast scrambling implies that $C_r\,(t) \sim O\,(1)\ \forall\, r$ in a time $t \sim \log\,(N)$. Fast scrambling is believed to be characteristic of black holes [30, 143] and holographic duals to theories of quantum gravity, e.g., the Sachdev-Ye-Kitaev (SYK) model [145, 146]. The highly complex structure of the latter, however, renders an experimental realization on current quantum simulation platforms challenging. Motivated by this, several proposals of simpler models that exhibit fast scrambling were brought forward lately [121–123, 147]. The proposals in Refs. [121, 122] follow a similar structure, that is, a fine tuned combination of a local spin-1/2 Hamiltonian and a nonlocal all-to-all interaction $\sim 1/r^0$. As these simple proposals are accessible in today's experimental environments, their nonequilibrium behavior is also of interest in a broader context, for example, with regard to quantum information processing.

In this chapter, we study one of these proposals and analyze the dynamics of quantum information similar to the previous chapters. In particular, we consider the proposal from Ref. [121] and present numerical results on entanglement growth and operator spreading in Sec. 5.1. Using these results and the previously developed connection between entanglement growth and operator dynamics, in Sec. 5.2 we discuss key differences between the fast scrambling model and the LRMFI model (4.1). Crucially, we demonstrate that these two models are associated fundamentally different operator dynamics, which motivates us to conjecture that fast scrambling is impossible in quantum lattice models with powerlaw interactions.

5.1. A Minimal Model for Fast Scrambling

In the following, we consider a relative of the MFI model (3.1), which is believed to be a fast scrambler. This model was recently proposed in Ref. [121] as a "*minimal model for fast scrambling*". In particular, its Hamiltonian is given by

$$\mathcal{H}_{\mathrm{FS}} = \mathcal{H} + \frac{g}{\sqrt{N}} \sum_{i<j\in Q} \mathcal{Z}_i \mathcal{Z}_j \, , \tag{5.1}$$

where $\mathcal{H}$ is the MFI Hamiltonian (3.1). As discussed in Chap. 3, the latter describes a system with local interactions, and quantum information therefore spreads ballistically. Hence, the additional all-to-all interaction in Eq. (5.1) is crucial to allow for fast scrambling, which essentially implies that the squared commutator is bounded by a logarithmic lightcone. Noteworthy, the normalization of the all-to-all interaction in Eq. (5.1) is proportional to $1/\sqrt{N}$. This scaling is crucial, as a recent work [130] proved that fast scrambling is prohibited in spin-1/2 models with a generic all-to-all interaction proportional to $1/N^{\gamma}$ if $\gamma > 1/2$. For further considerations, we set $g = J$, where J is the nearest-neighbor interaction strength associated with the MFI Hamiltonian (3.1). Moreover, we adopt the values of the magnetic fields in accordance with the previous chapters, i.e., $h_x/J = -1.05$, and $h_z/J = 0.5$. In the current, and the following section, we analyze the dynamics of quantum information regarding the fast scrambling Hamiltonian (5.1). We are particularly concerned with whether its dynamics differs from systems with (strong) powerlaw interactions. The latter may also feature a highly nonlinear ligthcone that bounds the squared commutator, as discussed in Chap. 4. Whether these systems also allow for fast scrambling, however, is yet not fully answered [47].

To begin with, let us discuss some numerical results on operator spreading regarding the fast scrambling Hamiltonian (5.1). In Fig. 5.1 (a), we display the spatiotemporal profile of the squared commutator (2.31). We evaluate the latter in the initial state

$|Y+\rangle$, and choose $\mathcal{W}, \mathcal{V} = \mathcal{Y}$. The data confirms an almost immediate growth of $C_r(t)$ for all r, resulting in a highly nonlinear lightcone. Note also the spacetime contours of constant value in Fig. 5.1 (a). Furthermore, $C_r(t)$ is nearly independent of r for large enough r, which agrees with our expectation for a fast scrambler. In the spirit of our previous investigations, we additionally consider the entanglement dynamics. Figure 5.1 (b) displays the temporal evolution of the half-chain entanglement entropy (2.6) following from a quench with initial state $|Y+\rangle$. We observe a rapid growth of entanglement entropy following a saturation at the Page value (2.22). Note also the comparison to the MFI Hamiltonian (3.1), which is obtained by setting $g = 0$. For the fast scrambling Hamiltonian, entanglement growth appears to be linear as well. However, in agreement with our expectation for a system with nonlocal interactions, the growth rate of entanglement entropy depends also on the volume of the region, which is most evident at early times and for small regions. Most importantly, however, is the absence of a slowdown of entanglement growth. Such a slowdown is characteristic for systems with (strong) powerlaw interactions, as discussed in the previous chapter. The fast scrambling Hamiltonian, therefore, induces fundamentally different entanglement dynamics compared to the LRMFI Hamiltonian (4.1). We want to emphasize that also for another recent proposal for a simple fast scrambler [122], no slowdown of entanglement growth was observed. The rapid entanglement growth regarding the fast scrambling Hamiltonian further results in a rapid approach toward local equilibrium in contrast to the LRMFI Hamiltonain. If we recollect the connection between entanglement growth and operator dynamics established in Sec. 4.5, we expect also different operator dynamics for these two systems. Confirming this expectation may potentially help to answer if systems with powerlaw interactions can exhibit fast scrambling, which we investigate further in the following section.

5.2. Fast Scrambling and Powerlaw Interactions

The apparent superballistic spread of quantum information in systems with powerlaw interactions motivates to ask whether these systems can exhibit fast scrambling. In this regard, it was proven recently that for decay exponents larger than the system's dimension, $\alpha > D$, lightcones are at best polynomial, which rules out fast scrambling in this regime [47]. If this remains true for $\alpha \leq D$ is an open question though. In Ref. [42], the authors derived lightcone shapes based on an effective stochastic model. According to their results, systems with powerlaw interactions allow for a logarithmic lightcone

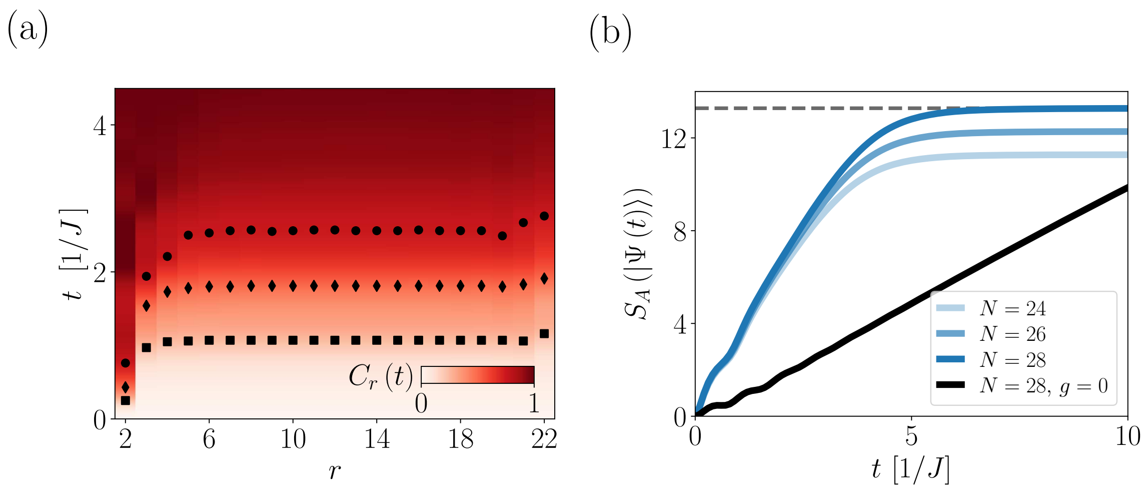

Figure 5.1.: Dynamics of quantum information regarding the fast scrambling Hamiltonian (5.1). (a) Spatiotemporal profile of the squared commutator (2.31), evaluated in the initial state $|Y+\rangle$. System size is $N = 22$ and we choose $\mathcal{W}, \mathcal{V} = \mathcal{Y}$. Crosses show spacetime contours of constant value, $C_r(t_\theta(r)) = \theta$, with $\theta = 0.25, 0.5, 0.75$ respectively. (b) Growth of half-chain entanglement entropy (2.6) following from a quench with initial state $|Y+\rangle$. System sizes of $N = 24, 26, 28$ are shown. Gray dashed line indicates the Page value (2.22) for $N = 28$. Black line shows the entanglement entropy for the local MFI Hamiltonian (3.1). Data is extracted from a numerical simulation (EXPM) of the respective Hamiltonians.

if $\alpha \leq D/2$. So far, however, this bound was not confirmed for an actual quantum many-body system, neither numerically nor analytically, and we will not try to do so here. Instead, motivated by the results from the previous section, we investigate whether a difference in entanglement dynamics infers different operator dynamics. Such a difference in operator dynamics may potentially have influence on the shape of the lightcone.

To set the stage, let us recapitulate the apparent differences and similarities between the fast scrambling Hamiltonian (5.1) and the LRMFI Hamiltonian (4.1). In Fig. 5.2 (a), we depict the lightcone, i.e., the spacetime contour $t_\theta(r)$ defined by a constant value of the squared commutator, for both of these models. We calculate $t_\theta(r)$ using TDVP, which allows us to reach system sizes up to $N = 32$ lattice sites. The results are consistent with the numerically exact method EXPM, see Appendix A.6 for further details. As already discussed in Chap. 4, for the LRMFI Hamiltonian, the lightcone becomes highly nonlinear for these small values of α. For $\alpha = 0.25$ in particular, the shape of the lightcone is very similar to that of the fast scrambler. Hence, regarding the lightcone shape, a system with sufficiently strong powerlaw interactions does not look too different from a fast scrambler, at least for the shown system size. However, for such small system sizes, it is extremely difficult, if not impossible, to reliably distinguish a logarithmic

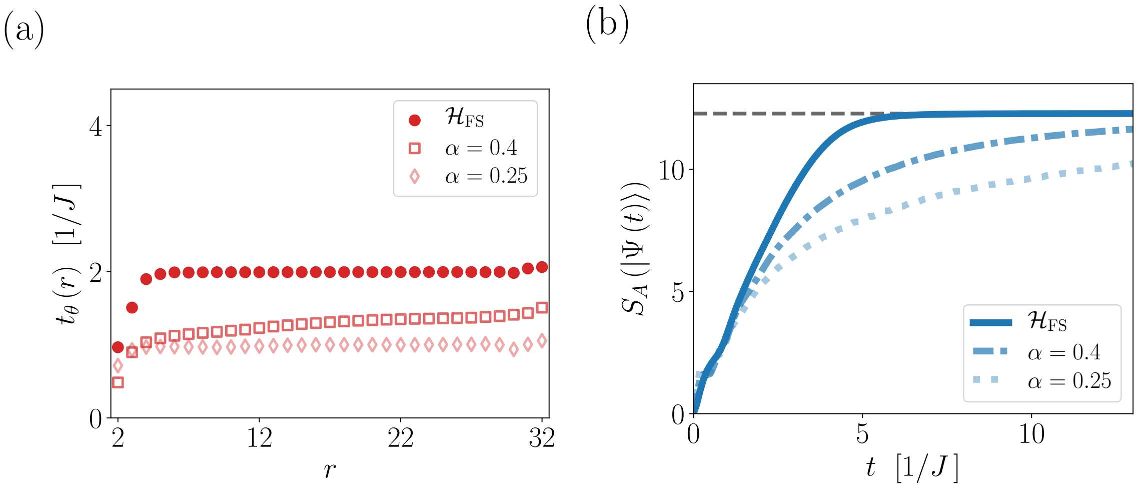

Figure 5.2.: Comparison between the fast scrambling Hamiltonian (5.1) and the LRMFI Hamiltonian (4.1) for $\alpha = 0.4$, and $\alpha = 0.25$ respectively. (a) Spacetime contour of the squared commutator (2.31) defined by $C_r(t_\theta(r)) = \theta$, where $\theta = 0.5$. Squared commutator is evaluated in the initial state $|Y+\rangle$, and we choose $\mathcal{W}, \mathcal{V} = \mathcal{Y}$. Data is extracted from a numerical simulation (TDVP) of the respective Hamiltonians for $N = 32$ lattice sites. (b) Growth of half-chain entanglement entropy (2.6) following from a quench with initial state $|Y+\rangle$. Gray dashed line indicates the Page value (2.22). Data is extracted from a numerical simulation (EXPM) of the respective Hamiltonians for $N = 26$ lattice sites.

lightcone from a polynomial lightcone. Considering entanglement growth though, these two systems follow evidently different dynamics. Figure 5.2 (b) shows the entanglement entropy following from a quench with initial state $|Y+\rangle$. Although we observe an initially rapid growth of entanglement entropy in all cases, the slowdown of entanglement growth seen for the LRMFI Hamiltonian with small decay exponents α is absent for the fast scrambler. As discussed in the previous chapter, this slowdown of entanglement growth is robust upon increasing the system size and a generic feature of quantum lattice models with powerlaw interactions.

Concerning the matter of entanglement growth, we further discussed that the apparent slowdown in systems with powerlaw interactions, such as the LRMFI Hamiltonian (4.1), diagnoses a slowdown of operator dynamics. Considering an initially local operator, this slowdown manifest in slow decay of the operator density behind the superballistically propagating front. Applying the same logic here, we expect that the fast scrambling Hamiltonian (5.1) does not exhibit such a slow decay of the operator density, and is thereby characterized by completely different operator dynamics. To confirm our understanding, we simulate the dynamics of a local operator $\mathcal{W} = \mathcal{Y}$, initially located at the left edge of the system, and analyze the decay of the operator density behind the operator front using

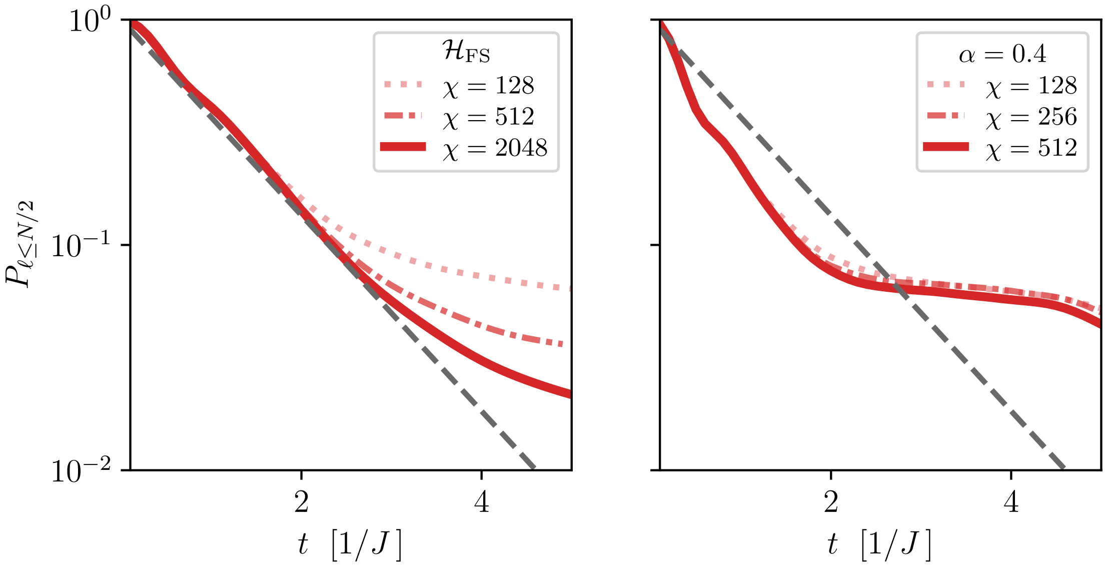

Figure 5.3.: Temporal evolution of the operator density on the left half of the system (5.2) for an initial operator $\mathcal{W} = \mathcal{Y}$ located at the left edge of the system. Left panel refers to the fast scrambling Hamiltonian (5.1) and the right panel to the LRMFI Hamiltonian (4.1) for $\alpha = 0.4$. The gray dashed line is proportional to $\exp(-t)$. Data is extracted from a numerical simulation (TDVP) of the respective Hamiltonians for $N = 24$ lattice sites.

TDVP. In particular, we consider the operator density in the left half of the system (2.37),

$$P_{\ell\leq N/2} = \sum_{\ell\leq N/2} p_\ell\,, \tag{5.2}$$

where p_ℓ is the operator density defined in Eq. (2.36). As mentioned several times, we expect Eq. (5.2) to become exponentially small in the system size at late times. In Fig. 5.3, we display the temporal evolution of $P_{\ell\leq N/2}$, for the fast scrambling Hamiltonian, and the LRMFI Hamiltonian with $\alpha = 0.4$. For the fast scrambler, $P_{\ell\leq N/2}$ approaches an exponential decay with increasing bond dimension χ, see the diagonal line as a guide. For the LRMFI Hamiltonian, however, we observe a drastic slowdown of this decay, which remains upon increasing bond dimension. We observe a similar slowdown for other small values of α, which we present in Appendix A.6. Moreover, a similar analysis as in Sec. 4.4 confirms that the observed slowdown in the saturation of the squared commutator is absent for the fast scrambler, see Appendix A.6.

To further support the TDVP results, we compute the dynamics of $\mathcal{W}(t)$ using ED. The latter grants us access to the operator density for all ℓ from which we compute the operator size defined in Eq. (2.38). The result of this computation is presented in Fig. 5.4 (a), where we display data for the fast scrambling Hamiltonian, and the LRMFI Hamiltonian with $\alpha = 0.4$, and $\alpha = 0.25$ respectively. Similar to earlier considerations, the operator size approaches L_{Haar} from Eq. (2.39) at late times for all considered Hamiltonians. At short to intermediate times, we observe a clear analogy between the operator size and the entanglement entropy following a quench, where the latter is additionally shown in Fig 5.4 (b) for the same system size. In particular, the operator size exhibits a slowdown for the LRMFI Hamiltonian, which is absent for the fast scrambler. Considering the operator density in the left half of the system, i.e., $P_{\ell \leq N/2}$ defined in Eq. (5.2), the ED results agree with the results from TDVP, which is depicted in Appendix A.6.

These numerical results agree with the developed connection between entanglement growth and operator dynamics presented in Sec. 4.5. That is, the rapid entanglement growth observed for the fast scrambling Hamiltonian (5.1), diagnoses a rapid decay of the operator density behind the superballistically propagating operator front. Thus, the fast scrambling Hamiltonian exhibits fundamentally different operator dynamics, compared to the LRMFI Hamiltonian (4.1). Crucially, this difference in operator dynamics is not immediately evident from the structure of the lightcone, at least not for system sizes of current numerical or experimental reach. However, based on our results, we conjecture that fast scrambling is prohibited in system with powerlaw interactions, as the slowdown of operator dynamics will ultimately influence the shape of the lightcone. In particular, since $\sum_\ell p_\ell = 1$ holds, a generally slower than exponential decay of p_ℓ behind the operator front will eventually slow down the latter, and thereby prohibit fast scrambling for large enough system sizes. The found connection between entanglement growth and operator dynamics further indicates that fast scrambling might be associated with unique entanglement dynamics. Deeper insights into this might help to better understand and characterize these extreme systems both experimentally and numerically.

Overall, the analysis of entanglement growth and operator spreading enables us to uncover two distinct classes of quantum information dynamics in systems with nonlocal interactions. The fast scrambling Hamiltonian (5.1) is associated with exponentially fast operator spreading accompanied by a rapid growth of entanglement. Thus, initially local information scrambles rapidly, which results in fast equilibration of local observables. The LRMFI Hamiltonian (4.1) is also associated with a superballistic spreading of initially local information over spatial degrees of freedom, which is diagnosed by a highly nonlinear lightcone and a rapid growth of entanglement at early times. However, in this case, the dynamics of quantum information is more diverse. Apparently, some information is not

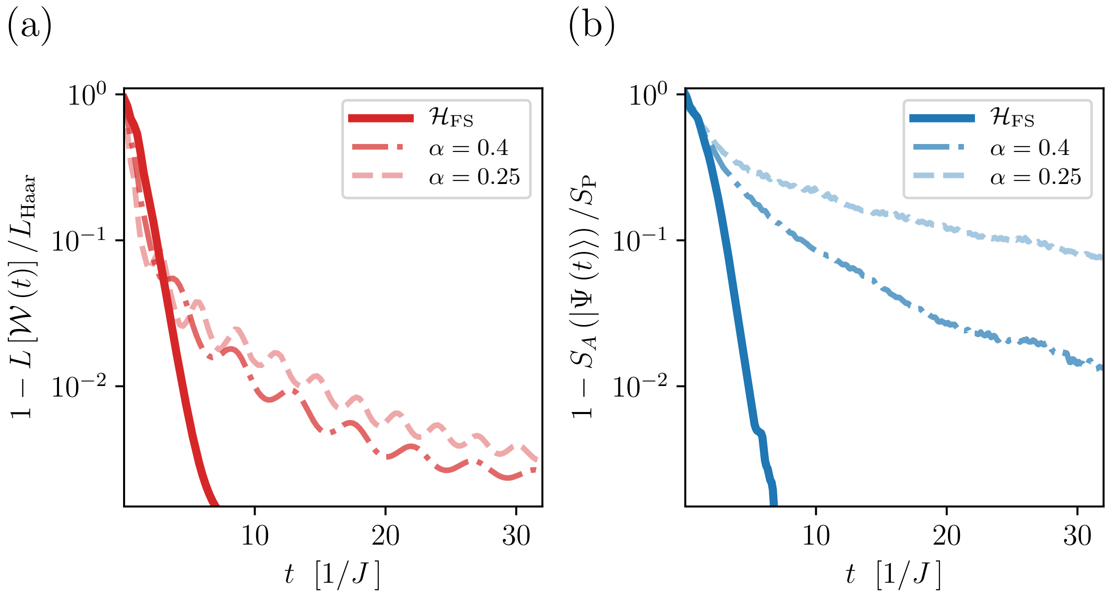

Figure 5.4.: Temporal evolution of operator size and entanglement entropy for the fast scrambling Hamiltonian (5.1) and the LRMFI Hamiltonian (4.1) with $\alpha = 0.4$, and $\alpha = 0.25$ respectively. (a) Approach of the operator size (2.38) towards its expected late-time value L_{Haar} defined in Eq. (2.39). (b) Approach of the half-chain entanglement entropy towards the Page value S_{P} defined in Eq. (2.22). Data is extracted from a numerical simulation (ED) of the respective Hamiltonians for $N = 16$ lattice sites.

scrambled as fast, which is diagnosed by a slow decay of the operator density behind the superballistically propagating operator front and a drastic slowdown of entanglement growth at intermediate times.

Chapter 6.

Discussions and Future Directions

“I’m smart enough to know that I’m dumb.”
— Richard Feynman

In this thesis, we explored the dynamics of quantum information in 1D quantum lattice models that describe interacting spin-1/2 degrees of freedom (qubits). One particular objective was to extend our understanding of quantum information dynamics regarding systems with local interactions to systems with nonlocal interactions, ubiquitous in many experimental platforms for quantum simulation and of high importance for future quantum technologies.

In Chap. 3, we developed a basic understanding of systems with local interactions. In particular, we considered the MFI model (3.1), a paradigmatic model of quantum information dynamics with rich thermalization behavior [138]. The analysis of the generalized Hayden-Preskill protocol in Sec. 3.1 underlines how the universal growth of entanglement in local systems (2.24) results in a ballistic spread of quantum information. Accordingly, the number of degrees of freedom necessary to recover the initial entanglement with the reference grows linear in time. Considering the dynamics following a quantum quench, the ballistic spread of quantum information is captured by the squared commutator (2.31). Our results on operator dynamics further show that state-independent quantities such as operator density (2.36) and operator size (2.38) agree with the effective picture of operator dynamics developed from studies on random unitary circuits [33, 124, 125]. The analysis of the operator state (3.4) in Sec. 3.3 further suggests that the process of operator spreading is connected to the growth of entanglement following a quantum quench, as the latter shows similarities to the entanglement growth of the operator state. Altogether, these results yield the following picture of quantum information dynamics in systems with local interactions. Under unitary evolution, information initially confined to a region A spreads ballistically over the system's spatial degrees of freedom. Hence, information becomes inaccessible to measurements on A once it spreads beyond A. This leakage of information due to information spreading manifests in the growth of entanglement entropy, which is linear in time with a growth rate that follows an area law, a consequence of the ballistic spreading of quantum information.

With the gathered knowledge for local interactions, we incorporated nonlocal, powerlaw interactions in Chap. 4, resulting in the LRMFI model (4.1). The results from Sec. 4.1 confirm that the strong thermalization behavior [138] is untouched by the presence of powerlaw interactions. However, the approach toward local equilibrium continues to slow down with decreasing decay exponent α, which becomes most severe for $\alpha < 1$.

We dived deeper into this issue in Sec. 4.2, where we investigated the quench dynamics of the TMI (2.13). Noteworthy, the TMI diagnoses an evident change in the correlation structure at $\alpha = 2$. In particular, our results suggest that the mutual information (2.11), a measure for total correlation, is monogamous for $\alpha > 2$, indicating that entanglement is the dominant correlation in this regime. In Ref. [72], we found a similar behavior of the TMI for the XY Hamiltonian with powerlaw interactions, which suggests the transition at $\alpha = 2$ might be a universal feature of spin-1/2 Hamiltonians with powerlaw interactions. This is further supported by the fact that for $\alpha > D + 1$, the entanglement entropy continues to follow the behavior expected in local systems (2.24), as proven in Ref. [107]. Thus, combining these results, we conjecture that the universal entanglement growth in local systems (2.24) enforces the monogamy of mutual information. Future works may review this conjecture and provide a definite answer.

For $\alpha \leq 2$, the dynamics of the TMI shows that the increasingly slower approach toward local equilibrium is accompanied by an increased localization of quantum information. Correspondingly, the decay of local correlations is significantly slower, emphasizing slower quantum information scrambling. Our analysis of the one-excitation subspace further suggests that the observed positivity of the TMI for sufficiently small decay exponents α originates from the confinement of the dynamics to a much smaller Hilbert space at early to intermediate times. Regarding future works, it remains an open question to what extent quantum states characterized by a positive value of the TMI are of practical use for quantum information processing. Due to their appearance in the quench dynamics of experimentally accessible systems, this may be an interesting route to consider.

The observed regimes of the TMI suggest a fundamental change in entanglement dynamics at $\alpha = 2$, hinting toward different regimes of quantum information dynamics. In Sec. 4.3, we further investigated these respective regimes, where we focused particularly on entanglement growth and operator spreading. The results presented in Sec. 4.3.1 support our speculation of a local regime for $\alpha > 2$, as both entanglement growth and operator spreading seem to follow effectively local dynamics. Moreover, the characteristic velocities of the two processes, i.e., the entanglement velocity v_{E} and the butterfly velocity v_{B}, show a similar dependence on the decay exponent α. Accordingly, within the local regime, both entanglement growth and operator spreading continue to slow down with decreasing α. This result is the first evidence of a deeper connection between entanglement growth and operator spreading. Moreover, it underlines that one can speed up or slow down the dynamics of quantum information by varying the decay exponent α within the local regime, which might be useful for future quantum technologies based on, for example, systems of trapped ions.

In the nonlocal regime, i.e., $\alpha \leq 2$, the dynamics of quantum information becomes radically different, which is particularly evident for $\alpha < 1$. While probes of operator spreading, such as the squared commutator (2.31), diagnose that initially local quantum information spreads superballistically over the system's spatial degrees of freedom, the growth of entanglement entropy (2.6) becomes sublinear, or even logarithmic, as discussed in Sec. 4.3.2. However, our analysis in Sec. 4.4 shows the connection between entanglement growth and operator spreading persists, even in the nonlocal regime. Our results for the operator state (3.4) and the saturation behavior of the squared commutator suggest that operator spreading becomes much more diverse in the nonlocal regime. That is, an initially local operator spreads with a superballistic operator front following a slow decay of the operator density behind the front. The derivation in Sec. 4.5 then connects these numerical observations to the known behavior of entanglement growth following a quantum quench. Accordingly, the superballistically propagating operator front manifests in fast entanglement growth at early times, with a growth rate that follows a volume law. The slow decaying operator density behind the front is responsible for the drastic slowdown of entanglement growth at intermediate times and the slowdown of thermalization. Future works may further investigate the relationship between the growth of entanglement following a quantum quench and the dynamics of Pauli strings under unitary evolution, as discussed in Sec. 4.5. What kind of universality one can ascribe to the latter is particularly interesting. Moreover, considering initial states with finite effective temperature, it could be interesting to investigate the correspondence between the reduced Pauli strings $\mathcal{S}_A(t)$ in Eq. (4.11), and the respective thermal ensemble. These insights may help to improve our understanding of prethermalization in systems with powerlaw interactions [10, 48, 49]. Another possible extension of these results is to study how they connect to operator dynamics of the time-evolution operator [105, 148].

At this point, we want to clarify a common misconception regarding the propagation of quantum information and thermalization. That is, how fast quantum information propagates directly corresponds to how fast a system thermalizes. Although this may be true for (effectively) local systems, this is certainly not the case in systems with strong powerlaw interactions, as our results from Chap. 4 underline. Ultimately, the timescale of thermalization is determined by entanglement growth, and a connection between the propagation of quantum information and thermalization in (effectively) local systems is due to a connection between entanglement growth and operator dynamics.

In Chap.5, we further examined the established connection between entanglement growth and operator dynamics by considering a recent proposal for a (simple) fast scrambling model [121]. Our results show that the different behavior of entanglement growth for the fast scrambling model (5.1) and the LRMFI model (4.1) implies also different operator dynamics. In particular, the slow decay of the operator density behind the operator front observed for the LRMFI model is absent for the fast scrambler, which further confirms the connection between entanglement growth and operator dynamics presented in Sec. 4.5. We used this apparent difference in operator dynamics to conjecture that fast scrambling is ultimately impossible in systems with powerlaw interactions. An explicit proof of this conjecture is challenging but highly desirable and may be subject to future works. Furthermore, these results suggest that fast scrambling might be associated with universal entanglement growth. Future theoretical works may explore the relationship between entanglement growth and fast scrambling in microscopic quantum systems, either through numerical studies of different models such as the proposals from Refs. [122, 123], or the SYK model [145, 146], or even better, through analytical insights starting from a logarithmic lightcone. Another interesting question is what role holography plays in this context [122]. Holographic models, for example, the SYK model, are expected to obey the monogamy of mutual information [67], which sets further restrictions on entanglement growth. A refined understanding of the relationship between entanglement growth and holography may result in explicit probes for holographic quantum matter.

In summary, these findings motivate us to generalize the effective picture of operator dynamics in local systems [31, 33, 34, 124, 125] to systems with nonlocal interactions. Based on the models we studied in this thesis, this results in two new classes of operator

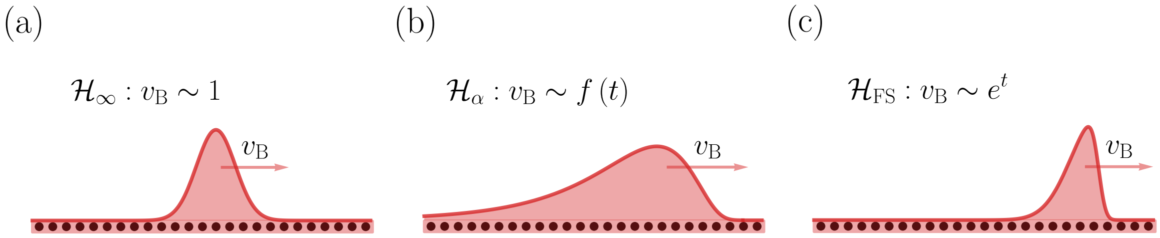
(a)
$\mathcal{H}_\infty : v_\mathrm{B} \sim 1$
v_B
(b)
$\mathcal{H}_\alpha : v_\mathrm{B} \sim f(t)$
v_B
(c)
$\mathcal{H}_\mathrm{FS} : v_\mathrm{B} \sim e^t$
v_B

Figure 6.1.: Pictorial illustration of operator dynamics regarding the respective Hamiltonians considered in this thesis. Depicted is the temporal evolution of the operator density of an initially local operator. (a) The local MFI Hamiltonian (3.1) is associated with a ballistic propagation of the operator front determined by a constant velocity v_B. (b) For sufficiently small decay exponents α, the LRMFI Hamiltonian (4.1) is associated with a superballistic propagation of the operator front. Behind the operator front the operator density decays considerably slower, though. (c) For the fast scrambling Hamiltonian (5.1), the operator front propagates exponentially fast with a rapid decay of the operator density behind the operator front.

dynamics, which are summarized in Fig. 6.1. Further quantitative insight into these classes may be subject to future works.

At last, let us emphasize that, to the best of our knowledge, there is no example where entanglement growth does not serve as a bottleneck of quantum information dynamics, i.e., where entanglement growth is ’faster’ than operator spreading. For example, subballistic operator spreading combined with linear entanglement growth. Considering the results of this thesis, we believe this is impossible. A solid understanding of the relationship between entanglement growth and operator spreading may improve our understanding of nonequilibrium phenomena and phases of quantum matter altogether.

Appendix A.

Numerics

A.1. Time-Evolution

The central object for the simulation of quantum many-body dynamics is the time-evolution operator

$$\mathcal{U}(t) = e^{-i\mathcal{H}t} \,. \tag{A.1}$$

Although easy to write down, access to Eq. (A.1) within a numerical treatment is difficult. The most straightforward is ED, i.e., one determines the eigenbasis of the Hamiltonian, $\{|E_i\rangle\}$, and then constructs Eq. (A.1) in accordance with

$$\mathcal{U}(t) = \sum_i e^{-iE_i t} |E_i\rangle\langle E_i| \,. \tag{A.2}$$

However, determining the eigenbasis of large matrices is a notoriously difficult task, and typically limited to small systems sizes N due to the exponential scaling of the Hilbert space. Moreover, the matrix representation of Eq. (A.2) is usually a *dense matrix*, i.e., the number of nonzero elements is not small compared to the total number of elements. Hence, even if we could construct Eq. (A.2), the required memory to store it grows exponentially with the system size N. Due to these limitations, the largest system size we can simulate using ED is $N = 16$.

On the other hand, the Hamiltonian $\mathcal{H}$ of a quantum many-body system is usually represented by a *sparse matrix*, i.e., the number of nonzero elements is small compared to the total number of elements. We can exploit this by storing only the nonzero elements and their respective positions. Although this does not allow the construction of the time-evolution operator (A.1), one can employ numerically exact techniques that determine the action of the time-evolution operator on an initial state $|\Psi_0\rangle$. We use such a technique (EXPM) in this thesis, where we utilize numerical routines from Ref. [139]. Within this technique, the largest system size we can simulate is $N = 28$.

A.2. Entanglement Entropy and the Partial Trace

Given a quantum state $|\Psi\rangle$, the most straightforward way to compute the entanglement entropy is the following. First, we construct the matrix $\rho = |\Psi\rangle\langle\Psi|$. From there, we can reshape ρ to a tensor and then trace over all indices that do not belong to the region A of interest, which gives us ρ_A. At last, we determine the eigenvalues of ρ_A and compute the entanglement entropy (2.6).

The approach described above has the same limitations as the construction of the time-evolution operator, discussed in Sec. A.1. In particular, ρ is also a dense matrix. However, all the necessary information is encoded in the state $|\Psi\rangle$, so constructing the projector is not necessary. A more efficient way is to reshape the state $|\Psi\rangle$ to a matrix, i.e., $|\Psi\rangle \to C$, where C has the shape $(\dim \mathbb{H}_A, \dim \mathbb{H}_B)$. The reduced state follows then by

$$\rho_A = C^\dagger C\,. \tag{A.3}$$

Since the size of the matrix ρ_A in Eq. (A.3) is exponentially smaller than the size of ρ, computing the eigenvalues is not an issue. Thus, if we can store the state $|\Psi\rangle$, we can compute the entanglement entropy.

A.3. Operator Dynamics

Let us first discuss how we can access the squared commutator (2.31) numerically. Within an ED computation, we can construct the Heisenberg operator directly, i.e.,

$$\mathcal{W}(t) = e^{i\mathcal{H}t}\mathcal{W}e^{-i\mathcal{H}t}\,. \tag{A.4}$$

Having access to Eq. (A.4), we can compute the squared commutator straightforwardly, with the same limitations of an ED computation discussed in Sec. A.1.

Additionally, we can compute the squared commutator using the EXPM technique discussed in Sec. A.1. In this case, we have to compute forward-, and backward time-evolution for two initial states. First, we evolve the initial states, $|\eta\rangle = |\Psi_0\rangle$, and $|\xi\rangle = \mathcal{V}_r|\Psi_0\rangle$ up to time t, i.e.,

$$|\eta\rangle \to e^{-i\mathcal{H}t}|\Psi_0\rangle\,, \qquad |\xi\rangle \to e^{-i\mathcal{H}t}\mathcal{V}_r|\Psi_0\rangle\,. \tag{A.5}$$

Afterward, we apply the operator $\mathcal{W}$ to both states in Eq. (A.5), obtaining

$$|\eta\rangle \to \mathcal{W}e^{-i\mathcal{H}t}|\Psi_0\rangle\,, \qquad |\xi\rangle \to \mathcal{W}e^{-i\mathcal{H}t}\mathcal{V}_r|\Psi_0\rangle\,. \tag{A.6}$$

Finally, we evolve both states in Eq. (A.6) back in time

$$|\eta\rangle \to e^{i\mathcal{H}t}\mathcal{W}e^{-i\mathcal{H}t}|\Psi_0\rangle\,, \quad |\xi\rangle \to e^{i\mathcal{H}t}\mathcal{W}e^{-i\mathcal{H}t}\mathcal{V}_r|\Psi_0\rangle\,. \tag{A.7}$$

With the resulting states in Eq. (A.7), the OTOC (2.33) is given by $\langle\eta|\mathcal{V}_r|\xi\rangle$ from which the squared commutator (2.31) follows immediately. If we want to evaluate the squared commutator at infinite temperature, we can follow the same procedure. In this case, we replace the initial state $|\Psi_0\rangle$ with a random state drawn from the Haar measure and average over several random states [134, 140]. This approach typically provides a good approximation of the trace.

The operator density (2.36) is more difficult to access. Within an ED computation, the operator density can be obtained as follows. Starting from the Heisenberg operator (A.4), we perform the partial trace with respect to all sites to the right of ℓ, i.e., we compute

$$\mathcal{W}_\ell\,(t) = \frac{1}{2^{N-\ell}}\,\mathrm{Tr}_{\overline{\mathcal{L}}}\,[\mathcal{W}\,(t)] = \sum_{|\mathcal{S}|\leq\ell} c_{\mathcal{S}}\,(t)\,\mathcal{S}\,, \tag{A.8}$$

where $\overline{\mathcal{L}}$ is the complement of $\{1,\ldots,\ell\}$. Note that $\mathcal{W}_\ell\,(t)$ is not unitary anymore. It follows then straightforwardly from Eq. (A.8) that

$$\mathrm{Tr}\,\{\mathcal{W}_\ell\,(t)\,\mathcal{W}_\ell\,(t)\} = \sum_{\ell'\leq\ell} p_{\ell'}\,(t)\ . \tag{A.9}$$

Thus, by computing Eq. (A.9) for all $1 \leq \ell \leq N-1$, one can reconstruct the operator density for all ℓ. In particular, we have

$$p_\ell\,(t) = \mathrm{Tr}\,\{\mathcal{W}_\ell\,(t)\,\mathcal{W}_\ell\,(t)\} - \mathrm{Tr}\,\{\mathcal{W}_{\ell-1}\,(t)\,\mathcal{W}_{\ell-1}\,(t)\}\ . \tag{A.10}$$

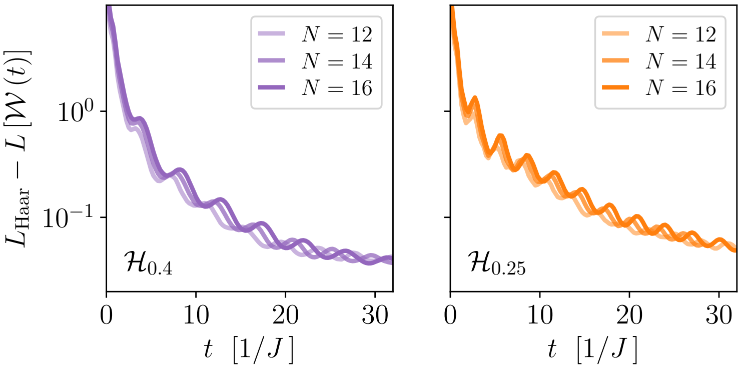

Figure A.1.: Slowdown of operator size for small values of the decay exponent α. The approach towards the expected late-time value L_{Haar} is displayed for $\mathcal{W} = \mathcal{Y}$ and different system sizes N. The left panel shows data for $\alpha = 0.4$ and the right panel for $\alpha = 0.25$. Data is obtained from a numerical simulation (ED) of the LRMFI Hamiltonian (4.1).

In principle, we can also compute the operator density using the EXPM technique. That is, we determine the coefficient $c_{\mathcal{S}}$ in the expansion (2.35) for every Pauli string that contributes to the desired operator density, i.e., we compute

$$c_{\mathcal{S}}(t) = \mathrm{Tr}\left\{\mathcal{W}(t)\,\mathcal{S}\right\} \tag{A.11}$$

for all $\mathcal{S}$ that contribute to $p_\ell(t)$. To compute Eq. (A.11), we us the same approach as for the squared commutator evaluated at infinite temperature. That is, we compute forward-, and backward time-evolution and approximate the trace using random states as discussed above. Although this works well, note that the number of strings $\mathcal{S}$ that contribute to p_ℓ is given by $3 \cdot 4^{\ell}$. Hence, this approach is limited to small ℓ.

A.4. Finite Size Scaling of Operator Size

We present additional data regarding the slow approach of the operator (2.38) size towards its late-time value for small decay exponents α in Fig. A.1. Accordingly, we display $L_{\mathrm{Haar}} - L\left[\mathcal{W}(t)\right]$ for $\mathcal{W} = \mathcal{Y}$ and different system sizes N. The left panel is associated with $\alpha = 0.4$ and the right panel with $\alpha = 0.25$. In both cases, the slowdown of operator size is robust upon increasing the system size N.

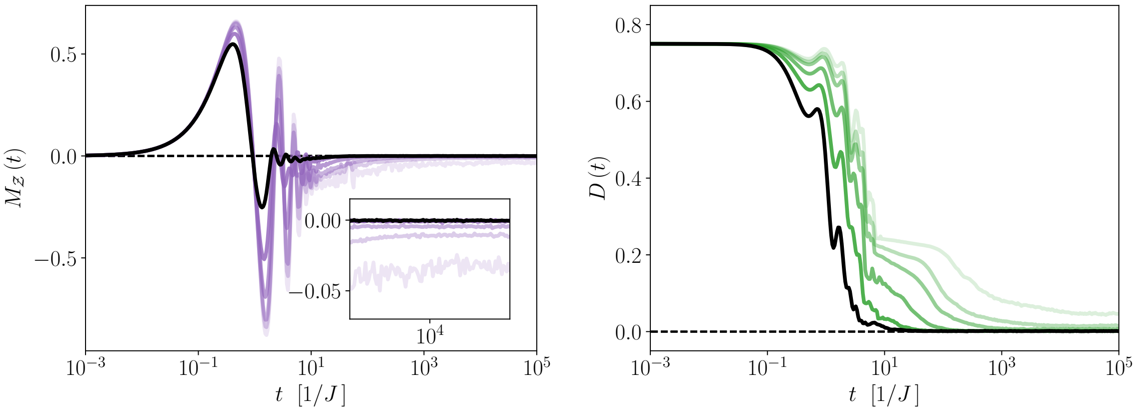

Figure A.2.: Strong thermalization in the LRMFI (4.1) following a quantum quench from the initial state $|\Psi_0\rangle = |Y+\rangle$ for various values of $\alpha = \{\infty, 2.3, 1.5, 1.0, 0.8, 0.5\}$. Darker colors indicate larger values of α. Interaction strength is rescaled by the Kac normalization. Data is extracted from a simulation of $N = 20$ lattice sites (EXPM). Left panel: Total magnetization in z-direction. Right panel: Distance between two-qubit reduced density matrix and the maximally mixed state.

A.5. Kac Normalization

In this section, we provide additional numerical data regarding the thermalization behavior of the LRMFI Hamiltonian (4.1) discussed in Sec. 4.1. In particular, we dress the interaction strength with *Kac normalization* [149], which is typically used to guarantee an extensive Hamiltonian for all values of the decay exponent α. Accordingly, we apply

$$J_{ij}^{\alpha} \to \frac{1}{\kappa} J_{ij}^{\alpha}\,, \quad \text{where} \quad \kappa = \frac{1}{N-1} \sum_{i<j} J_{ij}^{\alpha}\,.$$

Figure A.2 displays numerical data regarding the approach toward local equilibrium for various values of the decay exponent α. The left panel of Fig. A.2 shows the total magnetization in z-direction. Except for very small exponents, one can nicely see that the expectation value approaches the infinite temperature result at late times. The right panel of Fig. A.2 shows the distance between the reduced state of two qubits in the middle of the system and the maximally mixed state. Further analysis supports that the observed deviation for small exponents α is due to finite size effects. Figure A.3 shows the time average of the total magnetization in z-direction, i.e., $\overline{M}_{\mathcal{Z}}(t) = 1/t \int_0^t \mathrm{d}\tau \, M_{\mathcal{Z}}(\tau)$ for $\alpha = 0.5$ and various system sizes. With increasing system size, the deviation to the infinite temperature result systematically decreases, see also the inset of Fig. A.3.

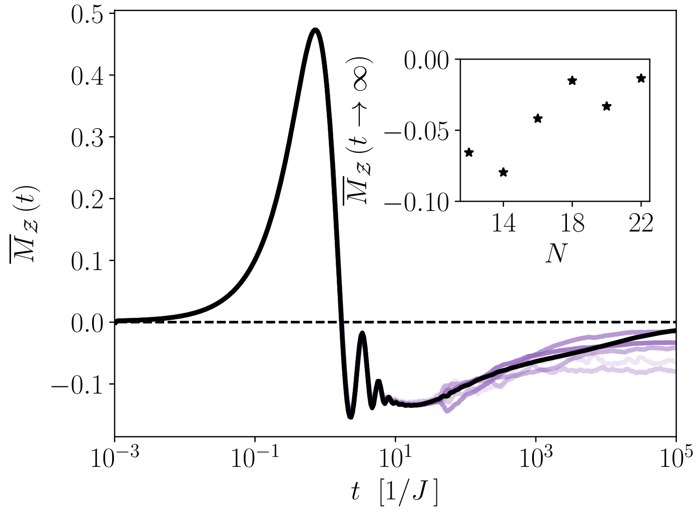

Figure A.3.: Strong thermalization in the LRMFI (4.1) following a quantum quench from the initial state $|\Psi_0\rangle = |Y+\rangle$. Interaction strength is rescaled by the Kac normalization. Data is extracted from a simulation (EXPM). Depicted is the time average of total magnetization in z-direction for various system sizes $N = \{12, 14, 16, 18, 20, 22\}$. Darker colors indicate larger values of N. Inset shows the late-time value as a function of N.

A.6. Additional TDVP Data

In this section, we provide additional details regarding our computations using matrix product states. All results have been obtained using a single site TDVP update [96]. For the calculation of the operator density (2.36) we used a state representation of the operator, defined in a doubled Hilbert space [42]. We have performed convergence checks of the quantities of interest with increasing bond dimension χ, which we present in the following.

Let us first discuss the calculated lightcone shapes presented in Fig. 5.2. For completeness, we also present the entanglement entropy (2.6) in the respective time intervals, which is shown in Fig. A.4. For the time intervals we considered, the entanglement entropy is clearly converged. Only small deviations at the end of the respective time intervals can be observed. The value of the squared commutator (2.31) at a fixed time t is shown in Fig. A.5. Apparently, the squared commutator seems to be more sensitive as a larger bond dimension is needed for convergence. This can be understood by the fact that one has to simulate forward and backward time-evolution, requiring effectively a simulation of twice the time scale.

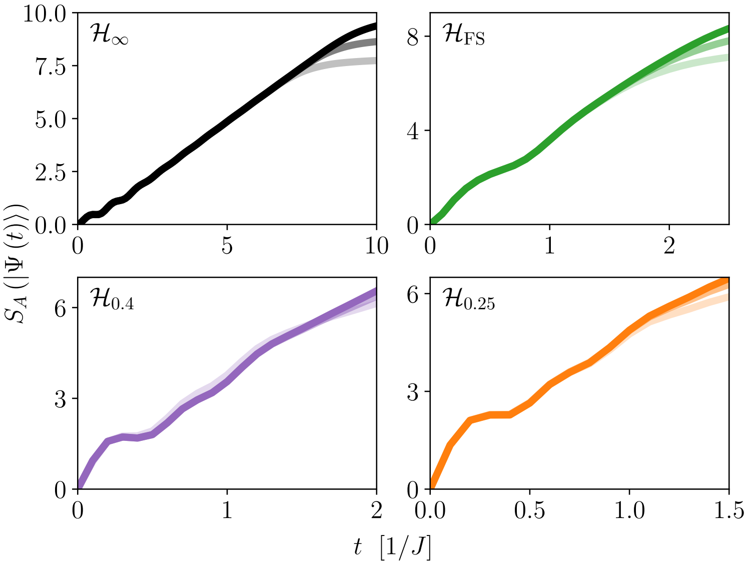

Figure A.4.: Half-chain entanglement entropy following a quench with initial state $|Y+\rangle$, $N = 32$, and various bond dimensions $\chi = \{256, 512, 1024\}$ (TDVP). Time step of the simulation is $\delta t = 0.1\,[1/J]$. Darker colors indicate larger bond dimension. MFI Hamiltonian (3.1) (upper left), fast scrambler (5.1) (upper right), LRMFI Hamiltonian (4.1) with $\alpha = 0.4$ (lower left) and $\alpha = 0.25$ (lower right).

In Fig. A.6, we display additional data regarding the operator density presented in Fig. 5.3. As discussed in Sec. 5.2, we observe a slowdown in the decay of the operator density also for other values of α, which is shown in Fig. A.6 (a) for $\alpha = 0.25$ and $\alpha = 0.6$ respectively. Also for these values, the slowdown remains upon increasing the bond dimension. Furthermore, the observed slowdown is robust against increasing the system size N, which is depicted in Fig. A.6 (b) for $\alpha = 0.25$ and $\alpha = 0.4$ respectively. Note that the ED results qualitatively match the TDVP results.

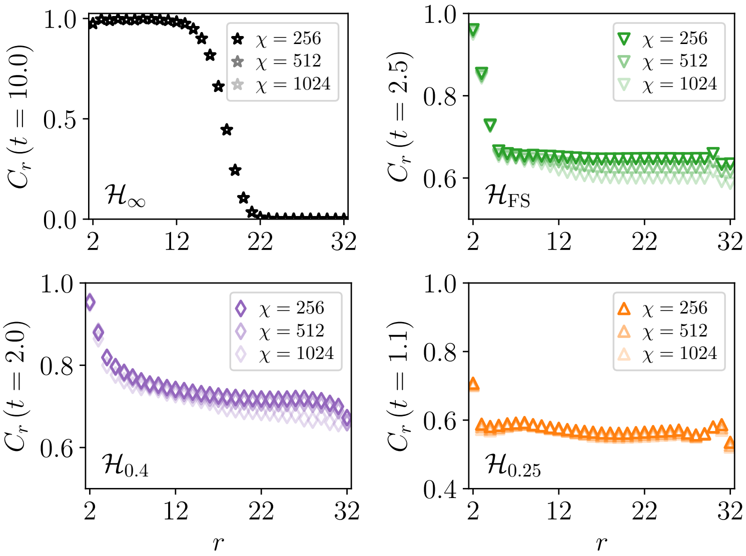

Figure A.5.: Squared commutator evaluated in the initial state $|Y+\rangle$ at a fixed time t for $\mathcal{W}, \mathcal{V} = \mathcal{Y}$, $N = 32$, and various bond dimensions $\chi = \{256, 512, 1024\}$ (TDVP). Time step of simulation is $\delta t = 0.1\,[1/J]$. MFI Hamiltonian (3.1) (upper left), fast scrambler (5.1) (upper right), LRMFI Hamiltonian (4.1) with $\alpha = 0.4$ (lower left), and $\alpha = 0.25$ (lower right).

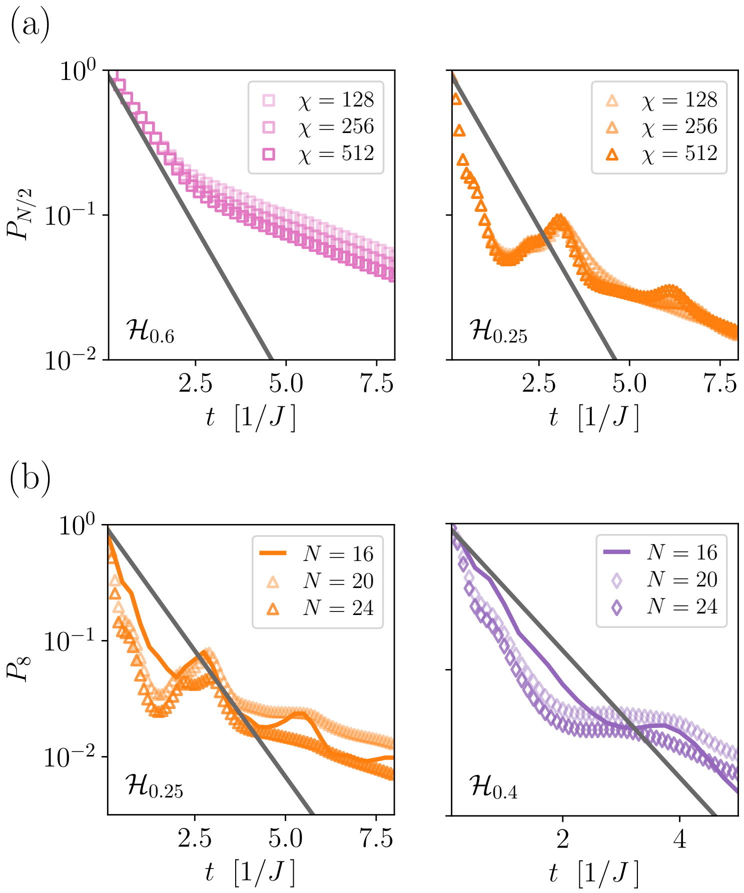

Figure A.6.: Operator dynamics in the LRMFI Hamiltonian (4.1). (a) Decay of operator density in the left half of the system for $\mathcal{W} = \mathcal{Y}$, various bond dimensions $\chi = \{256, 512, 1024\}$, and a system size of $N = 24$ (TDVP). The left panel shows data for $\alpha = 0.6$ and the right panel for $\alpha = 0.25$. (b) Operator density on the first eight sites for $N = 16, 20, 24$ respectively. The left panel is data for $\alpha = 0.25$ and the right panel for $\alpha = 0.4$. Data for $N = 20, 24$ is calculated using TDVP with $\chi = 512$, and data for $N = 16$ is calculated using ED.

Appendix B.

Derivations and Useful Relations

B.1. Derivation of Eq. (2.34)

Let us begin with the squared commutator (2.31) evaluated at infinite temperature, which we can write as

$$C_r\left(t\right) = \frac{1}{2^N}\operatorname{Tr}\left\{\mathcal{O}^\dagger\left(t\right)\mathcal{O}\left(t\right)\right\} = \frac{1}{2^N}\left|\left|\mathcal{O}\left(t\right)\right|\right|_{\mathrm{F}}^2 \,, \tag{B.1}$$

where $\mathcal{O}\left(t\right) = \left[\mathcal{W}\left(t\right), \mathcal{V}_r\right]$. Out of convenience, we have now dropped the factor of 1/2, which is present in Eq. (2.31). If we denote the singular values of $\mathcal{O}\left(t\right)$ with λ_i, it follows that

$$C_r\left(t\right) = \frac{1}{2^N}\sum_i \lambda_i^2 \,. \tag{B.2}$$

Since the operator norm is given by the largest singular value $\max\left\{\lambda_i\right\}$, it follows immediately that

$$\frac{1}{2^N}\sum_i \lambda_i^2 \leq \max\left\{\lambda_i\right\}^2 \tag{B.3}$$

holds, which implies

$$C_r\left(t\right) \leq \left|\left|\left[\mathcal{W}\left(t\right), \mathcal{V}_r\right]\right|\right|^2 \,. \tag{B.4}$$

If the expectation value is taken with respect to some pure state $|\Psi\rangle$, one can derive a similar bound. Since, by construction, $\mathcal{O}^\dagger(t)\,\mathcal{O}(t)$ is a hermitian operator, we have

$$\mathcal{O}^\dagger(t)\,\mathcal{O}(t) = \sum_i \lambda_i^2 |i\rangle\langle i| \,, \tag{B.5}$$

where the set $\{|i\rangle\}$ spans a complete orthonormal basis of $\mathbb{H}$. We can, therefore, write the respective state as $|\Psi\rangle = \sum_i c_i |i\rangle$, where $\sum_i |c_i|^2 = 1$. The squared commutator then reads

$$C_r(t) = \langle\Psi|\mathcal{O}^\dagger(t)\,\mathcal{O}(t)\,|\Psi\rangle = \sum_i \lambda_i^2\,|c_i|^2 \leq \max\{\lambda_i\}^2 \,. \tag{B.6}$$

Thus, Eq. (2.34) holds for both the infinite temperature ensemble and an arbitrary pure state $|\Psi\rangle$.

B.2. Further Operator Relations

This section provides further details on the relationship between the operator density (2.36) and the squared commutator (2.31). To this end, let us consider the squared commutator, where the operator $\mathcal{W}$ is initially placed at the left edge of the system, and the operator $\mathcal{V}$ at site r

$$C_r^{\mathcal{V}}(t) = \frac{1}{2}\left\langle [\mathcal{W}(t)\,,\mathcal{V}_r]^\dagger\,[\mathcal{W}(t)\,,\mathcal{V}_r]\right\rangle \,. \tag{B.7}$$

Here, we use $\langle\ldots\rangle = 2^{-N}\,\mathrm{Tr}\{\ldots\}$, which is the expectation value in the infinite temperature ensemble. Furthermore, we assume $\mathcal{W}$ and $\mathcal{V}$ to be local Pauli operators. Let us first consider $r = N$, Eq. (B.7) then reads

$$\frac{1}{2}\left\langle [\mathcal{W}(t)\,,\mathcal{V}_N]^\dagger\,[\mathcal{W}(t)\,,\mathcal{V}_N]\right\rangle = \left\langle [\mathbb{P}_N\mathcal{W}(t)]^2\right\rangle - \left\langle [\mathbb{P}_N\mathcal{W}(t)\,\mathcal{V}_N]^2\right\rangle \,, \tag{B.8}$$

where we defined $\mathbb{P}_N\mathcal{W}(t) = \sum_{|\mathcal{S}|=N} c_{\mathcal{S}}\mathcal{S}$ as the projection of $\mathcal{W}(t)$ onto strings that act nontrivially on site N. The first term in Eq. B.8 then reads

$$\left\langle [\mathbb{P}_N\mathcal{W}(t)]^2\right\rangle = \sum_{|\mathcal{S}|=|\mathcal{S}'|=N} c_{\mathcal{S}}^* c_{\mathcal{S}'}\,\langle\mathcal{S}\mathcal{S}'\rangle = \sum_{|\mathcal{S}|=N} |c_{\mathcal{S}}|^2 = p_N(t) \,, \tag{B.9}$$

which is just the operator density for $r = N$. For the second term, we obtain

$$\left\langle \left[\mathbb{P}_N \mathcal{W}\left(t\right) \mathcal{V}_N\right]^2 \right\rangle = \sum_{|\mathcal{S}|=|\mathcal{S}'|=N} c_{\mathcal{S}}^* c_{\mathcal{S}'} \left\langle \mathcal{S} \mathcal{V}_N \mathcal{S}' \mathcal{V}_N \right\rangle = \sum_{|\mathcal{S}|=N, \mathcal{S}_N = \mathcal{V}} \left|c_{\mathcal{S}}\right|^2 - \sum_{|\mathcal{S}|=N, \mathcal{S}_N \neq \mathcal{V}} \left|c_{\mathcal{S}}\right|^2 . \tag{B.10}$$

The convention $\mathcal{S}_N = \mathcal{V}$ in Eq. (B.10) should be understood such that the sum runs over all strings $\mathcal{S}$, which have the operator $\mathcal{V}$ at site N. The second equality in Eq. (B.10) follows from the fact that $\mathcal{V}_N \mathcal{S} \mathcal{V}_N = \pm \mathcal{S}$, where we obtain a negative sign if the string $\mathcal{S}$ at site N is not $\mathcal{V}$. Combining Eq. (B.9) and (B.10) we obtain

$$C_N^{\mathcal{V}}\left(t\right) = 2 \sum_{|\mathcal{S}|=N, \mathcal{S}_N \neq \mathcal{V}} \left|c_{\mathcal{S}}\right|^2 . \tag{B.11}$$

Note that Eq. (B.11) depends on the choice of $\mathcal{V}$. Using Eq. (B.11), we can define an average square commutator to get rid of this dependence, i.e.,

$$\overline{C}_N\left(t\right) = \frac{1}{4} \sum_{\mathcal{V} \in \mathcal{P}} C_N^{\mathcal{V}}\left(t\right) = \sum_{\mathcal{S}_N \neq \mathbf{1}} \left|c_{\mathcal{S}}\right|^2 , \tag{B.12}$$

where $\mathcal{P} = \{\mathbf{1}, \mathcal{X}, \mathcal{Y}, \mathcal{Z}\}$. Hence, we can establish the following equality between the squared commutator and the operator density

$$p_N\left(t\right) = \overline{C}_N\left(t\right) . \tag{B.13}$$

Equation (B.13) is a special case. In general, the average squared commutator $\overline{C}_r\left(t\right)$ is determined by all coefficients $c_{\mathcal{S}}$ that belong to strings $\mathcal{S}$ that act nontrivially on site r. For $r = N$, this coincides with all coefficients that belong to strings of size N. In the general case, we obtain

$$p_r\left(t\right) = \overline{C}_r\left(t\right) - \sum_{|\mathcal{S}|>r, \mathcal{S}_r \neq \mathbf{1}} \left|c_{\mathcal{S}}\right|^2 . \tag{B.14}$$

Thus, in general, the operator density is bounded from above by the average squared commutator, i.e.,

$$p_r\left(t\right) \leq \overline{C}_r\left(t\right) , \; r > 1 . \tag{B.15}$$

Moreover, the total operator density on all strings of size $\ell \geq r$, i.e., $P_{\ell\geq r}(t) = \sum_{\ell\geq r} p_\ell(t)$ upper bounds the average squared commutator. Accordingly, we have

$$p_r(t) \leq \overline{C}_r(t) \leq P_{\ell\geq r}(t) \ . \tag{B.16}$$

Given a single site i, another useful relation is

$$\frac{1}{4}\sum_{\mathcal{W}_i\in\mathcal{P}} \mathcal{W}_i\mathcal{S}\mathcal{W}_i = \begin{cases} 0\,, \text{if}\, \mathcal{S}_i \neq \mathbf{1} \\ \mathcal{S}\,, \text{if}\, \mathcal{S}_i = \mathbf{1} \end{cases} \quad , \tag{B.17}$$

where $\mathcal{S}$ can be any Pauli string.

Bibliography

[1] A. Einstein, B. Podolsky, and N. Rosen, Phys. Rev. **47**, 777 (1935).

[2] R. Horodecki, P. Horodecki, M. Horodecki, and K. Horodecki, Rev. Mod. Phys. **81**, 865 (2009).

[3] M. A. Nielsen and I. L. Chuang, *Quantum Computation and Quantum Information* (Cambridge University Press, Cambridge, 2000).

[4] G. Vidal, J. I. Latorre, E. Rico, and A. Kitaev, Phys. Rev. Lett. **90**, 227902 (2003).

[5] M. Levin and X. G. Wen, Phys. Rev. Lett. **96**, 110405 (2006).

[6] N. Schuch, M. M. Wolf, F. Verstraete, and J. I. Cirac, Phys. Rev. Lett. **100**, 030504 (2008).

[7] J. Eisert, M. Friedsdorf, and C. Gogolin, Nat. Phys. **11**, 124 (2015).

[8] R. P. Feynman, Int. J. Theor. Phys. **21**, 467 (1982).

[9] R. Blatt and C. Roos, Nat. Phys. **8**, 277 (2012).

[10] B. Neyenhuis *et al.*, Sci. Adv. **3**, e1700672 (2017).

[11] I. Bloch, J. Dalibard, and S. Nascimbene, Nat. Phys. **8**, 267 (2012).

[12] C. Gross and I. Bloch, Science **357**, 995 (2017).

[13] H. Labuhn, D. Barredo, and S. Ravets *et al.*, Nature **534**, 667 (2016).

[14] H. Bernie, S. Schwartz, and A. Keesling *et al.*, Nature **551**, 579 (2017).

[15] L. W. Cheuk *et al.*, Phys. Rev. Lett. **114**, 193001 (2015).

[16] D. Mitra *et al.*, Nat. Phys. **14**, 173 (2018).

[17] A. M. Kaufman *et al.*, Science **353**, 794 (2016).

[18] J. Zeiher *et al.*, Phys. Rev. X **7**, 041063 (2017).

[19] N. Friis *et al.*, Phys. Rev. X **8**, 021012 (2018).

[20] N. Linden, S. Popescu, A. J. Short, and A. Winter, Phys. Rev. E **79**, 061103 (2009).

[21] T. Mori, T. N. Ikeda, E. Kaminishi, and M. Ueda, J. Phys. B **51**, 112001 (2018).

[22] J. M. Deutsch, Phys. Rev. A **43**, 2046 (1991).

[23] M. Srednicki, Phys. Rev. E **50**, 888 (1994).

[24] D. A. Abanin, E. Altman, I. Bloch, and M. Serbyn, Rev. Mod. Phys. **91**, 021001 (2019).

[25] M. Serbyn, D. A. Abanin, and Z. Papić, Nat. Phys. **17**, 675 (2021).

[26] B. Swingle, Nat. Phys. **14**, 988 (2018).

[27] R. J. Lewis-Swan, A. Safavi-Naini, A. M. Kaufman, and A. M. Rey, Nat. Rev. Phys. **1**, 627 (2019).

[28] X. L. Qi, Nat. Phys. **14**, 984 (2018).

[29] P. Hayden and J. Preskill, J. High Energy Phys. **09**, 120 (2007).

[30] Y. Sekino and L. Susskind, J. High Energy Phys. **10**, 065 (2008).

[31] D. E. Parker, X. Cao, A. Avdoshkin, T. Scaffidi, and E. Altman, Phys. Rev. X **9**, 041017 (2019).

[32] E. H. Lieb and D. W. Robinson, Commun. Math. Phys. **28**, 251–257 (1972).

[33] C. W. von Keyserlingk, T. Rakovszky, F. Pollmann, and S. L. Sondhi, Phys. Rev. X **8**, 021013 (2018).

[34] T. Rakovszky, F. Pollmann, and C. W. von Keyserlingk, Phys. Rev. X **8**, 031058 (2018).

[35] P. Calabrese and J. Cardy, J. Stat. Mech. P04010 (2005).

[36] G. De Chiara, S. Montangero, P. Calabrese, and R. Fazio, J. Stat. Mech. P03100 (2006).

[37] H. Kim and D. A. Huse, Phys. Rev. Lett. **111**, 127205 (2013).

[38] M. Mezei and D. Stanford, J. High Energy Phys. **05**, 065 (2017).

[39] A. Blackmore *et al.*, Quantum Sci. Technol. **4**, 014010 (2019).

[40] M. Lu, N. Q. Burdick, and B. L. Lev, Phys. Rev. Lett. **108**, 215301 (2012).

[41] B. Yan *et al.*, Nature **501**, 521 (2013).

[42] T. Zhou, S. Xu, X. Chen, A. Guo, and B. Swingle, Phys. Rev. Lett. **124**, 180601 (2020).

[43] Z. Eldredge *et al.*, Phys. Rev. Lett. **119**, 170503 (2017).

[44] T. Kuwahara and K. Saito, Phys. Rev. X **10**, 031010 (2020).

[45] M. C. Tran *et al.*, Phys. Rev. X **10**, 031009 (2020).

[46] M. C. Tran, A. Y. Guo, A. Deshpande, A. Lucas, and A. V. Gorshkov, Phys. Rev. X **11**, 031016 (2021).

[47] T. Kuwahara and K. Saito, Phys. Rev. Lett. **126**, 030604 (2021).

[48] M. Marcuzzi, J. Marino, A. Gambassi, and A. Silva, Phys. Rev. Lett. **111**, 197203 (2013).

[49] T. Mori, J. Phys. A **52**, 054001 (2019).

[50] J. Schachenmayer, B. P. Lanyon, C. F. Roos, and A. J. Daley, Phys. Rev. X **3**, 031015 (2013).

[51] A. S. Buyskikh, M. Fagotti, J. Schachenmayer, F. Essler, and A. J. Daley, Phys. Rev. A **93**, 053620 (2016).

[52] A. Lerose and S. Pappalardi, Phys. Rev. Research **2**, 012041(R) (2020).

[53] J. S. Bell, Physics **1**, 3 (1964).

[54] A. Aspect, P. Grangier, and G. Roger, Phys. Rev. Lett. **49**, 91 (1981).

[55] A. Aspect, J. Dalibard, and G. Roger, Phys. Rev. Lett. **49**, 1804 (1981).

[56] A. Peres and D. R. Terno, Rev. Mod. Phys. **76**, 93 (2004).

[57] C. H. Bennett *et al.*, Phys. Rev. Lett. **70**, 1895 (1993).

[58] D. Bouwmeester *et al.*, Nature **390**, 575–579 (1997).

[59] A. K. Ekert, Phys. Rev. Lett. **67**, 661 (1991).

[60] R. Ursin *et al.*, Nat. Phys. **3**, 481–486 (2007).

[61] H. Araki and E. H. Lieb, Commun. Math. Phys. **18**, 60–170 (1970).

[62] E. H. Lieb and M. B. Ruskai, J. Math. Phys. **14**, 1938 (1973).

[63] B. Groisman, S. Popescu, and A. Winter, Phys. Rev. A **72**, 032317 (2005).

[64] M. M. Wolf, F. Verstraete, M. B. Hastings, and J. I. Cirac, Phys. Rev. Lett. **100**, 070502 (2008).

[65] V. Coffman, J. Kundu, and W. K. Wootters, Phys. Rev. A **61**, 052306 (2000).

[66] A. Streltsov, G. Adesso, M. Piani, and D. Bruß, Phys. Rev. Lett. **109**, 050503 (2012).

[67] P. Hayden, M. Headrick, and A. Maloney, Phys. Rev. D **87**, 046003 (2013).

[68] A. Kitaev and J. Preskill, Phys. Rev. Lett. **96**, 110404 (2006).

[69] S. Pappalardi *et al.*, Phys. Rev. B **98**, 134303 (2018).

[70] A. Seshadri, V. Madhok, and A. Lakshminarayan, Phys. Rev. E **98**, 052205 (2018).

[71] E. Iyoda and T. Sagawa, Phys. Rev. A **97**, 042330 (2018).

[72] D. Wanisch and S. Fritzsche, Phys. Rev. A **104**, 042409 (2021).

[73] Z. H. Sun, J. Cui, and H. Fan, Phys. Rev. A **104**, 022405 (2021).

[74] A. Hosur, X. L. Qi, D. A. Roberts, and B. Yoshida, J. High Energy Phys. **02**, 004 (2016).

[75] O. Schnaack *et al.*, Phys. Rev. B **100**, 224302 (2019).

[76] S. Xu and B. Swingle, arXiv:2202.07060 .

[77] M. B. Hastings and T. Koma, Commun. Math. Phys. **265**, 781 (2006).

[78] M. Foss-Feig, Z. X. Gong, C. W. Clark, and A. V. Gorshkov, Phys. Rev. Lett. **114**, 157201 (2015).

[79] C. F. Chen and A. Lucas, Phys. Rev. Lett. **123**, 250605 (2019).

[80] D. V. Else, F. Machado, C. Nayak, and N. Y. Yao, Phys. Rev. A **101**, 022333

(2020).

[81] A. Y. Guo, M. C. Tran, A. M. Childs, A. V. Gorshkov, and Z. X. Gong, Phys. Rev. A **102**, 010401(R) (2020).

[82] M. C. Tran *et al.*, Phys. Rev. Lett. **127**, 160401 (2021).

[83] P. Hauke and L. Tagliacozzo, Phys. Rev. Lett. **111**, 207202 (2013).

[84] J. Eisert, M. van den Worm, S. R. Manmana, and M. Kastner, Phys. Rev. Lett. **111**, 260401 (2013).

[85] P. Richerme *et al.*, Nature **511**, 198 (2014).

[86] P. Jurcevic *et al.*, Nature **511**, 202 (2014).

[87] L. Amico, R. Fazio, A. Osterloh, and V. Vedral, Rev. Mod. Phys. **80**, 517 (2008).

[88] J. Eisert, M. Cramer, and M. B. Plenio, Rev. Mod. Phys. **82**, 277 (2010).

[89] M. B. Hastings, J. Stat. Mech. P08024 (2007).

[90] F. Verstraete, V. Murg, and J. I. Cirac, Advances in Physics **57**, 143 (2008).

[91] U. Schollwöck, Rev. Mod. Phys. **77**, 259 (2005).

[92] J. M. Deutsch, H. Li, and A. Sharma, Phys. Rev. E **87**, 042135 (2013).

[93] L. Vidmar and M. Rigol, Phys. Rev. Lett. **119**, 220603 (2017).

[94] C. Murthy and M. Srednicki, Phys. Rev. E **100**, 022131 (2019).

[95] D. N. Page, Phys. Rev. Lett. **71**, 1291 (1993).

[96] J. Haegeman *et al.*, Phys. Rev. Lett. **107**, 070601 (2011).

[97] A. Daley, C. Kollath, U. Schollwöck, and G. Vidal, J. Stat. Mech. P04005 (2004).

[98] J. Couch, S. Eccles, P. Nguyen, B. Swingle, and S. Xu, Phys. Rev. B **102**, 045114 (2020).

[99] D. F. V. James, P. G. Kwiat, W. J. Munro, and A. G. White, Phys. Rev. A **64**, 052312 (2001).

[100] M. Carmer *et al.*, Nat. Commun. **1**, 149 (2010).

[101] R. Islam *et al.*, Nature (London) **528**, 77 (2015).

[102] B. Vermersch, A. Elben, M. Dalmonte, J. I. Cirac, and P. Zoller, Phys. Rev. A **97**, 023604 (2018).

[103] A. Elben, B. Vermersch, M. Dalmonte, J. I. Cirac, and P. Zoller, Phys. Rev. Lett. **120**, 050406 (2018).

[104] T. Brydges *et al.*, Science **364**, 260 (2019).

[105] T. L. Lezama and D. J. Luitz, Phys. Rev. Research **1**, 033067 (2019).

[106] J. H. Bardarson, F. Pollmann, and J. E. Moore, Phys. Rev. Lett. **109**, 017202 (2012).

[107] Z. X. Gong, M. Foss-Feig, F. G. S. L. Brandao, and A. V. Gorshkov, Phys. Rev. Lett. **119**, 050501 (2017).

[108] A. Lerose and S. Pappalardi, Phys. Rev. A **102**, 032404 (2020).

[109] S. Sugimoto, R. Hamazaki, and M. Ueda, Phys. Rev. Lett. **129**, 030602 (2022).

[110] A. L. Burin, Phys. Rev. B **91**, 094202 (2015).

[111] S. Schiffer, J. Wang, X.-J. Liu, and H. Hu, Phys. Rev. A **100**, 063619 (2019).

[112] A. Safavi-Naini, M. L. Wall, O. L. Acevedo, A. M. Rey, and R. M. Nandkishore, Phys. Rev. A **99**, 033610 (2019).

[113] J. E. Campbell, Proc. London Math. Soc. 28 **1**, 381 (1897).

[114] B. Vermersch, A. Elben, L. M. Sieberer, N. Y. Yao, and P. Zoller, Phys. Rev. X **9**, 021061 (2019).

[115] M. K. Joshi *et al.*, Phys. Rev. Lett. **124**, 240505 (2020).

[116] M. Gärttner *et al.*, Nat. Phys. **13**, 781 (2017).

[117] J. Braumüller *et al.*, Nat. Phys. **18**, 172 (2021).

[118] F. Heyl, M.and Pollmann and B. Dóra, Phys. Rev. Lett. **121**, 016801 (2018).

[119] D. Yuan, S.-Y. Zhang, Y. Wang, L.-M. Duan, and D.-L. Deng, Phys. Rev. Research **4**, 023095 (2022).

[120] M. Frías-Pérez and M. C. Bañuls, Phys. Rev. B **106**, 115117 (2022).

[121] R. Belyansky, P. Bienias, Y. A. Kharkov, A. V. Gorshkov, and B. Swingle, Phys.

Rev. Lett. **125**, 130601 (2020).

[122] Z. Li, S. Choudhury, and W. V. Liu, Phys. Rev. Research **2**, 043399 (2020).

[123] G. Bentsen *et al.*, Phys. Rev. Lett. **123**, 130601 (2019).

[124] A. Nahum, S. Vijay, and J. Haah, Phys. Rev. X **8**, 021014 (2018).

[125] V. Khemani, A. Vishwanath, and D. A. Huse, Phys. Rev. X **8**, 031057 (2018).

[126] D. A. Roberts, D. Stanford, and A. Streicher, J. High Energy Phys. **06**, 122 (2018).

[127] T. Zhou, A. Guo, S. Xu, X. Chen, and B. Swingle, Phys. Rev. B **107**, 014201 (2023).

[128] S. Omanakuttan, K. Chinni, P. D. Blocher, and P. M. Poggi, Phys. Rev. A **107**, 032418 (2023).

[129] D. A. Roberts, D. Stanford, and L. Susskind, J. High Energy Phys. **03**, 051 (2015).

[130] C. Yin and A. Lucas, Phys. Rev. A **102**, 022402 (2020).

[131] J. Bensa and M. Znidaric, Phys. Rev. Research **4**, 013228 (2022).

[132] J. Rammensee, J. D. Urbina, and K. Richter, Phys. Rev. Lett. **121**, 124101 (2018).

[133] B. Kobrin *et al.*, Phys. Rev. Lett. **126**, 030602 (2021).

[134] D. J. Luitz and Y. Bar Lev, Phys. Rev. A **99**, 010105(R) (2019).

[135] L. Colmenarez and D. J. Luitz, Phys. Rev. Research **2**, 043047 (2020).

[136] S. H. Shenker and D. Stanford, J. High Energy Phys. **03**, 067 (2014).

[137] P. Jordan and E. Wigner, Zeitschrift für Physik **47**, 631 (1928).

[138] M. C. Banũls, J. I. Cirac, and M. B. Hastings, Phys. Rev. Lett. **106**, 050405 (2011).

[139] P. Weinberg and M. Bukov, SciPost Phys. **2**, 003 (2017).

[140] F. Jin *et al.*, J. Phys. Soc. Jpn. **90**, 012001 (2021).

[141] W. Dür, G. Vidal, and J. I. Cirac, Phys. Rev. A **62**, 062314 (2000).

[142] C. J. Lin and O. I. Montrunich, Phys. Rev. A **95**, 023621 (2017).

[143] N. Lashkari, D. Stanford, M. Hastings, T. Osborne, and P. Hayden, J. High Energy Phys. **04**, 022 (2013).

[144] J. Maldacena, S. H. Shenker, and D. Stanford, J. High Energy Phys. **08**, 106 (2016).

[145] S. Sachdev and J. Ye, Phys. Rev. Lett. **70**, 3339 (1993).

[146] A. Kitaev, KITP Program: Entanglement in Strongly-Correlated Quantum Matter (2015).

[147] M. Tezuka, O. Oktay, E. Rinaldi, M. Hanada, and F. Nori, arXiv:2208.12098 .

[148] T. Zhou and D. J. Luitz, Phys. Rev. B **95**, 094206 (2017).

[149] M. Kac and C. J. Thompson, J. Math. Phys. **10**, 1373 (1969).

Ehrenwörtliche Erklärung

Ich erkläre hiermit ehrenwörtlich, dass ich die vorliegende Arbeit selbstständing, ohne unzulässige Hilfe dritter und ohne Benutzung anderer als der angegebenen Hilfsmittel und Literatur angefertigt habe. Die aus anderen Quellen direkt oder indirekt übernommenen Daten und Konzepte sind unter Angabe der Quelle gekennzeichnet. Bei der Anfertigung dieser Arbeit haben mir meine Betreuer und die Koautoren oben genannter Publikationen geholfen.

Weitere Personen waren an der inhaltlich-materiellen Erstellung der vorliegenden Arbeit nicht beteiligt. Insbesondere habe ich hierfür nicht die entgeltliche Hilfe von Vermittlungs- bzw. Beratungsdiensten (Promotionsberater oder andere Personen) in Anspruch genommen.

Niemand hat von mir unmittelbar oder mittelbar geldwerte Leistungen für Arbeiten erhalten, die im Zusammenhang mit dem Inhalt der vorgelegten Dissertation stehen. Die Arbeit wurde bisher weder im In- noch im Ausland in gleicher oder ähnlicher Form einer anderen Prüfungsbehörde vorgelegt. Die geltende Promotionsordnung der Physikalisch-Astronomischen Fakultät ist mir bekannt. Ich versichere ehrenwörtlich, dass ich nach bestem Wissen die reine Wahrheit gesagt und nichts verschwiegen habe.

Jena,

Darvin Wanisch

Curriculum Vitae

Personal Information

Name	Darvin Wanisch
Born	January 24, 1994

Academic Education

2019–2023	Ph.D in physics, Friedrich-Schiller-Universität, Jena, Germany
2017–2019	M.Sc. in physics, RWTH Aachen, Aachen, Germany
2016–2017	M.Sc. in physics, TU Dortmund, Dortmund, Germany
2013–2016	B.Sc. in physics, TU Dortmund, Dortmund, Germany

School Education

2004–2013	High school, Friedrich Harkort Gymnasium, Herdecke, Germany
2000–2004	Elementary school, Freiherr vom Stein Grundschule, Hagen, Germany

Employment

2019–2022	Research fellow, Helmholtz Institut Jena, Germany